1994

Lithium Binding to Human RBC Membranes and Substrates of Second Messenger Systems

Qinfen Rong
Loyola University Chicago

LOYOLA UNIVERSITY OF CHICAGO

LITHIUM BINDING TO HUMAN RBC MEMBRANES AND SUBSTRATES OF SECOND MESSENGER SYSTEMS

A DISSERTATION SUBMITTED TO

THE FACULTY OF THE GRADUATE SCHOOL

IN CANDIDACY FOR THE DEGREE OF

DOCTOR OF PHILOSOPHY

DEPARTMENT OF CHEMISTRY

BY

QINFEN RONG

CHICAGO, ILLINOIS

JANUARY 1994

ACKNOWLEDGEMENTS

I am indebted to my research advisor, Dr. Duarte Mota de Freitas for all his excellent guidance, his generous financial support and his willingness to help at any time. I am grateful to him for his patience and time in reading this thesis and for all the help that he rendered in its preparation.

My grateful appreciation goes to my committee members, Dr. David Lynn, Dr. Kenneth Olsen, Dr. Charles Thompson and Dr. David Crumrine for all their valuable suggestions and constructive criticisms on this thesis.

I am most thankful to Dr. Carlos F.G.C. Geraldes for his greate help on the data analysis.

I would like to thank all my labmates Suilan Mo, Aida Abraha, Lisa Wittenkeller, Wanrong Lin, Yuling Chi, Cherian Zachariah, Chandra Srinivasan, Hanan Hasan, and Louis Amari, and especially Dr. Elizabeth Dorus, for their friendly encouragement and corporation.

Grateful acknowledgements are made for the support of all faculty, staff, secretaries and graduate students of the Chemistry Department, and especially our graduate advisor, Dr. Albert Herlinger. Special thanks to Dr. Olsen, Dr. Thompson, Dr. Mary Boyd and their groups, especially Qunying Zhang, He Huang and Jing Lin, for their assistance on my projects and for allowing me to use their equipment. I also wish to acknowledge the Graduate School for the financial support, the Arthur J. Schmitt Foundation for awarding me the Schmitt Dissertation Fellowship, and the Chemistry Department for awarding me the Dumbach

medal.

I wish to express my sincere thanks to my parents and siblings for their constant encouragement and generosity throughout my life, and their special love and great care for my daughter, Ellen. My special appreciation for my husband, who encouraged me to go abroad to pursue the Ph.D. degree and whose love, understanding and tolerance helped me coming through all those energy barriers during these years.

Finally, I would like to covey my deepest love to Ellen over the sea.

To my dear husband and lovely daughter

LIST OF PUBLICATIONS

A. Refereed Articles:

1. "Competition Between Lithium and Magnesium Ions for Guanosine Di- and Triphosphates in Aqueous Solution: A Nuclear Magnetic Resonance Study". Q. Rong, D. Mota de Freitas, C.F.G.C. Geraldes. Lithium, 1992: 3, 213-220.

2. "Effect of Hematocrit on the Rate of Lithium Uptake in Human Erythrocyte Suspensions". D. Mota de Freitas, Q. Rong, and C.F.G.C. Geraldes. Lithium, 1992: 3, 281-285.

3. "Reinvestigation of the Transmembrane Difference in ^{7}Li NMR T_1 Values in Li^+-Loaded Human Erythrocyte Suspensions". D. Mota de Freitas, Q. Rong, S. Mo. Magn. Reson. Med., 1993: 29, 256-259.

4. "Relationship Between Lithium Ion Transport and Phospholipid Composition in Erythrocytes from Bipolar Patients Receiving Lithium Carbonate". D. Mota de Freitas, A. Abraha, Q. Rong, J. Silberberg, W. Whang, G. F. Borge, and E. Elenz. Lithium, accepted for publication.

5. "^{7}Li NMR Relaxation Study of Li^+ Binding in Human Erythrocytes". Q. Rong, M. Espanol, D. Mota de Freitas, C.F.G.C. Geraldes. Biochemistry, accepted for publication.

6. "Competition between Li^+ and Mg^{2+} for the Phosphate Groups in the Human Erythrocyte Membrane and ATP: An NMR and Fluorescence Study". D. Mota de Freitas, L. Amari, C. Srinivasan, Q. Rong, R. Ramasamy, A. Abraha, C.F.G.C. Geraldes. in preparation.

B. Abstracts:

1. "Competition Between Li^+ and Mg^{2+} for Purine Nucleoside Di- and Triphosphates in Aqueous Solution: A Multinuclear NMR Study". A. Abraha, D. Mota de Freitas, Q. Rong, M.M.C.A. Castro and C.F.G.C. Geraldes. J. Inorg. Biochem., 1991: 43, 389

2. "Elucidation of Transport Mechanisms for Alkali Cations in Human RBCs by Metal NMR". D. Mota de Freitas, A. Abraha, Q. Rong, S. Mo, L. Wittenkeller. J. Inorg. Biochem., 1991: 43, 386.

3. "Correlations Between Lithium Ion Transport and Phospholipid Composition in

Erythrocytes From Manic-Depressive Patients Receiving Lithium Carbonate and Matched Normal individuals". D. Mota de Freitas, A. Abraha, Q. Rong. SMRM Book of Abstracts, 1992: 2, 2205.

4. "^{7}Li NMR Relaxation Study of Li^{+}-Loaded Human Erythrocytes". Q. Rong, M. Espanol, D. Mota de Freitas. SMRM Book of Abstracts, 1993: 3, 1166.

TABLE OF CONTENTS

Page

ACKNOWLEDGEMENTS iii

LIST OF PUBLICATIONS v

LIST OF FIGURES xii

LIST OF TABLES xiv

LIST OF ABBREVIATIONS xvi

CHAPTER

I. INTRODUCTION 1

1. Lithium in Medicine 1

2. Proposed Mechanisms of Lithium Action 2

3. G Protein Structure and Function 8

4. Techniques for Li^+ Analysis 17

A. Conventional Methods 17

B. NMR Method 18

II. STATEMENT OF THE PROBLEMS 25

III. EXPERIMENTAL APPROACH 28

1. Materials 28

A. Reagents 28

B. Blood Samples 29

2. Sample Preparation 29

A. Metal Nucleotide Complexes in Aqueous Solution 29

B. Preparation of Shift Reagent 30

C. Preparation of Li^+-Loaded RBC 31

D. Preparation of Deoxy and Carbon Monoxy (CO) Li^+-loaded RBC 31

E. Preparation of COHb, DeoxyHb and MetHb 32

F. Preparation of Unsealed RBC Membrane 33

G. Preparation of IOV and ROV 33

H. Preparation of Spectrin 34

I. Extraction and Analysis of Phospholipids 34

3. Data Analysis 35

A. Determination of Metal-Nucleotide Binding Constants from ^{31}P NMR Chemical Shifts 35

B. $^7Li^+$ NMR Determination of Li^+ Concentration, and Time Constants for Li^+ Uptake in RBC Suspensions 36

C. Calculation of Binding Constants to RBC Membrane and ATP from ^7Li T_1 Values 37

D. Protein Concentration Determination 39

E. Statistical Analysis 39

4. Instrumentation 39

A. Nuclear Magnetic Resonance Spectrometer 39

B. Atomic Absorption Spectrophotometer 40

C. UV/Vis Spectrophotometer 40

D. Centrifuge 40

E. Osmometer 42

F. Hemofuge 42

G. Lyophilizer 42

H. Viscometer 42

IV. RESULTS 43

1. Competition Between Li^+ and Mg^{2+} for Substrates of Second Messenger Systems, and RBC Membrane 43

A. Competition Between Li^+ and Mg^{2+} for GDP and GTP in Aqueous Solution 43

a. $^7Li^+$ NMR T_1 Measurements 43

b. ^{13}C and ^1H NMR Chemical Shift Measurements 48

c. Measurements of ^{31}P NMR Chemical Shifts and Metal Ion Binding Constants 48

B. Interactions of Li^+ and Mg^{2+} with cAMP, AMP and IP_3 56

C. Competition Between Li^+ and Mg^{2+} for RBC Membrane and ATP 75

2. Multinuclear NMR Study of Li^+-Loaded Erythrocytes 80

A. The Effects of Hematocrit on ^7Li NMR T_1 Values, and on the Rate of Lithium Uptake in Human RBC Suspensions 80

B. Identification of Li^+ Binding Sites in Erythrocytes 83

a. ^7Li Intracellular Relaxation Study in Li^+-Loaded RBCs 83

b. Interactions of Li^+ with RBC Components 91

c. Li^+ Interaction with IOV and ROV 98

d. ^7Li Relaxation Behavior in RBC Membrane Suspensions 102

3. Relationship Among Na^+/Li^+ Countertransport Rates, Phospholipid Composition, and Li^+ Binding to Human RBC Membranes from Bipolar Patients Receiving Lithium Carbonate 105

A. Demography of Patients and Controls 105

B. Na^+/Li^+ Countertransport Rates 108

C. Interaction of Li^+ with RBC Membranes 111

D. Phospholipid Composition Analysis 117

E. Correlation Analysis 120

V. DISCUSSION 122

1. Competition Between Li^+ and Mg^{2+} for Substrates of Second Messenger Systems, and RBC Membrane 122

2. Transmembrane Difference on ^7Li NMR T_1 Values, and on the Rate of Li^+ Uptake in Human RBCs 133

3. Identification of Li^+ Binding Sites in Erythrocytes 140

4. ^7Li Relaxation Behavior in RBC Membrane Suspensions 144

5. Relationship Among Na^+/Li^+ Countertransport Rates, Phospholipid Composition, and Li^+ Binding to Human RBC Membranes from Bipolar Patients Receiving Lithium Carbonate 147

REFERENCES 152

VITA 167

LIST OF FIGURES

Page

1. G Protein Regulation of Adenylate Cyclase and Phosphoinositide Turnover 4
2. Schematic Drawing of Guanine Nucleotide Binding Domain 11
3. Scheme for G Protein Signal Transduction 15
4. Rotating Frame Energy Level Diagrams for an Isolated I=3/2 System 20
5. Structure of GTP 44
6. ^{7}Li T_1 Values for Li-GTP and Li-GDP in the Presence of Increasing Concentrations of Mg^{2+} 46
7. ^{13}C NMR Spectrum of GTP 49
8. ^{1}H NMR Spectrum of GTP 51
9. ^{31}P NMR Spectra of GTP 54
10. Structures of cAMP, AMP and IP_3 62
11. ^{7}Li T_1 Values for Li^{+}-IP_3 Solution Containing Various Mg^{2+} Concentrations 69
12. ^{1}H and ^{31}P NMR Spectra of IP_3 71
13. ^{7}Li T_1 Values for Membrane Suspensions in Presence of Various Concentrations of Mg^{2+} 76
14. Hematocrit Dependence of Intra- and Extracellular $^{7}Li^{+}$ T_1 Values for Human RBC Suspensions at 37 °C 81
15. Time Dependence of RBC Intracellular Li^{+} Uptake at 37 °C and

at 44% or at 85% Hematocrit 84

16. ^{31}P NMR Spectra of Packed RBCs in Various Oxygenation States 89

17. ^{7}Li T_1 Values for Li^+-Containing IOV and ROV 100

18. Partially Relaxed ^{7}Li NMR Spectra in RBC Membrane Suspension 103

19. James-Noggle Plot of RBC Membrane Suspension Containing Li^+ 106

20. ^{7}Li T_1 Values of RBC Membrane Samples at Different Concentrations of Li^+ from Patient 4 and Normal Individual 4 in the Presence of Increasing Concentrations of Li^+ 115

21. ^{31}P NMR Spectra of Phospholipid Extracts From Human RBC Membrane 118

22. Logarithmic Plot of Mg^{2+} and Li^+ Conditional Binding Constants to the RBC Membrane against Free ATP Concentration 131

LIST OF TABLES

Page

1. NMR Parameters of Nuclei Invesgated at 7.0 T 41
2. ^{1}H and ^{13}C NMR Chemical Shifts of GTP and GDP 53
3. ^{31}P NMR Chemical Shifts of GTP with Various Li^{+} and Mg^{2+} Concentrations ... 57
4. ^{31}P NMR Chemical Shifts of GDP with Various Li^{+} and Mg^{2+} Concentrations .. 58
5. ^{31}P NMR Chemical Shift Data Analysis in the Presence of LiCl or $MgCl_2$ Alone 59
6. ^{31}P NMR Chemical Shift Data Analysis in the Presence of Both LiCl and MgCl2 61
7. ^{7}Li T_1 Values of cAMP and AMP 64
8. ^{13}C NMR Chemical Shifts of cAMP and AMP 66
9. ^{31}P Chemical Shifts of cAMP and AMP 67
10. ^{7}Li T_1 Values of Li^{+}-Containing IP_3 Solutions 68
11. ^{1}H Chemical Shifts of IP_3 With or Without Li^{+} and Mg^{2+} 73
12. ^{31}P Chemical Shifts of IP_3 74
13 ^{7}Li T_1 Values in ATP Aqueous Solutions in Presence of Various Concentrations of Mg^{2+} 78
14. Effect of Hematocrit on Li^{+} Transport Parameters in Human RBC Suspensions 86

15. ^{7}Li T_1 and T_2 Relaxation Values of Packed Li^+-Loaded RBCs 87

16. ^{7}Li T_1 and T_2 Relaxation Values of 2.7 mM Hemoglobin Solutions 93

17. ^{7}Li T_1 and T_2 Relaxation Values in Aqueous Solutions of ATP and DPG 94

18. ^{7}Li T_1 and T_2 Relaxation Values of Spectrin Solutions 95

19. ^{7}Li T_1 and T_2 Relaxation Values of RBC Membrane Suspensions 96

20. ^{7}Li Relaxation Values for RBCs and Its Components at 1.5 mM Li^+ Concentration 97

21. ^{7}Li T_1 Relaxation Values for IOV and ROV 99

22. Demography of Bipolar Patients 109

23. Demography of Matched Normal Individuals 110

24. Na^+-Li^+ Exchange Rates, Phospholipid Composition, and Li^+ Binding Constants to RBC Membranes of Bipolar Patients Receiving Lithium Carbonate 112

25. Na^+-Li^+ Exchange Rates, Phospholipid Composition, and Li^+ Binding Constants to RBC Membranes of Matched Normal Individuals 113

26. Pearson Product Moment Correlation For Li^+ Binding and Transport Parameters in RBCs from Bipolar Patients Receiving Lithium Carbonate and from Matched Normal Individuals 121

LIST OF ABBREVIATIONS

AA	atomic absorption
AAPC	alkylacyl derivative of PC
ADP	adenosine 5'-diphosphate
AMP	adenosine 5'-monophosphate
AT	acquisition time
ATP	adenosine 5'-triphosphate
cAMP	adenosine 3',5'-cyclic monophosphate
BSA	bovine serum albumin
^{13}C	carbon-13 isotope
COHb	carbon monoxy hemoglobin
CPMG	Carl-Purcell-Meiboom-Gill sequence
CWS	112 mM choline chloride, 10 mM glucose, 85 mM sucrose, and 10 mM HEPES, pH 7.4
DAG	diacylglycerol
DPG	2,3-diphosphoglycerate
DTNB	5,5'-dithio-bis(2-nitrobenzoic acid)
δ	chemical shift
$\delta_{\alpha\beta}$	chemical shift separation of alpha and beta phosphate groups of GTP or GDP

$\Delta\nu_{1/2}$	NMR signal line width at half intensity
$\Delta\nu_{1/8}$	NMR signal line width at one-eigth intensity
EDTA	[Ethylenediamine]tetraacetic acid
GDP	guanosine 5'-diphosphate
GTP	guanosine 5'-triphosphate
5H8	5 mM HEPES, pH 8
Hb	hemoglobin
HEPES	4-(2-hydroxyethyl)-1-piperazineethanesulfonic acid
Ins(1,2,6)P_3	inositol 1,2,6 triphosphate
IOV	inside-out vesicle
IP_3	inositol 1,4,5 triphosphate
^{6}Li	lithium-6 isotope
^{7}Li	lithium-7 isotope
metHb	methemoglobin
MIR	modified inversion recovery
NMR	nuclear magnetic resonance
^{31}P	phosphorus-31 isotope
0.3P7.6	0.3 mM sodium phosphate, pH 7.6
5P8	5 mM sodium phosphate, pH 8
0.5P8	0.5 mM sodium phosphate, pH 8
0.5P8-0.1Mg	0.5 mM sodium phosphate, 0.1 mM $MgSO_4$, pH 8
PBS	150 mM NaCl, 5 mM sodium phosphate, pH 7.4
PC	phosphatidyl choline

PE	phosphatidyl ethanolamine
PE_p	PE plasmalogen
PI	phosphatidyl inonsitol
PIP_2	phosphatidyl inonsitol 4,5 diphosphate
P_i	inorganic phosphate
PKC	protein kinase C
PS	phosphatidyl serine
PW	pulse width
RBC	red blood cell
ROV	right-side-out vesicle
Sph	sphingomyelin
SR	shift reagent
SW	spectral width
T_1	spin-lattice relaxation time
T_2	spin-spin relaxation time
TMP	trimethyl phosphate
TMS	trimethylsilane
Tris	tris(hydroxymethyl)aminomethane
UV/VIS	ultraviolet-visible spectrophotometry

CHAPTER I

INTRODUCTION

I.1. Lithium in Medicine

Lithium was discovered in 1817. Though it has been used medically for more than a century, some of the applications are now considered useless or contra-indicated (1,2). After the success of lithium in the treatment of mania which was introduced by Cade in 1949 (3), lithium has been used more widely in psychiatry. It is a primary drug in the treatment of manic and depressive symptoms (1).

Manic-depression (or bipolar illness) is a psychiatric disorder that is characterized by severe mood swings cycling between manic and depressive states. It is a common psychiatric disease; it is estimated that at least one in every thousand individuals in the United States, Great Britain and Scandinavian countries are undergoing lithium therapy (1).

Lithium is most commonly administered to patients as lithium carbonate, and given in doses of 500-1800 mg per day. The most common side effects of lithium treatment are hand tremor, weight gain, increased urination and thirst. Patients with cardiovascular, kidney or thyroid disease need to take lithium carefully (4). The uptake of the lithium ion in biological tissue is slow; it takes 5-14 days to reach the therapeutic level of 0.3-1.0 mM in sera (1). The toxic level of lithium in the plasma is 2 mM. Loss of appetite, aversion to food, nausea and vomiting are common early signs of lithium toxicity (4). Although not fully evaluated

yet, it is possible to speed up lithium uptake and decrease the therapeutic effective extracellular Li^+ levels by enriching the drug preparation with the ^6Li isotope (5) or by using Li^+-selective ionophores (6).

Lithium is also used in the treatment of low white blood cell count resulting from anti-cancer chemotherapy and conditions caused by the Herpes Simplex virus (1), aggression, inflammatory disease and dermatoses (7). The mechanism of lithium action in the treatment of manic-depressive illness, however, is still not clear.

I.2. Proposed Mechanisms of Lithium Action

Two molecular interrelated mechanisms for the pharmacologic action of lithium have been proposed. One mechanism is based on competition between lithium and magnesium ions for magnesium binding sites in biomolecules (8,9); the other involves a cell membrane abnormality (10,11,12).

Lithium interacts with various enzymes and regulates certain metabolic processes (13). Its pharmacological effects may result from its regulation of second messenger systems through guanosine nucleotide binding proteins (G proteins). Activation of G proteins stimulates the enzyme adenylate cyclase, which enhances the synthesis of cyclic adenosine monophosphate (cAMP) from ATP to mediate cell function. Moreover, the activated G proteins influence phosphoinositide turnover via phospholipase C, triggering the release of intracellular stores of calcium which, subsequently, influence cell regulation and ion channel coupling.

At plasma concentrations of 0.6 mM, lithium blocks the activity of two types of G proteins, one with stimulatory and the other with inhibitory properties. These two types of

G proteins may provide a common site for the antimanic and antidepressive therapeutic effects of lithium (14).

G proteins are known to play an important role in triggering cellular response to outside stimulants. They carry information between hormone receptors and specific effectors to regulate different intracellular processes. The signal-transducing processes mediated by G proteins involve interaction of stimulatory agonists with G proteins, GTP binding to G proteins followed by hydrolysis to GDP, and are activated by Mg^{2+} (14,15). The synthesis of cAMP from ATP and the phosphoinositide turnover (Fig. 1) are stimulated by G proteins; the adenylate cyclase is also magnesium dependent (16) whereas the phosphoinositide turnover system has many potential binding sites for Mg^{2+}.

The structure of the guanine nucleotide binding domain has been investigated in *ras* protein by two dimensional NMR and X-ray techniques (17-21). Conformational changes were observed in active and inactive states. The triggering mechanism for activation of G proteins is thought to involve a change in the coordination of the Mg^{2+} ion at the active site (20,21). The three-dimensional structure of inositol monophosphatase was also recently studied by X-ray crystallography (22); the binding site for Li^+ was identified and was proposed to be the target for Li^+ therapy.

Lithium belongs to group IA of the periodic table of elements. Its ionic radius of 0.60 Å is nearly identical to that of the Mg^{2+} ion (0.65 Å). The existence of a diagonal relationship between Li^+ and Mg^{2+} in the periodic table results in similar chemical properties, allowing for competition between these two metal ions for Mg^{2+} binding sites in biomolecules (8,9). Competition was observed between these two cations for ATP and ADP in aqueous solution (23) and for ATP in red blood cells (9). No studies have yet addressed the question

Figure 1. G Protein Regulation of Adenylate Cyclase and Phosphoinositide Turnover (adapted from reference 15).

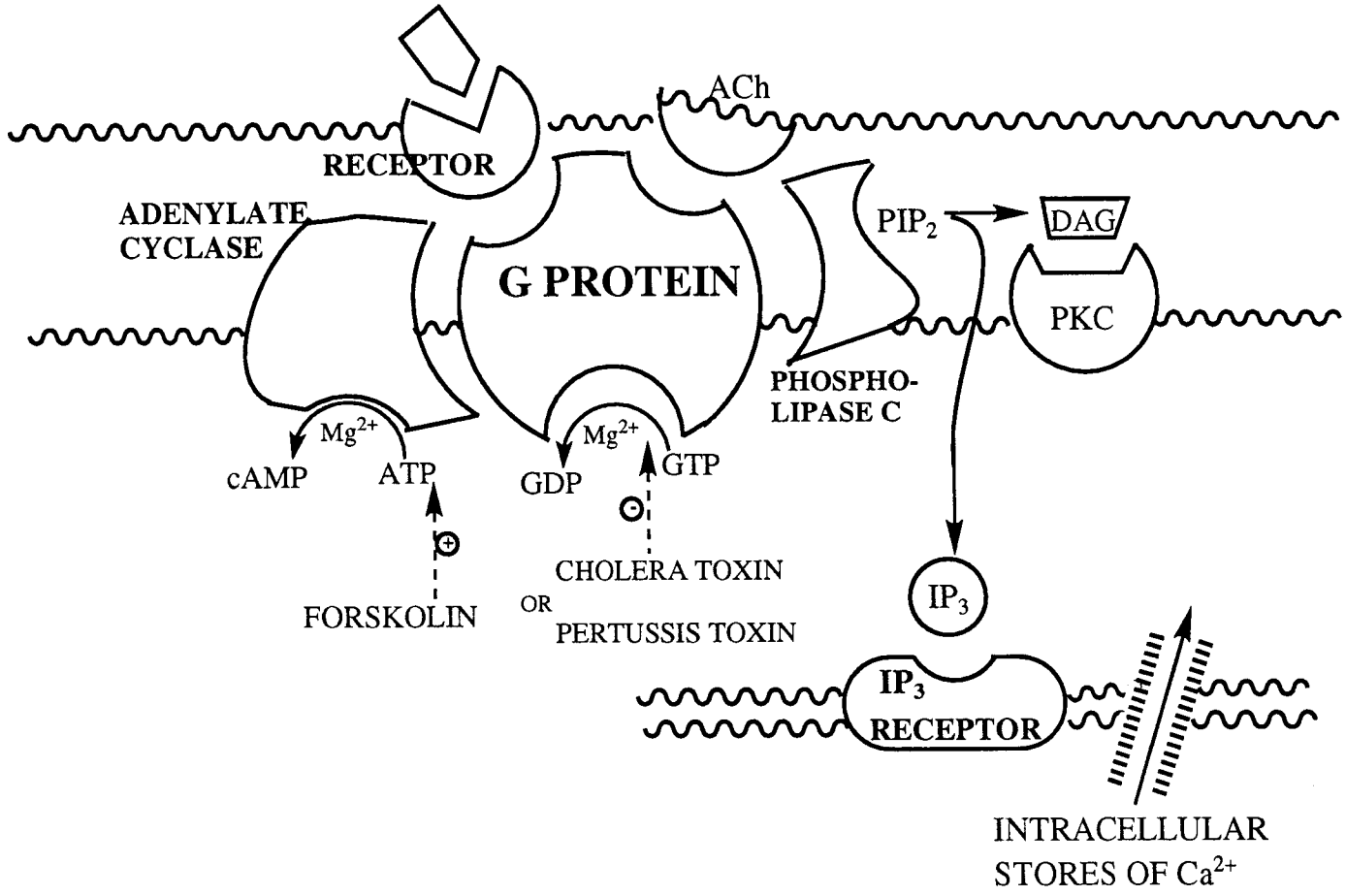
ACh
RECEPTOR
ADENYLATE CYCLASE
G PROTEIN
PIP2
DAG
PKC
PHOSPHO-LIPASE C
Mg2+
Mg2+
cAMP
ATP
GDP
GTP
FORSKOLIN
CHOLERA TOXIN
OR
PERTUSSIS TOXIN
IP3
IP3 RECEPTOR
INTRACELLULAR STORES OF Ca2+

of competition between Li^+ and Mg^{2+} ions for substrates of G proteins (24).

A membrane abnormality has been suggested in the etiology of hypertension (25) and manic-depressive (10,11,12) illness. The cell membrane dysfunction may involve different interactions between G proteins and hormone receptors, leading to abnormal signal-transduction.

Human erythrocytes are used in research for studying biological process because of their simplicity and availability. Evidence for abnormal phospholipid composition in platelets and red blood cell (RBC) membranes of manic-depressive patients was found by thin-layer chromatography (26). We and others (10,11,27) have shown that the rates of Na^+-Li^+ exchange in RBCs were significantly lower for manic-depressive patients receiving lithium carbonate than for normal individuals. In contrast, some investigators did not observe difference between patients receiving lithium carbonate and normal individuals (28-33). In a systematic investigation of manic-depressive patients withdrawn from lithium carbonate for at least three weeks, no differences between patients and normal individuals occurred (34-36).

The "Rate constant" is a characteristic of a transmembrane ion transport system and is sometimes expressed in the following way:

$$v=k[M^+] \qquad (1)$$

where v is the flux rate of the metal ion M^+, $[M^+]$ is the external M^+ concentration in influx transport experiments or the internal concentration under efflux transport conditions, and k is the "rate constant". This equation presupposes a linear relationship between influx (or efflux) of M^+ and its external (or internal) concentration, but in most cases this assumption is not valid. Equation (1) should then be replaced by the Michaelis-Menten equation:

$$v = V_{max}[M^+]/(K_m + [M^+]) \quad (2)$$

In this equation, the relationship between v and $[M^+]$ is governed by the maximal flux rate of M^+, V_{max}, and the metal ion M^+ dissociation constant K_m. Equation (2) can be simplified to an equation resembling equation (1) when $[M^+]$ is substantially lower than K_m:

$$v = V_{max}[M^+]/K_m \quad (3)$$

Thus, the rate constant k is equal to the ratio V_{max}/K_m. The rate constant may vary with changes in both maximal rate and metal ion affinity (37); however, the ratio V_{max}/K_m, and thus the rate constant k, will remain the same if both V_{max} and K_m increase or decrease by the same factor.

The standard assay for sodium and lithium countertransport activity measures Li^+ efflux from Li^+ loaded RBCs into media containing either Na^+ at 150 mM or choline-Cl at 112 mM. The transport rate is obtained by subtracting the rate in the choline medium from that in the Na^+ medium. The level of intracellular Li^+ is adequate to saturate internal ion-binding sites; the flux rate is maximal for intracellular Li^+ levels of 6 to 8 mM. The concentration of Na^+ in the medium is not sufficient to saturate outer membrane Na^+ sites (38). The Na^+ affinity for external ion-binding sites is 148 mM, which is similar to the concentration of Na^+ in the transport medium. The Na^+/Li^+ exchange rate is not at a maximum at physiologic extracellular Na^+ levels; the extracellular Na^+ level affects the activity observed in the standard assay. As discussed above, variations in Na^+ affinity (K_m) or maximal velocity (V_{max}) could change the observed rates. Nevertheless, results obtained under the same experimental conditions are still comparable (37). To avoid misinterpretation of transport assay data, measurements of binding constants as well as maximum transport rates are however required (37).

The RBC membrane is made up mostly of proteins and phospholipids, which play an important role in determining the ionic permeability of the membrane. A genetically controlled RBC membrane protein effects Na^+-Na^+ exchange under physiologic conditions and, when lithium carbonate is administered, Na^+-Li^+ exchange (39). The major phospholipids present in the RBC membrane are phosphatidyl choline (PC), phosphatidyl ethanolamine (PE), sphingomyelin (Sph), phosphatidyl serine (PS), and phosphatidyl inositol (PI). PC, PE and Sph have neutral head groups at the membrane surface; in contrast, PS and PI possess negatively charged head groups that could act as potential binding sites for the Li^+ ion. They are distributed asymmetrically between the bilayer (40). The outer leaflet contains predominately neutral charged phospholipids (40-50% PC, 40-50% Sph and 10-15% PE) while the inner leaflet contains predominately negatively charged phospholipids (10-20% PC, 10% Sph, 40-50% PE and 20-30% PS).

One possible consequence of a membrane abnormality is that changes in lipid-protein interactions within the RBC membrane may result in alterations in the Li^+ transport properties of the Na^+-Li^+ exchange protein and abnormal Li^+ interactions with the RBC membrane. The reduced transport rate of bipolar patients receiving lithium carbonate could be related to a larger extent of Li^+ binding to some RBC components. Thus, lithium binding studies in RBCs may reveal the mystery of lithium action.

I.3. G Protein Structure and Function

G proteins are membrane bound proteins that play an obligatory role in the transduction of extracellular, receptor-detected signals across the cell membrane to various intracellular effectors (41,42). G proteins consist of three subunits, designated as α, β and γ, which are

associated with the plasma membrane. G proteins are $\alpha\beta\gamma$ heterotrimers. Large diversity occurs in the α subunits, which are thought to directly modulate the activities of various effectors; diversity also exists in the β and γ subunits.

The α subunits behave as hydrophilic molecules while the $\beta\gamma$ subunits are generally hydrophobic. The $\beta\gamma$ subunits may anchor the α subunits to the membrane (43). The α subunits may be able to reach the channel directly from the aqueous phase and interact with membrane, whereas $\beta\gamma$ may be required for insertion into the membrane (44).

It is possible to isolate G proteins from different sources. For example, oncogene human *ras* proteins have been cloned in *E coli*, and G proteins were extracted by biochemical methods from RBC membranes (45). The α subunit subtypes are highly conserved across species, with interspecies differences in amino acid sequence of less than 3%; this observation suggests that each subtype has a specific role in signal transduction (44). The most conserved regions are thought to make up the guanine nucleotide binding site on the basis of their similarity to the oncogene *ras* proteins and bacterial EFTu (46-50). The differences in amino acid sequence that distinguish one subtype from another are clustered in well defined regions of each α subunit (46). The variability occurs between amino acids 85 and 125; it has been proposed that this region might be involved in effector interactions (46), but the function of this region is still not completely known (44).

The $\beta\gamma$ subunits are heterogeneous. This heterogeneity may arise partially through stable combinations of similar β subunits with different γ subunits. The $\beta\gamma$ subunits can also vary in hydrophobicity (44) from very hydrophobic (brain $\beta\gamma$) to hydrophilic (RBC $\beta\gamma$). The variable hydrophobicity is not due to the amino acid sequence but to interaction between the β and γ components. Because native β and γ do not dissociate unless treated with detergent,

the $\beta\gamma$ dimer is believed to form a single functional unit. Either covalent modifications of β or variations in the γ subunit create the observed differences in hydrophobicity.

Determination that stimulation of adenylyl cyclase activity requires both hormones and GTP encouraged further research (51). It was demonstrated that β-adrenergic agonists stimulated GTPase activity in RBC and that guanine nucleotides or similar non-hydrolyzable analogues [Gpp(NH)p or GTPβS] modulated the affinity of this receptor for agonists but not antagonists. The site of GTP's action may be on a protein distinct from both hormone receptor and adenylyl cyclase.

The structure of the guanine-nucleotide-binding domain was studied in *ras* p21 proteins by X-ray (19-21), two-dimensional NMR (17,18) and EPR (52) methods. *ras* p21 proteins are small guanine-nucleotide-binding proteins (53). They constitute a group of highly conserved proteins that function in cell signalling, proliferation and differentiation (54-56). Therefore, *ras* p21 is a useful model for guanine-nucleotide-binding proteins in general.

Figure 2 is a schematic picture of guanine nucleotide binding domain containing guanosine-5'-(β,γ- imido)-triphosphate [Gpp(NH)p]. Gpp(NH)p is a non-hydrolyzable analogue of GTP. The guanine base is sandwiched between the aromatic side chain of Phe 28 and the aliphatic part of the side chain of Lys 117. The amino group of Lys 117 is only 3.5 Å away from endocyclic oxygen of the ribose which is close enough to the main chain carbonyl group of Gly 13 in the phosphate binding loop. There are many conformational differences in the Mg^{2+} binding domain between the active GTP binding state and the inactive GDP binding state. The detailed structures were obtained at a 2.6-Å resolution by using X-ray crystallography (20). In the GTP binding structure, Mg^{2+} ion is coordinated to the nucleotide by the γ- and β- phosphate groups (pro-R oxygen) and to the protein by hydroxyl

Figure 2. Schematic Drawing of Guanine Nucleotide Binding Domain (from reference 19)

Hydrogen bonds are indicated by open arrows (⇒), bonds between Mg^{2+} and its ligands are shown by solid arrows (→).

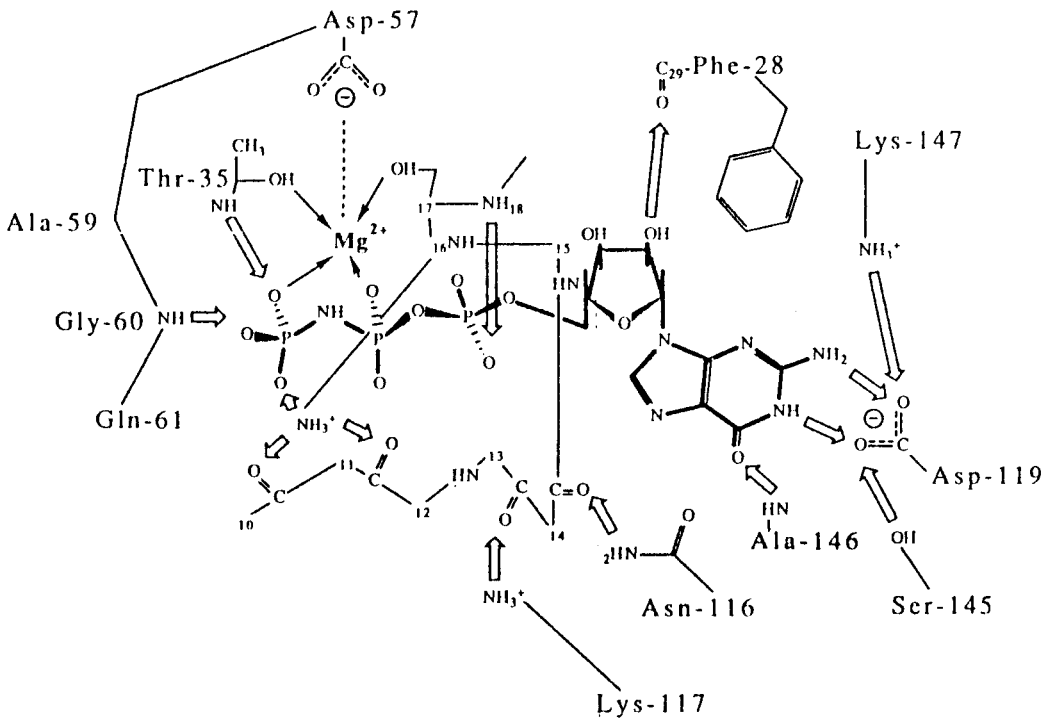
Asp-57
Thr-35
Ala-59
Gly-60
Gln-61
Mg2+
C29-Phe-28
Lys-147
Asp-119
Ala-146
Ser-145
Asn-116
Lys-117

groups of Ser 17 and Thr 35. Since Mg^{2+} is normally hexacoordinated, two molecules of water are also coordinated to the metal ion, one of them providing a bridge to the carboxyl group of Asp 57 (20). But only the latter has been identified in the p21 GTP structure. Asp 57 is close in sequences to residue 59 where substitution can influence the transforming properties of the protein (57). The ε-amino group of Lys 16 interacts with an oxygen of the γ-phosphate, and more weakly, with the β-phosphate. The β- and γ-phosphate groups are doubly coordinated with Mg^{2+} and the NH_3^+ group of Lys 16.

Several differences were observed at the active site of GDP state when compared with the GTP state, which are directly or indirectly due to the loss of γ-phosphate group. Lys 16 still interacts with the backbone carbonyl group of residues 10 and 11, but not with the β-phosphate. The distance between the amino group of Lys 16 and the oxygens of the β-phosphate group is now too large for interaction. The coordination of Mg^{2+} is similar to that in the GTP state, but only one interaction with the nucleotide at the β-phosphate group. The interaction with Asp 57 is direct, and not through a water molecule as in the triphosphate structures. The distance of Mg^{2+} to Thr 35 increases and is too large for direct interaction.

Due to a change in the position of Mg^{2+}, large differences in the effector-binding region (residues 32-40) between the two states also occurred. Main variabilities were observed between residues 32-36. This is the part of the molecule that is thought to interact with GAP (GTPase activating protein) (58). Tyr 32 interacts more strongly with the pyrrolidone ring of Pro 34 in the GDP structure; it seems likely that a conformational change is associated with this interaction. The mechanism of GTP hydrolysis is still controversial (21,59), but Gln 61 is believed to play a major role in it.

Based on their function, G proteins are referred to as G_i, G_s, G_o and G_t. G_s is involved

in the stimulation of adenylyl cyclase while G_i is involved in inhibition. G_k is a unique protein which opens potassium channels without any other intervening metabolic steps in heart (60,61). G_o, in contrast, is one kind of G protein in brain whose function is unknown. Molecular cloning techniques have revealed that at least four or more other proteins exist (62). It was found that G_i-like proteins also activate phospholipase C which hydrolyses phosphatidylinositol 4,5-bisphosphate to generate diacylglycerol and inositol 1,4,5-triphosphate and modulates the activity of specific ion channels (41,42,63,64). The study of G_o proteins in brain tissue led to the understanding that G proteins are a family of homologous proteins serving diverse roles in a wide variety of receptor-mediated extracellular signals to various intracellular second messenger systems (41,42,63,64).

G protein cycles between an inactive GDP-bound oligomeric ($\alpha\beta\gamma$) form and an active GTP-bound monomeric (α) form (Fig. 3). These two forms of α subunit are described as the "off" and "on" positions of a carefully timed molecular switch (42,65). This cycle starts from a stimulatory agonist recognized by a receptor. Activation of a receptor by an agonist induces a conformational change in the receptor, allowing it to interact with the G protein, and forms a short-lived "high affinity ternary complex" consisting of α, β and γ components. The receptor-G protein interaction facilitates the replacement of GDP by GTP on the α subunit of G protein. The binding of GTP is a crucial step which causes the G protein to dissociate from the receptor and promote dissociation into α-GTP and $\beta\gamma$ subunits. The α-GTP complex (G_s) activates the effector system (enzyme or ion channel). The continued activation is terminated by the action of GTPase which hydrolyses GTP to GDP. The formation of α-GDP causes the dissociation of α_s from effector and reassociation of α-GDP with $\beta\gamma$ which is thermodynamically stable (51).

Figure 3. Scheme for G Protein Signal Transduction (adapted from references 44 and 51)

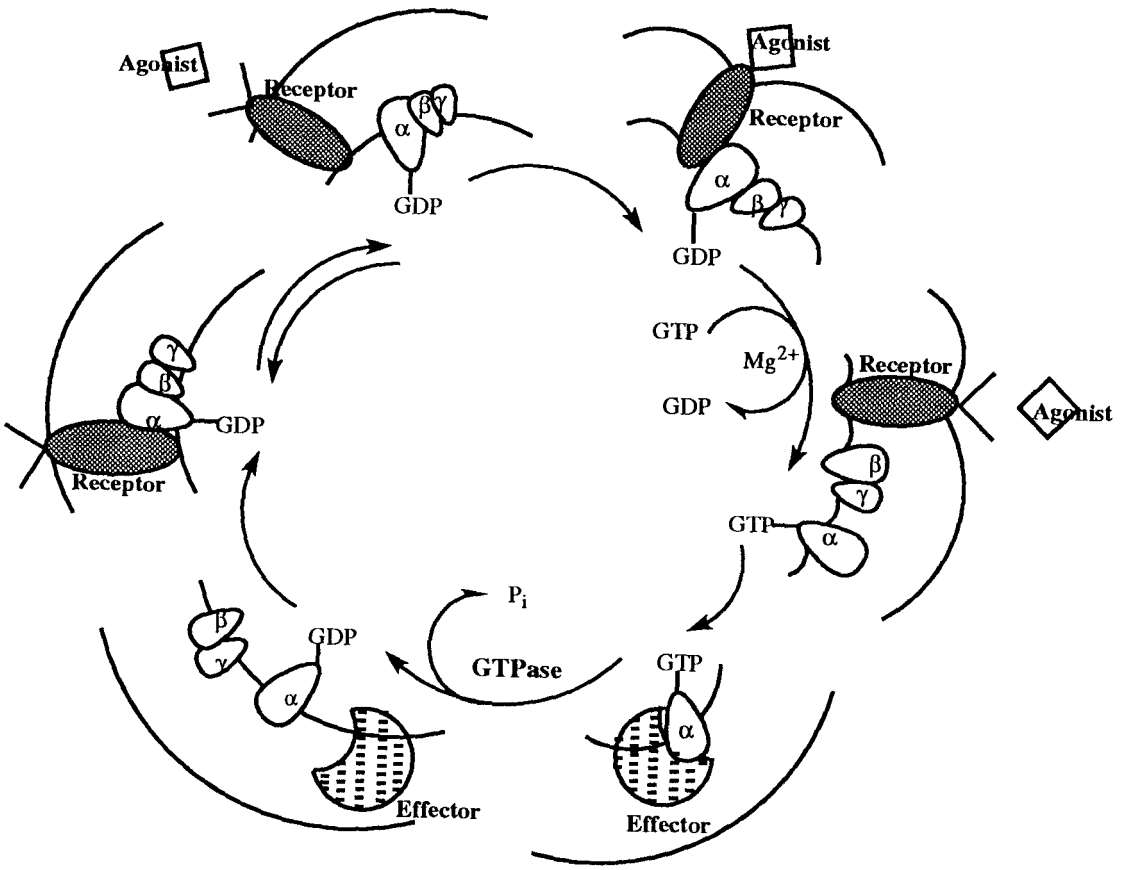
Agonist
Receptor
α
βγ
GDP
Agonist
Receptor
α
β
γ
GDP
GTP
Mg2+
GDP
Receptor
Agonist
β
γ
GTP
α
Pi
GTPase
GTP
α
Effector
β
γ
GDP
α
Effector
γ
β
α
GDP
Receptor

Inhibitory effects on adenylyl cyclase is based on two distinct mechanisms. First, there appears to be a direct inhibitory effect of the α subunit of G_i on the catalytic unit of adenylyl cyclase which acts as a parallel system to G_s. Second, the $\beta\gamma$ subunits which are released by receptor activation of G_i, may by mass action attenuate the dissociation of G_s. Since the concentration of G_i is substantially greater than G_s, $\beta\gamma$ subunits may be more potent inhibitors of adenylyl cyclase (42,66). When G_s is stimulated by a hormone or neurotransmitter, α_i is the primary mediator of inhibition of adenylyl cyclase; the $\beta\gamma$ exerts a major role in the inhibition of basal- and postreceptor-stimulated adenylyl cyclase activity.

G proteins serve a critical role in a second messenger system. They amplify or attenuate extracellular generated neural signals and then transmit these integrated signals to effectors, thus forming the basis for a complex information processing network (67). Abnormalities in the function and/or expression of G proteins is implicated in a variety of pathophysiologic states: pseudohypoparathyroidism type I, heart failure, certain endocrine tumors, McCune-Albright syndrome, diabetes, alcoholism, schizophrenia, mitral valve prolapse, chronic cocaine/opiate ingestion, aging, hypo/hyperthyroidism, and adrenalectomy/corticosteroid administration (51). G protein dysfunction appears to be a primary cause of pathology in Albright's hereditary osteodystrophy, endocrine tumors, and McCune-Albright syndrome; in several other conditions, G protein abnormalities are probably secondary, but are nonetheless implicated in the pathophysiology of the condition (51).

I.4. Techniques for Li^+ Analysis

I.4A. Conventional Methods

Several conventional methods, including atomic absorption (AA), flame emission (FE),

UV/VIS, fluorescence, ion-selective electrodes and neutron activation analysis, have been applied to monitor Li^+ levels in biological tissues and aqueous solution (68). Among these methods, AA has been used most frequently; it is very selective in that each element emits or absorbs radiation at a specific wavelength, and therefore, less prone to interference effects. It is also highly sensitive and is able to trace very small amounts of Li^+ in biological tissues.

However, all these techniques require physical separation of cells from plasma by centrifugation and cell lysing. The intra- or extracellular Li^+ level is then determined by comparison to standard Li^+ solutions with a composition similar to the biological tissue being analyzed. The invasive nature of these methods may lead to errors due to nonspecific ion binding to membranes and cell metabolites and additional ion transport during sample processing (68). Moreover, most conventional methods are only useful for obtaining total Li^+ concentrations. No information can be obtained about free and bound states of the Li^+ ion. Fluorescence and ion-electrodes are the exceptions. The major difficulty is however finding a reagent that is highly selective for Li^+ ion and yet does not disturb its distribution across the cellular membrane. Some success has recently been achieved in this area (69-72).

I.4.B. NMR Method

The major advantage of the NMR method is its non-invasiveness which gives clinicians and researchers access to physiological information unattainable with conventional methodology (73). NMR spectroscopy is however not as sensitive as some of the conventional methods, in particular atomic absorption.

Lithium has two isotopes, ^7Li and ^6Li. The natural abundance of ^7Li (92.6%) is considerably higher than that of ^6Li (7.4%). Moreover, the receptivity, an NMR parameter

which considers the effects of nature abundance, gyromagnetic ratio γ and the nuclear spin I, is substantially higher for ^{7}Li than for ^{6}Li. These factors make the detection of ^{7}Li routine. The lower receptivity of ^{6}Li can be circumvented in biological applications by using lithium salts enriched with the ^{6}Li isotope (5,74).

Both ^{6}Li and ^{7}Li are quadrupolar with nuclear spins equal to 1 and 3/2, respectively. The quadrupole moments are very small in both cases, giving rise to narrow NMR lines (75). The dipolar relaxation mechanism predominates in the case of ^{6}Li, and is also important in the case of ^{7}Li (76).

Because ^{7}Li has a spin at 3/2, in the presence of a magnetic field it has four nuclear energy states and undergoes three transitions when pulsed with the correct radio frequency (77) (Fig. 4). In general, in a homogeneous system, the energy gaps corresponding to the three transitions are the same. Only one "extreme narrowed" peak is observed. Upon distortion of the nuclear environment, the nuclear energies may change. As a result, a single crystal-like spectrum of three peaks may be observed. Between these two extreme cases, there are the homogeneous "biexponential" ("super-Lorentzian") state (78), which only has an effect on relaxation, and the inhomogeneous "powder" ("pseudosuper-Lorentzian") state (78), in which chemical shifts start to split.

A $\Delta\nu_{1/8}/\Delta\nu_{1/2}$ ratio of $7^{1/2}$ is characteristic for a Lorentzian line shape (79), where $\Delta\nu_{1/8}$ and $\Delta\nu_{1/2}$ are the spectral line widths at one-eighth and half intensities of the NMR resonance, respectively. If the ratio of $\Delta\nu_{1/8}/\Delta\nu_{1/2}$ is larger than $7^{1/2}$, the resonance is non-Lorentzian (80). It can be deconvoluted into a narrow Lorentzian curve responsible for the slow relaxation component and a broad Lorentzian curve which is due to the fast component (81). The narrow component is associated with the -1/2 to +1/2 transition, whereas the broad components relate to the -3/2 to -1/2 and +1/2 to +3/2 transitions (75,80).

Figure 4. Rotating Frame Energy Level Diagrams for an Isolated I=3/2 System (adapted from reference 77)

a) Homogeneous 'extreme narrowed' spectrum

b) Single crystal-like spectrum

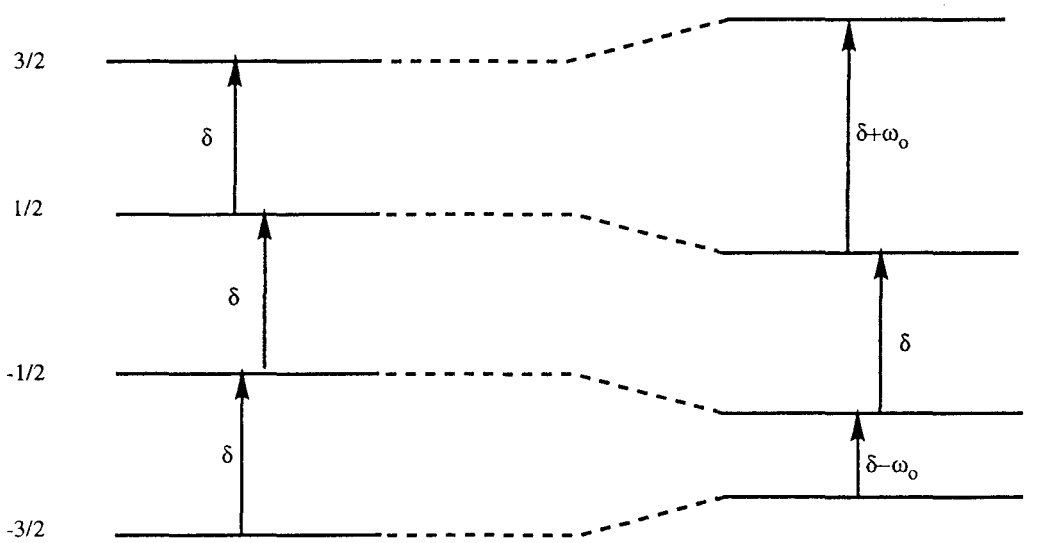

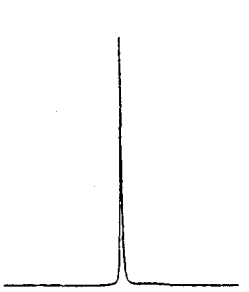

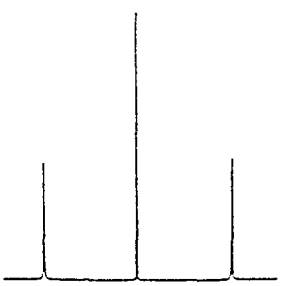

Homogeneous

Distorted

a

b

Correlation time, τ_c, is a parameter that describes molecular motion. When τ_c is much shorter than the NMR observation frequency, ω, the extreme narrow condition applies ($\omega^2\tau^2 << 1$); the spin-lattice (T_1) and spin-spin (T_2) relaxation times are equal and undergo a monoexponential decay. The equation is:

$$1/T_1 = 1/T_2 = 3(2I+3)\chi^2\tau_c/40I^2(2I-1) \qquad (4)$$

where χ is the product of the quadrupolar coupling constant, $e^2qQ/\hbar$, and the asymmetry factor, $1+\eta^2/3$ (75). The eq term is the electric field gradient, eQ is the electric quadrupole moment, and $\hbar$ is the Planck constant, h, divided by 2π. In a homogeneous magnetic field, T_2 is inversely proportional to the line width at half-intensity of the signal, $\Delta\nu_{1/2}$, and is given by the equation:

$$1/T_2 = \pi\Delta\nu_{1/2} \qquad (5)$$

When Li^+ is bound to proteins or intracellular components, τ_c is sufficiently large and comparable to the NMR observation frequency which results in the T_1 values being much larger than the T_2 values. For ^6Li, though, the relaxation decay is still monoexponential while for ^7Li it is biexponential (76,82). Fast relaxation decay contributes to slow motion, and slow relaxation decay is due to free motion. Two components can be observed in the longitudinal, $M_Z(t)$, and transverse, $M_T(t)$, relaxation mechanisms for I=3/2; they are expressed by equations 6 and 7, respectively (76,81,82).

$$M_Z(t) = M_Z(0)[0.2\ \exp(-t/T_1') + 0.8\ \exp(-t/T_1'')] \qquad (6)$$

$$M_T(t) = M_T(0)[0.6\ \exp(-t/T_2') + 0.4\ \exp(-t/T_2'')] \qquad (7)$$

where single and double primed symbols denote the relaxation times of the two components. When the mole fraction of bound species, p_b, is very small compared to that of the free species, p_f, in solution:

$$1/T_1' = 1/T_{1f} + p_b\chi^2/10[\tau_c/(1+\omega^2\tau_c^2)] \quad (8)$$

$$1/T_1'' = 1/T_{1f} + p_b\chi^2/10[\tau_c/(1+4\omega^2\tau_c^2)] \quad (9)$$

$$1/T_2' = 1/T_{2f} + p_b\chi^2\tau_c/20[1 + 1/(1+\omega^2\tau_c^2)] \quad (10)$$

$$1/T_2'' = 1/T_{2f} + p_b\chi^2\tau_c/20[1/(1+4\omega^2\tau_c^2) + 1/(1+\omega^2\tau_c^2)] \quad (11)$$

Subscripts f and b stand for free and bound states.

Li^+ ions are in the fast exchange in the ^7Li NMR time scale. The observed ^7Li chemical shift and relaxation values represent the weighted average of free and bound Li^+ ions. The chemical shifts of ^7Li are insensitive to Li^+ binding. On the contrary, the relaxation values are sensitive to motion (75). Since ^7Li is quadrupolar, changes in the symmetry of the Li^+ environment are expected to alter the relaxation. However, components of motion at the resonance frequency contribute to both T_1 and T_2, while slow motions only contribute to T_2. Therefore, large differences exist between T_1 and T_2 for bound Li^+ ions. Thus, ^7Li NMR relaxation times constitute a good probe for obtaining information on Li^+ interaction with biological tissues.

Because the chemical shifts of lithium are generally insensitive to solvation or complexation by biomolecules (76,82), a shift reagent (SR) method was developed to discriminate intra- and extracellular signals (83,84). Negatively charged lathanide shift reagents are soluble in aqueous solution and insoluble in hydrophobic cell membranes, and are repelled by the negatively charged head groups of phospholipids at the surface of cell membranes. SRs are cell impermeable and remain in the cell suspensions except when SR decomposition occurs or when cell membranes are leaky. The most popular shift reagents used in biological applications of ^7Li NMR are $Dy(PPP)_2^{7-}$ (dysprosium(III) triphosphate) and $Dy(TTHA)^{3-}$ (dysprosium (III) triethylenetetraminehexaacetate). Because the lanthanide ion

in shift reagents is paramagnetic, the NMR resonance of extracellular Li^+ is subject to a pseudocontact shift, and therefore, is separated from the intracellular signal. $Dy(PPP)_2^{7-}$ induces an upfield shift whereas a downfield shift is induced by $Dy(TTHA)^{3-}$. The opposite direction of pseudocontact shifts for Li^+ resonance are due to the different locations of the Li^+ ion relative to the cones around the effective magnetic axes of these shift reagents (74). Since the overall negative charge is different for these two SRs, the pseudocontact shift induced by $Dy(PPP)_2^{7-}$ is larger than that by $Dy(TTHA)^{3-}$ at same concentration (84). These two SRs can also be used in ^6Li NMR studies (5). In a ^7Li NMR investigation of Na^+/Li^+ exchange in RBC suspensions, it was found that $Dy(PPP)_2^{7-}$ in the suspension medium could alter the rates and membrane potential (85,86,87). Because of the high negative charge of $Dy(PPP)_2^{7-}$, the amount of extracellular Li^+ bound to shift reagent is considerable.

In addition to the SR method, the Modified Inversion Recovery (MIR) method can also be used to discriminate between intra- and extracellular ^7Li NMR signals in human RBC suspensions (85,86). The MIR pulse sequence $(D_1\text{-}180°\text{-}D_2\text{-}60°\text{-}AQ)_n$ takes advantage of large differences between ^7Li T_1 relaxation values and was applied to human RBC suspensions to eliminate the extracellular ^7Li resonance and selectively observe the intracellular NMR signal (86,88,89).

CHAPTER II

STATEMENT OF THE PROBLEMS

The purpose of this thesis is: 1. to address the competition between lithium and magnesium ions for substrates of second messenger systems, and RBC membranes; 2. to characterize the major lithium binding sites in human erythrocytes; and 3. to investigate the cell membrane abnormality in RBCs of lithium-treated manic-depressive patients.

Li^+ may exert its antimanic and antidepressive effect by competing with Mg^{2+} for biomolecules. Li^+ and Mg^{2+} have similar chemical properties because of the diagonal relationship between these two cations; several studies have provided evidence for competition between Li^+ and Mg^{2+} for biological ligands (8,9,23). Li^+ can also modulate the activity of Mg^{2+}-activated enzymes involved in second messenger systems (14,90,91).

^{31}P, ^{13}C, ^{1}H NMR spectroscopic methods will be applied to the substrates of second messenger systems including cAMP, AMP, IP_3, GTP and GDP. The changes in chemical shifts induced by the presence of various concentrations of Li^+ and Mg^{2+} on the phosphate, sugar and base moieties can be monitored to determine which part of the nucleotide structure contributes to Li^+ and Mg^{2+} binding. Measurements of spin-lattice (T_1) relaxation values by the inversion recovery pulse sequence will be used to investigate whether competition between Li^+ and Mg^{2+} ions for the same binding sites exist in aqueous solutions of nucleotides.

NMR relaxation is characterized by spin-lattice (T_1) and spin-spin (T_2) relaxation values.

They are similar when molecular motion is fast but different when motion is slow, i.e., strong binding and electric field gradient. Previous NMR studies in our laboratory (92,93) showed that Li^+ binds to intracellular components of RBCs; T_1 for RBCs loaded with 1.5 mM Li^+ is 6.0 s, whereas T_2 is 0.30 s, indicating that strong Li^+ binding exists in RBCs. It is however not known which component contributes mostly to Li^+ binding in human RBCs. Measurements of ^7Li NMR relaxation values with different RBC components will establish which component contributes more toward Li^+ binding. The larger the difference between T_1 and T_2, the stronger the interaction between Li^+ and that RBC component.

The viscosity and magnetic properties of intact RBC suspensions are two factors that may influence the relaxation times. Hematocrit may affect the viscosity of a RBC suspension. The higher the hematocrit, the more viscous the sample. On the other hand, RBCs contain hemoglobin which is a mixture of oxy and deoxy. Oxy hemoglobin is diamagnetic while deoxy hemoglobin is paramagnetic. Carbon monoxide (CO)- and nitrogen (N_2)-treated RBCs were used in our experiments to examine the paramagnetic contribution of hemoglobin to relaxation times.

By using ^7Li relaxation measurements, I investigated the Li^+ binding sites in human erythrocytes via the investigation of the interaction of Li^+ with the RBC components: hemoglobin, ATP, DPG, membrane, spectrin-actin network and vesicles. Three forms of hemoglobin were used: CO-treated hemoglobin is an irreversible analogue of oxy hemoglobin, and is diamagnetic; deoxy hemoglobin and methemoglobin are paramagnetic. Vesicles were of two types: inside-out (inner membrane surface outside; IOV) and right-side-out (outer membrane surface outside; ROV) vesicles. ^7Li NMR relaxation measurements will be used to investigate whether Li^+ binding to internal RBC components contributes significantly to the

relaxation parameters observed in intact RBC suspensions. The measurements in vesicle suspensions will be made to examine which side of the RBC membrane contributes mostly to Li^+ binding.

To understand the ^7Li relaxation behavior in RBC membrane suspensions, partially relaxed ^7Li NMR spectra will be measured in RBC membrane suspensions containing various amounts of Li^+, and in Li^+-containing glycerol-water mixtures.

Abnormal phospholipid composition in platelets and RBC membranes and lower Na^+/Li^+ exchange rates were observed in RBCs of manic-depressive patients receiving lithium carbonate (10,11,26,27). To address the question of a cell membrane abnormality, AA analysis, ^7Li NMR relaxation measurements and ^{31}P NMR will be used to investigate the Na^+/Li^+ exchange rates in RBCs, the interaction of Li^+ with RBC membranes and the phospholipid components, respectively, from blood of manic-depressive patients taking lithium carbonate, and from matched normal individuals. Correlations among Na^+/Li^+ exchange rates, Li^+ binding to membrane, and phospholipid composition in lithium-treated patients were determined.

CHAPTER III

EXPERIMENTAL APPROACH

III.1. Materials

III.1A. Reagents

Tris salts of guanosine 5'-triphosphate (GTP) and guanosine 5'-diphosphate (GDP), Tris salt of adenosine 3',5'-cyclic monophosphate (cAMP), adenosine 5'-triphosphate (ATP), free acid form of adenosine 5'-monophosphate (AMP), 2,3-diphosphoglycerate (DPG), Tris-base, DEAE-Sephadex A-50, Sephadex G-25, Dowex-50W resin, antifoaming reagent A, [Ethylenedinitrilo]tetraacetic acid (EDTA, 99%), Triton X-100, bovine serum albumin (BSA), DL-cysteine, DL-glyceraldehyde-3-phosphate, 5,5'-dithio-bis(2-nitrobenzoic acid) (DTNB), acetylthiocholine chloride, sodium pyrophosphate, sodium arsenate, and β-NAD were obtained from Sigma. Magnesium chloride ($MgCl_2$) hexahydrate, lithium chloride (LiCl), sodium chloride (NaCl), potassium chloride (KCl), tetramethylammonium hydroxide, trimethyl phosphate (TMP), trimethyl silane (TMS), dysprosium nitrate [$Dy(NO_3)_3$], sodium triphosphate (Na_5PPP), 4-(2-hydroxyethyl)-1-piperazineethanesulfonic acid (HEPES), ouabain, potassium cyanide (KCN), potassium ferricyanide [$K_3Fe(CN)_6$], choline chloride, glucose, sucrose, methanol (anhydrous), chloroform ($CHCl_3$), deuterated chloroform ($CDCl_3$), and D_2O (99.5%) were purchased from Aldrich. The lithium salt of inositol 1,4,5 triphosphate (IP_3)

was from Calbiochem, and the sodium salt was from Research Biochemicals Inc. The protein assay dye reagent was purchased from Bio-Rad Chem. Co., and Dextran T70 was from Pharmacia. All reagents were used without further purification except for Na_5PPP, which was recrystallized three times from 40% ethanol and then dried.

III.1B. Blood Samples

Fresh packed human red blood cells (RBCs) were obtained from a blood bank (Chicago Chapter of Life Source). Whole blood from eight male and two female bipolar patients who were receiving lithium carbonate, and from ten normal individuals were obtained from the Department of Psychiatry, Loyola University Medical Center, Maywood, IL. Each bipolar patient was matched to a normal individual according to gender, race, age, and weight. Patients were diagnosed according to the Diagnostic and Statistical Manual of Mental Disorders (DSM-IIIR, 1990) (94). The patients in this study received between 300 and 2100 mg of lithium carbonate per day and had been taking lithium for a minimum of 3 weeks or for as long as 17 years. Some patients were taking other psychotropic drugs, including phenothiazines and benzodiazepines. Because Na^+-Li^+ exchange rates are related to the occurrence of hypertension (95,96), blood pressure was measured at the time of blood drawing, and individuals suffering from hypertension were excluded from the study.

III.2. Sample Preparation

III.2A. Metal Nucleotide Complexes in Aqueous Solution

The NMR samples for studies of GTP, GDP, cAMP and AMP were buffered at pH 7.4 with Tris-Cl and tetramethylammonium hydroxide, and the ionic strength was adjusted with

Tris-Cl to 0.15 M. The temperature was maintained at 37 °C with the variable-temperature unit of the NMR spectrometer. We maintained the pH, ionic strength, and temperature in all of our experiments except for ^{13}C and ^{1}H NMR experiments, in which the ionic strength was not adjusted, because the Tris resonance overlapped with the nucleotide peaks. The nucleotide concentrations used were in the 5 mM to 10 mM range. The concentration of LiCl was varied from 5 mM to 150 mM, whereas the $MgCl_2$ concentration was in the range of 0.5 - 50 mM.

For the Li^+ and Mg^{2+} competition study using ^{7}Li relaxation measurements, IP_3 in the Li^+ form was dissolved in 99.5% D_2O at a concentration of 2 mM and the pH of the solution was adjusted to 7.4 with tetramethylammonium hydroxide. For ^{1}H and ^{31}P NMR chemical shift measurements, and the ^{7}Li relaxation study in Li^+-containing solution without Mg^{2+}, IP_3 in the Na^+ form was dissolved in 99.5% D_2O in the concentration range of 2 to 4 mM and the pH of 9.5 was obtained by titration with NaOH.

III.2B. Preparation of Shift Reagent

The K^+ form of the shift reagent dysprosium triphosphate, $Dy(PPP)_2^{7-}$, was prepared according to a published procedure (97) and contained 16% residual Na^+, as measured by atomic absorption (AA) spectrophotometry. K_5PPP was added dropwise to $Dy(NO_3)_3$ until complete formation of the complex, $Dy(PPP)_2^{7-}$, which is indicated by the clearance of the solution (75). The final ratio of $Dy(NO_3)_3$ and K_5PPP was approximately 1:2.5 to 1:3. K_5PPP was obtained by passage of recrystallized Na_5PPP through a Dowex-50W column saturated with KCl, then freeze-dried overnight.

III.2C. Preparation of Li^+-Loaded RBC

RBCs were washed at least three times in an isotonic choline wash solution (CWS) containing 100 mM choline chloride, 10 mM glucose, 85 mM sucrose, and 10 mM HEPES, pH 7.4. They were then centrifuged at 7000 g for 5 min at 4 °C in a Savant refrigerated centrifuge. Washed RBCs were separated from the plasma and buffy coat by aspiration and then kept at 4 °C before use. Li^+-loaded RBCs were prepared by incubating washed packed RBCs at 37 °C in an isotonic Li^+-loading medium containing 150 mM LiCl, 10 mM glucose, and 10 mM HEPES, pH 7.4. Two Li^+ loading conditions were applied; one being incubation of RBCs in a loading medium at 10% hematocrit for 20-75 minutes, the other being at 16% hematocrit for 3 hours (95). Under these loading conditions, the intracellular Li^+ concentrations were approximately 1 mM to 3.5 mM and 8 mM, respectively, as measured by AA. After incubation, the Li^+-loaded cells were washed five times using CWS by centrifugation at 7000 g for 5 min to remove extracellular Li^+.

III.2D. Preparation of Deoxy and Carbon Monoxy (CO) Li^+-Loaded RBC

Deoxygenated Li^+-loaded RBCs (deoxyRBC) were prepared by gentle passage of moist nitrogen gas for 30 min through a suspension of washed Li^+-loaded RBCs (intracellular $[Li^+]$ approximately 3.0 mM) in the isotonic CWS at 25% hematocrit. Carbon monoxygenated RBCs (CORBC) were prepared in a similar way by bubbling of the Li^+-loaded RBC suspensions for 30 min with CO gas. DeoxyRBC and CORBC were then washed twice with the isotonic choline medium and repacked; their oxygenation states were verified by examination of their ^{31}P NMR spectra (98,99).

III.2E. Preparation of Carbon Monoxy Hemoglobin, Deoxy Hemoglobin and Methemoglobin (100-102)

Packed RBCs were washed three times by centrifugation at 2000 g for 10 minutes, with isotonic buffer containing 150 mM NaCl and 5 mM sodium phosphate, pH 8 (PBS) at 4°C. The plasma and buffy coat were removed by aspiration. The washed cells were suspended in two volumes of cold distilled water, stirred gently for 30 minutes at 4 °C and restirred for another 30 minutes after addition of 1/4 volume of neutral saturated ammonium sulphate solution whose pH was adjusted to pH 7 with NaOH. A precipitate was formed and the Hb solution was separated by centrifugation for 10 minutes at 18,000 g. Then, it was dialyzed against 0.05 M Tris, 0.001 M KCN buffer pH 8.5 (adjusted with HCl); the buffer was changed at least three times every 4 hours till SO_4^{2-} was not present. Purification of hemoglobin was carried out by DEAE Sephadex A-50 chromatography. The column was prebalanced to pH 8.5 with Tris-CN buffer. Elution of the various hemoglobin fractions was carried out by using a pH gradient produced by a Tris-CN buffer (pH 8.5-7.2) with a flow rate of 20 mL per hour.

To obtain COHb and deoxy Hb, purified Hb was bubbled with carbon monoxide and N_2 for one hour, respectively. Deoxy Hb is very unstable and easily converted to the oxy form in air; all deoxy Hb experiments were therefore performed under N_2. MetHb was prepared by oxidation of the purified Hb solution (which was prepared as above except that the Tris buffer did not contain CN^-) with a slight excess of potassium ferricyanide and passage down a column of Sephadex G-25. The oxygenation states and concentrations of Hb were determined by optical spectroscopy (102,103). The COHb preparation was more than 97% pure with less than 3% metHb; the metHb preparation contained approximately 87% metHb,

10% hemichrome, and 3% oxyHb. The deoxyHb preparation contained less than 3% metHb. The Hb solution, containing 0.1% antifoaming reagent A, was purged with N_2 gas for 1 hr, to convert most of the Hb to the deoxy form. The viscosity of the Hb solutions was adjusted to 5 cP with glycerol.

III.2F. Preparation of Unsealed RBC Membrane (104)

Washed, packed RBCs were lysed in 20 to 40 volumes of hypotonic buffer, 5P8 (5 mM sodium phosphate, pH 8). The membrane suspension was washed by centrifugation at 22,000 g and 4 °C until the membrane was pale white. To avoid the possible interference of Na^+ in our Li^+ binding study, a modification of a literature method (104) was used to prepare unsealed RBC membranes; 5H8 (5 mM HEPES, pH 8) was used instead of 5P8.

III.2G. Preparation of IOV and ROV (104,105)

Unsealed membrane (1 mL) which was extracted in 5P8 buffer was diluted to 40 mL with 0.5P8 (0.5 mM sodium phosphate, pH 8). After 0.5 to 30 hours incubation on ice, the membranes were pelleted at 28,000 g for 30 minutes and resuspended to 1 mL in 0.5P8 by vortex mixing, passed 3-5 times through a No. 27 gauge needle to complete vesiculation. The vesicle suspension (2 mL) was overlayed on 3 mL of dextran barrier (4.46 g Dextran T-70 dissolved in 100 mL 0.5P8, pH 8.3-8.5, d=1.015 mg/mL). After centrifugation for 40 minutes at 29,000 g, the top band was collected and washed with 40 volumes of 0.5P8 buffer at 29,000 g for 30 minutes. The preparation of ROVs was similar to IOVs except for addition of 0.1 mM $MgSO_4$ (0.5P8-0.1Mg) after incubation on ice, and the incubation time was 1 to 1.5 hour.

The two types of vesicle preparations were characterized using sidedness assays of acetylcholinesterase and glyceraldehyde-3-phosphate dehydrogenase (G3PD) (104). The RBC membrane is asymmetric; the inner surface contains glyceraldehyde 3-phosphate dehydrogenase, while the acetylcholinesterase is at the outer surface. DTNB is used in the assay of acetylcholinesterase, which follows the appearance of free thiol groups during the hydrolysis of acetylthiocholine at 412 nm. The G3PD assay follows the reduction of NAD by glyceraldehyde-3-phosphate by the change in its absorbance at 340 nm.

III.2H. Preparation of Spectrin (106)

RBC membranes were prepared from 5P8 buffer as section III.2F. The membranes were then twice suspended in the extraction buffer, 0.3P7.6 (0.3 mM sodium phosphate, pH 7.6), followed by centrifugation at 20,000 g for 30 minutes, and incubation in 3 volumes of extraction buffer at 37 °C for 20 minutes. Finally, the fragmented membranes were pelleted by centrifugation at 80,000 g for 1 hour at 2 °C. Spectrin dimers, actins and other water-soluble proteins were in the supernatant. The products were characterized by SDS electrophoresis and the sample was found to contain 85 - 90% spectrin.

III.2I. Extraction and Analysis of Phospholipids

Extraction of phospholipids in RBC membranes for analysis by ^{31}P NMR spectroscopy was conducted as follows (107). RBC membrane (1 - 2 mL) was added slowly to methanol (17 mL) and mixed for 10 min. Chloroform (33 mL) was then added, and the sample was mixed for an additional 15 min. The resulting extract was filtered through a sintered glass funnel and washed with 50 mL of a chloroform/methanol (2:1) solvent mixture. The filtrate

was mixed thoroughly with 0.1 M KCl (in a 1:0.2 ratio) for removal of all non-lipid impurities. The bottom chloroform layer was separated with a separatory funnel fitted with a teflon stopper. The purified phospholipids were dried in a rotary evaporator at 30 °C, the lipid extract was suspended in solvent mixtures of deuterated chloroform/methanol/deuterated EDTA at ratios of 100:40:10 or 125:8:3. The deuterated EDTA reagent was prepared by titration of free acid EDTA with tetramethylammonium hydroxide to pH 6, followed by lyophilization and by solubilization in D_2O to a final concentration of 0.2 M. The sample was then placed in a 10 mm NMR tube and allowed to stand for a few minutes until the aqueous phase had separated. The spinning turbine was adjusted along the NMR tube so that only the chloroform phase was in the region of signal detection. Integration of the ^{31}P NMR resonances was conducted using the software provided by the NMR manufacturer. Each ^{31}P NMR resonance in the phospholipid extract of RBC membrane was assigned either by comparison to spectra of pure phospholipid standards that were recorded alone or by spiking of the extract samples with known amounts of pure phospholipids. The ^{31}P NMR spectra were run at 27 °C and locked on the deuterium resonance of deuterated chloroform, which ensured magnetic field stabilization. Proton decoupling was applied only during data acquisition with WALTZ-16 decoupling sequence, as previously reported (108).

III.3. Data Analysis

III.3A. Determination of Metal-Nucleotide Binding Constants from ^{31}P NMR Chemical Shifts

Three different models were applied, which assumed the formation of either 1:1 or 2:1 species alone or a mixture of 1:1 and 2:1 species. For the first model, which assumed 1:1

stoichiometry for the Li^+ complex of GTP, we used the following equations to calculate the binding constant, K_{LiGTP}, for the LiGTP complex:

$$\delta_{obs} = x_{GTP}\delta_{GTP} + x_{LiGTP}\delta_{LiGTP}, \qquad (12)$$

$$[Li^+]_{eq} + K_{LiGTP}[Li^+]_{eq}[GTP]_{eq} - [Li^+]_o = 0, \qquad (13)$$

where δ_{GTP} and δ_{LiGTP}, represent the limiting chemical shifts for the free GTP and LiGTP species, and δ_{obs} represents the observed chemical shift in GTP solutions containing Li^+ in the 0 to 100 mM concentration range; x_{GTP} and x_{LiGTP} are the mole fractions for the same species; and the subscripts eq and o denote the equilibrium and starting Li^+ concentrations, respectively. Equations similar to (12) and (13) were used to calculate the binding constants of 1:1 Li^+ complexes of GDP, or of 1:1 Mg^{2+} complexes of GTP and GDP. For the second model, which assumed 2:1 stoichiometry for the Li^+ complex of GTP, we used equations (14) and (15) instead to calculate the binding constant, β_{Li_2GTP}, for Li_2GTP species:

$$\delta_{obs} = x_{GTP}\delta_{GTP} + x_{Li_2GTP}\delta_{Li_2GTP}, \qquad (14)$$

$$[Li^+]_{eq} + 2\beta_{Li_2GTP}[Li^+]_{eq}[GTP]_{eq} - [Li^+]_o = 0, \qquad (15)$$

where the symbols have the same meaning as above. We used equations similar to (14) and (15) to calculate the binding constants of 2:1 Li^+ complexes of GDP, or of 2:1 Mg^{2+} complexes of GTP and GDP. The third model, which assumed a mixture of 1:1 and 2:1 species, was based on equations which were combinations of equations (12) and (14) or of equations (13) and (15).

III.3B. ^{7}Li NMR Determination of Li^+ Concentration, and Time Constants for Li^+ Uptake in RBC Suspensions

Intra- and extracellular Li^+ can be separated by ^{7}Li NMR by using a shift reagent. The

areas under the intracellular ^7Li NMR resonance curve were measured and were converted into intracellular Li^+ concentrations at a certain time, t, $[Li^+]_t$, with the equation

$$[Li^+]_t = [Li^+]_o \times (1 - Ht)/[Ht \times (1 + A_{out}/A_{in})], \qquad (16)$$

where A_{in} and A_{out} are the peak areas of the intra- and extracellular $^7Li^+$ NMR resonances at time t, $[Li^+]_o$ is the known starting extracellular Li^+ concentration, and Ht is the hematocrit of the RBC suspension. We obtained relative peak areas by means of the integration routines included in the software for the Varian VXR-300 NMR spectrometer. The equation above assumes 100% visibility for the intracellular ^7Li NMR signal. The visibility factor for ^7Li NMR resonances in RBC suspensions is still a matter of controversy (86). Because the visibility of intra- and extracellular ^7Li NMR signals in RBC suspensions is the same (109), however, this factor does not affect the conclusions from our Li^+ uptake studies.

We calculated the time constants k and $[Li^+]^\infty_{in}$, the limiting intracellular Li^+ concentrations after a steady state was reached, by fitting the ^7Li NMR peak areas at several incubation times t to the equation

$$[Li^+]_t = [Li^+]^\infty_{in} \times [1 - \exp(-t/k)] \qquad (17)$$

by means of nonlinear least-squares approximations.

III.3C. Calculation of Binding Constants to RBC Membrane and ATP form ^7Li T_1 Values

Li^+ binding constants (K_b) to the unsealed RBC membranes were determined from James-Noggle plots (110) of ^7Li T_1 values observed in RBC membrane suspensions titrated with Li^+ at increasing concentrations. A two-state model (free Li^+ and Li^+ bound to the RBC membrane) undergoing fast chemical exchange in the NMR time scale was assumed when

we calculated the Li^+ K_b values from the following equations (110-112):

$$R_1 = 1/T_1 = R_{1f}X_f + R_{1b}X_b \quad (18)$$

$$(\Delta R)^{-1} = (R_1 - R_{1f})^{-1} = K_b^{-1}\{[B](R_{1b} - R_{1f})\}^{-1} + [Li^+]\{[B](R_{1b} - R_{1f})\}^{-1} \quad (19)$$

where R_1, R_{1f}, and R_{1b} are the observed, free, and bound relaxation rates of Li^+ ions in RBC membrane samples, X_f and X_b are the mole fractions of free and bound Li^+, and $[Li^+]$ and [B] are the total concentrations of Li^+ and membrane binding sites. Equation (19) assumes one to one stoichiometry for binding at a microscopic level when $[B] << [Li^+]$ (110), which is valid under our experimental conditions. The K_b values were obtained from the slope/intercept ratios of linear James-Noggle plots of $(\Delta R)^{-1}$ against $[Li^+]$.

In the Li^+ and Mg^{2+} competition study, the binding constants obtained from equation 19 are apparent Li^+ binding constants, K_{ap}, in the presence of Mg^{2+}. Li^+ and Mg^{2+} binding constants were then obtained from the equation:

$$1/K_{ap} = 1/K_{Li\text{-}M}\,(1 + K_{Mg\text{-}M}[Mg^{2+}]) \quad (20)$$

where $K_{Li\text{-}M}$, $K_{Mg\text{-}M}$ are the Li^+ and Mg^{2+} binding constants, and $[Mg^{2+}]$ is the total Mg^{2+} concentration. $K_{Mg\text{-}M}$ was obtained from the ratio of slope and intercept using a plot of $1/K_{ap}$ versus Mg^{2+} concentration. The reciprocal of the y-intercept was the Li^+ binding constant.

Li^+ and Mg^{2+} binding constants to ATP were generated as described in section III.3A for the GTP/GDP system. Three different models were considered for Li^+ binding. Instead of ^{31}P chemical shifts (δ), we used ^7Li spin-lattice relaxation rates (R) as parameters, in which R was the reciprocal of T_1. The conditional binding constants of Li^+ ($K'_{Li\text{-}M}$) and Mg^{2+} (K'_{Mg-M}) to RBC membranes in presence of ATP were obtained by the following equations:

$$K'_{Mg\text{-}M} = K_{Mg\text{-}M}/(1 + [ATP]_f K_{MgATP}) \quad (21)$$

$$K'_{Li\text{-}M} = K_{Li\text{-}M}/(1 + [ATP]_f K_{LiATP} + 2[ATP]_f[Li^+]_f \beta_{Li_2ATP}) \quad (22)$$

where $[ATP]_f$ and $[Li^+]_f$ are the free concentrations of ATP and Li^+, respectively.

III.3D. Protein Concentration Determination

Protein concentration was determined by the "Bradford Assay" method at 595 nm (113). The dye reagent (purchased from Bio-Rad Chem. Co.) was diluted five-fold in deionized water and filtered through a Whatman No. 1 paper. Standards of protein were prepared from bovine serum albumin (BSA).

III.3E. Statistical Analysis (114)

The statistical significance of the differences between bipolar patients receiving lithium carbonate and normal individuals for the RBC Li^+ transport and binding parameters, and for the phospholipid composition of the RBC membrane, were analyzed by use of a paired Student's t-test. Correlation coefficients among Li^+ transport and binding parameters and phospholipid composition were obtained by using a Pearson product-moment correlation. Correlation coefficients ≥ 0.4 were considered significant ($p \leq 0.05$) for a sample size of 10.

III.4. Instrumentation

III.4A. Nuclear Magnetic Resonance Spectrometer

^1H, ^{13}C, ^{31}P and ^7Li NMR measurements were obtained at 300, 74.6, 121.4 and 116.5 MHz, respectively, on a Varian VXR-300 NMR spectrometer using a multinuclear probe. The spin rate with the 10 mm probe was 16 Hz, and 20 Hz with 5 mm probe. All RBC samples were run without spinning to avoid cell settling. Spin-lattice relaxation time (T_1)

measurements were performed by the inversion recovery method (180°-τ-90° pulse sequence); spin-spin relaxation time (T_2) measurements were conducted by using the Carl-Purcell-Meiboom-Gill sequence [90°-(τ-180°-τ)$_n$]. The spacing between pulse sequence was at least $5T_1$ for both methods. Table 1 shows the NMR parameters that were used.

III.4B. Atomic Absorption Spectrophotometer

A Perkin Elmer 5000 spectrometer equipped with a flame source and a graphite furnace was used for AA studies. Li^+ measurements were performed at a wavelength of 607.8 nm and a slit width of 1.4 nm. Acetylene and compressed air were used as fuel and oxidant, respectively. The flow rate of fuel to oxidant was 45/50.

III.4C. UV/Vis Spectrophotometer

All studies were conducted on an IBM UV/Vis 9420 spectrometer. The protein concentration was determined at 595 nm by using the "Bradford Assay" (113); oxygenation stage and concentration of hemoglobin were determined in the range of 400 to 700 nm (102,103).

III.4D. Centrifuge

A Savant refrigerated centrifuge, model HSC 10000, was used for general blood processing. Membranes were prepared by using a Beckman J2-21 refrigerated centrifuge equipped with JA-14 and JA-20 fixed angle rotors. A Sorvall refrigerated ultra centrifuge, model OTD 65B, equipped with a T865 rotor, was used for the spectrin preparation.

Table 1. NMR Parameters of Nuclei Investigated at 7.0 T.

	^{1}H	^{13}C	^{31}P	^{7}Li
Frequency /MHz	300.0	74.6	121.4	116.5
SW /KHz	10	16	10	4.5
AT /s	3.8	1.3	1.5	1.2
PW 90 /μs	20	17.5	12	27[a], 33[b], 12[c]
Flip angle /degree	60	45	45	45
Delay /s	0	1 - 3	0 - 4	30

[a]90° pulse width in low ionic strength solutions (0 - 20 mM) in the 10 mm probe. [b]90° pulse width in high ionic strength solutions (150 mM) in the 10 mm probe. [c]90° pulse width in low ionic strength solutions (0 - 20 mM) in the 5 mm probe.

III.4E. Osmometer

The osmolarity of all RBC suspension media was checked with a Wescor vapor pressure osmometer model 5500 and adjusted to 300 $\pm$ 10 mosM with sucrose and distilled water.

III.4F. Hemofuge

Hematocrits (cell volume percentage) were measured using an IEC model MB IM116 hemofuge.

III.4G. Lyophilizer

Recrystalizations of K_5PPP and EDTA-$N(CH_3)_4OH$ salts were performed on a FDX Flexi-Dry 1-54 freezer drier after freezing.

III.4H. Viscometer

The viscosities of Hb, DPG and spectrin were measured with a Brookfied Cone Plate Viscometer, equipped with a 8° CP-40 cone, at 12 rpm; they were adjusted with glycerol to 5 cP to correspond to the viscosity inside RBCs (115).

CHAPTER IV

RESULTS

IV.1. Competition Between Li^+ and Mg^{2+} for Substrates of Second Messenger Systems, and RBC Membrane

IV.1A. Competition Between Li^+ and Mg^{2+} for GDP and GTP in Aqueous Solution

Figure 5 depicts the structure of GTP. We investigated whether metal ion binding to GTP and GDP takes place via the base, sugar, or phosphate moiety. We probed metal ion binding to the base and sugar domains by using ^1H and ^{13}C NMR, whereas we studied metal ion binding to the phosphate groups by ^{31}P NMR. We also studied competition between Li^+ and Mg^{2+} ions for binding sites in guanine nucleotides by using ^7Li NMR relaxation measurements and ^{31}P NMR chemical shifts.

IV.1A.a. $^7Li^+$ NMR T_1 Measurements

Figure 6 shows the T_1 values for ^7Li in solutions of GTP or GDP containing both Li^+ and Mg^{2+} ions. Li^+ ions are in fast exchange on the ^7Li NMR time scale; the observed ^7Li chemical shift and T_1 values therefore represent the weighted average of free and bound Li^+ ions. Because the $^7Li^+$ nucleus has a narrow chemical shift range (76), the ^7Li NMR chemical shifts were not sensitive to Li^+ binding to nucleotides. In contrast, ^7Li T_1 relaxation times are sensitive to motion. Free nuclei have long T_1 values, whereas those that are tightly bound,

Figure 5. Structure of GTP. The primed symbols indicate the numbering of the sugar atoms, and the unprimed symbols the numbering of the base atoms. The positions of phosphate groups are denoted by α, β, and γ. In GDP, the γ phosphate is not present.

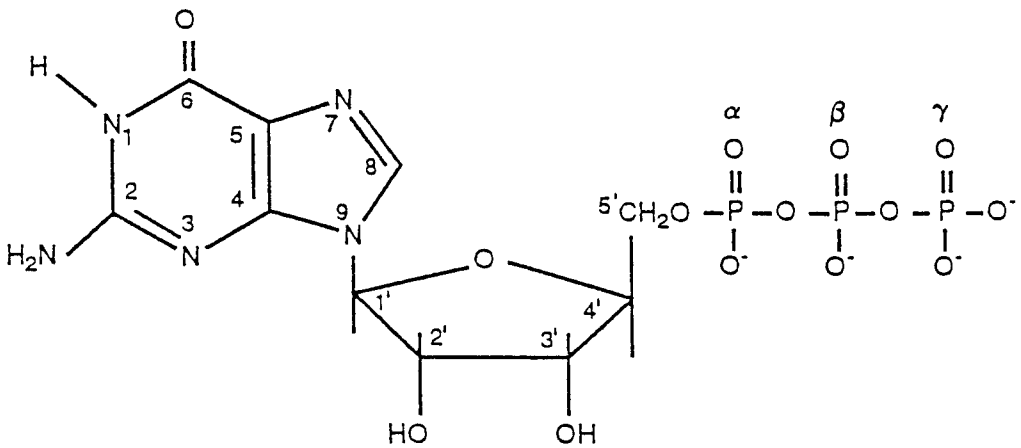
O
H
N1
6
5
7
N
8
2
4
9
N
3
N
H2N
O
1'
4'
2'
3'
HO
OH
5'CH2O
α
β
γ
P
O-

Figure 6. ^{7}Li T_1 Values for Li-GTP (open symbols) and Li-GDP (closed symbols) in the Presence of Increasing Concentrations of Mg^{2+}. The Li^{+} concentration was 5.0 mM in all samples. The nucleotide concentrations were 3.0 mM (circles), 5.0 mM (squares), and 7.0 mM (triangles). Each value is an average of two readings made on separately prepared samples.

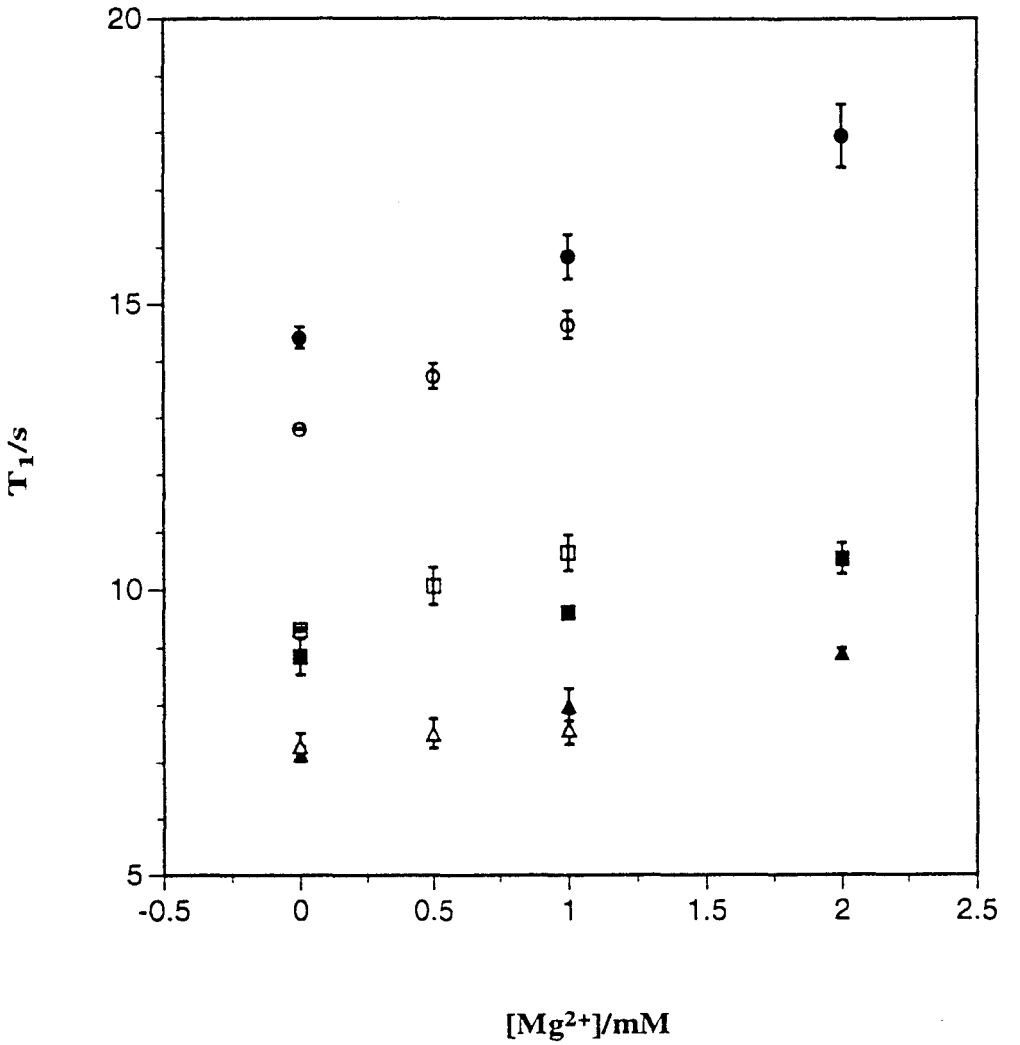
20
15
10
5
-0.5
0
0.5
1
1.5
2
2.5
T1/s
[Mg2+]/mM

if visible by ^{7}Li NMR, have relatively short T_1 values (116). The T_1 values for ^{7}Li decreased in the presence of increasing concentrations of GTP and GDP (Figure 6). In the presence of increasing concentrations of Mg^{2+}, the ^{7}Li T_1 values increased.

IV.1A.b. ^{13}C and ^{1}H NMR Chemical Shift Measurements

Figures 7 and 8 are ^{13}C and ^{1}H NMR spectra of GTP, respectively. Table 2 shows ^{1}H and ^{13}C NMR chemical shifts of the base and sugar moieties of GTP and GDP in the absence and presence of saturating amounts of Li^{+} and Mg^{2+}. The H_8 proton resonance of the base and the $H_{1'}$ proton resonance of the sugar of GTP and GDP showed almost no changes in chemical shifts upon addition of either excess LiCl or excess $MgCl_2$. No other proton resonances for GTP or GDP were observed because the large water envelope and line broadening was induced by rapid exchange between NH or OH protons in the base and sugar domains and the solvent protons. The ^{13}C chemical shift changes that occurred upon addition of saturating amounts of LiCl or $MgCl_2$ were also very small.

IV.1A.c. Measurements of ^{31}P NMR Chemical Shifts and Metal Ion Binding Constants

Figure 9 shows the ^{31}P NMR spectra of GTP. The changes in the ^{31}P NMR chemical shifts indicate that metal ions bind to the phosphate moiety of nucleotides. The chemical shift of the γ-phosphate resonance, to a greater extent that of the β-phosphate, moved downfield upon addition of metal ions. Very small ^{31}P chemical shift changes were observed for the α-phosphate resonance. The chemical shift separation between the α- and β-phosphate resonances of GTP ($\delta_{\alpha\beta}$) indicates the state of metal ion complexation of GTP. The value of $\delta_{\alpha\beta}$ varies from its maximum value of 10.93 ppm in free GTP (Fig. 9A) to its minimum value

Figure 7. ^{13}C NMR Spectrum of GTP. The GTP concentration was 10 mM. All experiments were conducted at pH 7.4 and 37 °C. Chemical shifts were referenced relative to an external standard of tetramethylsilane (TMS). Refer to figure 5 for structure assignments.

C6
C2
C4
C8
C5
C1'
C4'
C3'
C2'
C5'
160
140
120
100
80
60
40
20
0 PPM

Figure 8. ^{1}H NMR Spectrum of GTP. (A) with water suppression; (B) without water suppression, and at 37 °C. The GTP concentration was 10 mM. All samples were prepared in 95% D_2O, adjusted to pH 7.4. The presaturation technique was employed to suppress the water resonance in (A). Chemical shifts were referenced relative to an internal reference of t-butanol. Refer to figure 5 for structure assignments.

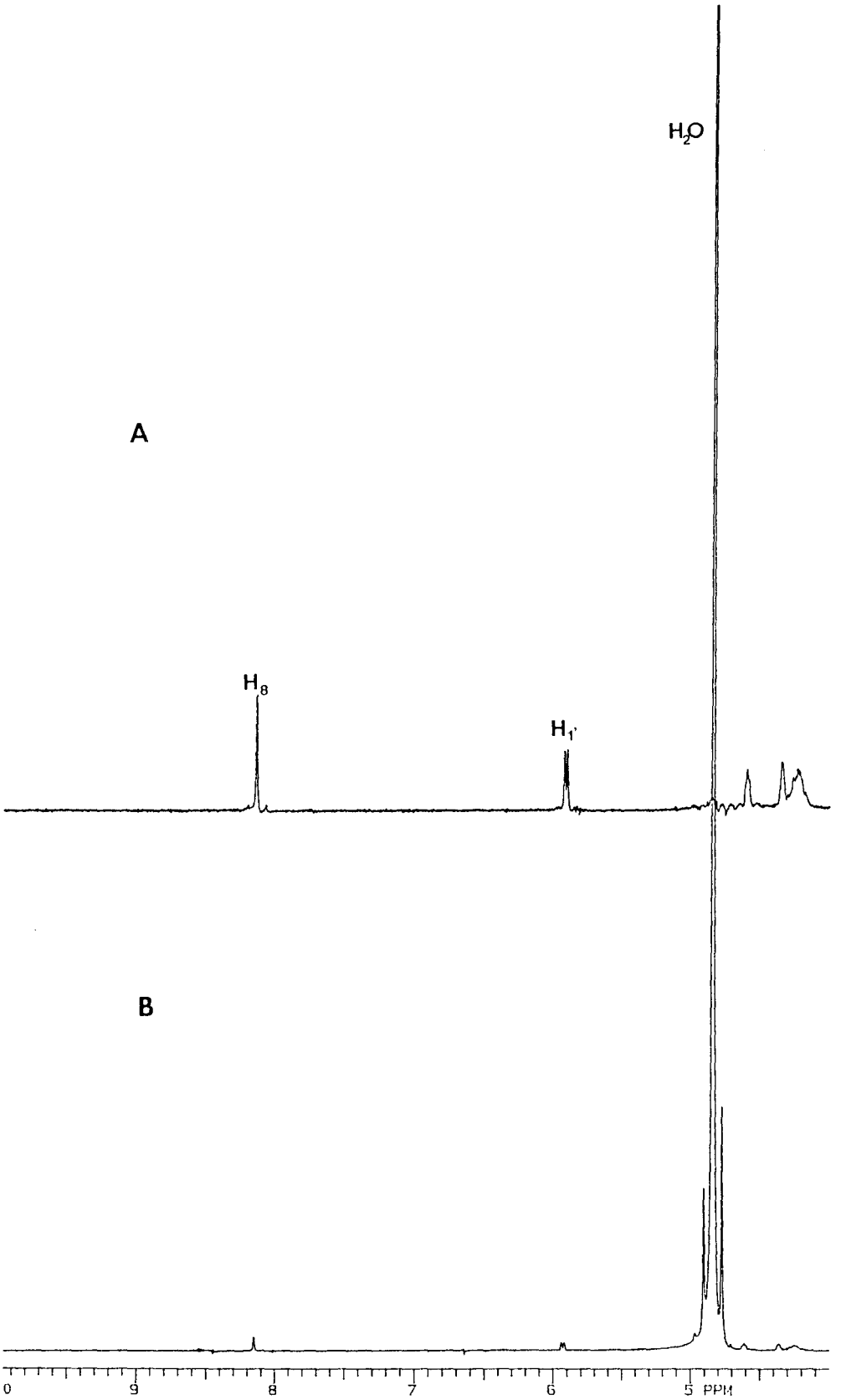
H2O
A
H8
H1'
B
0
9
8
7
6
5 PPM

Table 2. ^{1}H and ^{13}C NMR Chemical Shifts (in ppm) of GTP and GDP [a,b]

	GTP			GDP		
Resonance	No metals	w/ Li^+	w/ Mg^{2+}	No Metals	w/ Li^+	w/ Mg^{2+}
H_8	8.12	8.11	8.12	8.11	8.15	8.12
$H_{1'}$	5.90	5.90	5.90	5.90	5.93	5.92
C_2	157.7	157.7	157.7	157.7	157.7	157.6
C_4	155.4	155.3	155.4	155.2	155.3	155.4
C_5	120.0	119.8	119.9	120.0	120.1	119.8
C_6	162.6	162.6	162.7	162.8	162.8	162.6
C_8	141.5	141.4	141.4	141.5	141.4	141.3
$C_{1'}$	90.5	90.6	90.5	90.7	90.6	90.3
$C_{2'}$	74.2	74.1	74.0	73.9	74.1	74.2
$C_{3'}$	77.3	77.7	77.4	77.4	77.4	77.5
$C_{4'}$	87.8	87.1	87.4	87.5	87.5	87.4
$C_{5'}$	59.1	58.9	59.2	59.0	58.5	58.9

[a]Primed resonances are due to sugar protons or carbons, whereas unprimed resonances are due to atoms in the guanine base. [b]The concentration of nucleotide was 10 mM, and the concentrations of LiCl and $MgCl_2$ were 150 mM and 50 mM, respectively. Each value is an average of two readings on separately prepared samples. The errors are less than 0.02 ppm for ^{1}H NMR and less than 0.5 ppm for ^{13}C NMR.

Figure 9. ^{31}P NMR Spectra of GTP. (A) 5.0 mM Tris-GTP, (B) 5.0 mM Tris-GTP with 100 mM LiCl, (C) 5.0 mM Tris-GTP with 100 mM LiCl and 1.5 mM $MgCl_2$, and (D) 5.0 mM GTP with 5.0 mM $MgCl_2$. Ionic strength, pH, and temperature were maintained at 0.15 M, 7.4, and 37 °C, respectively. No line broadening was used, and trimethyl phosphate served as the external reference.

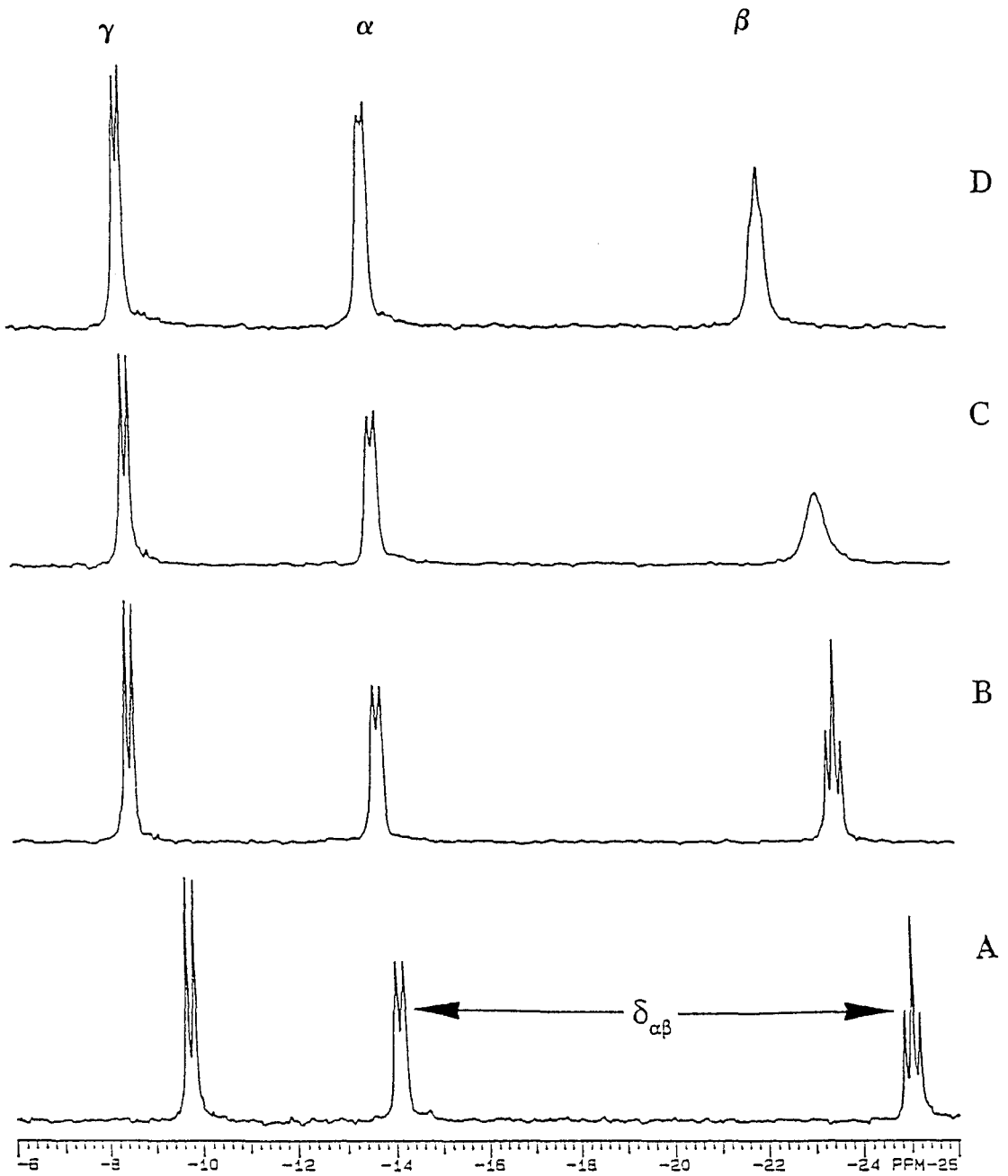
γ
α
β
D
C
B
A
$\delta_{\alpha\beta}$
-6
-8
-10
-12
-14
-16
-18
-20
-22
-24
PPM-26

of 8.59 ppm in Mg^{2+}-saturated GTP (Fig. 9D). The values of $\delta_{\alpha\beta}$ for Li^+-saturated GTP (9.84 ppm; Fig. 9B) or GTP in the presence of a mixture of Li^+ and Mg^{2+} ions (9.39 ppm; Fig. 9C) are intermediate between those observed for free GTP and for Mg^{2+}-saturated GTP alone.

We fitted the ^{31}P NMR chemical shifts for the phosphate resonances of GTP and GDP (Tables 3 and 4), as measured in the absence or presence of LiCl or $MgCl_2$ alone and for LiCl/$MgCl_2$ mixtures, to three different models (see III.3A.) to generate binding constants (Tables 5 and 6). Because of the lower charge and correspondingly lower affinity of Li^+ relative to Mg^{2+} for both GTP and GDP, we used larger concentrations of Li^+ (0 to 100 mM) than of Mg^{2+} (0 to 15 mM) in the Li^+ and Mg^{2+} titration of both nucleotides. In ion competition experiments, the Mg^{2+} concentration was kept constant at 1.5 mM for GTP and at 3.0 mM for GDP; the Li^+ concentration ranged from 0 to 100 mM. Under these conditions, we observed appreciable changes in ^{31}P chemical shifts in individual nucleotide titration with Li^+ or Mg^{2+} alone and in ion competition experiments.

IV.1B. Interactions of Li^+ and Mg^{2+} with cAMP, AMP and IP_3

Figure 10 shows the structures of cAMP, AMP and IP_3. A similar experimental approach to that used for GTP and GDP was applied to these three substrates.

^7Li NMR relaxation measurements (Table 7) showed that the T_1 values remained constant with increasing concentrations of either cAMP or AMP, indicating no interaction between Li^+ and AMP or cAMP under these conditions; the T_1 values observed were similar to those of LiCl in the absence of nucleotides. Very small changes were observed in the ^{13}C chemical shifts of AMP and cAMP upon addition of either saturating concentrations of Li^+

Table 3. ^{31}P NMR Chemical Shifts of GTP with Various Li^+ and Mg^{2+} Concentrations (n=2)[a]

$[Mg^{2+}]$/mM	$[Li^+]$/mM	δ_α/ppm	δ_β/ppm	δ_γ/ppm
0	0	-14.19 ± 0.03	-25.12 ± 0.06	-9.80 ± 0.09
0	15	-14.10 ± 0.04	-24.80 ± 0.04	-9.60 ± 0.04
0	30	-14.06 ± 0.05	-24.49 ± 0.07	-9.47 ± 0.04
0	45	-13.98 ± 0.01	-24.31 ± 0.05	-9.26 ± 0.05
0	60	-13.92 ± 0.01	-24.07 ± 0.05	-9.05 ± 0.02
0	75	-13.86 ± 0.03	-23.89 ± 0.05	-8.87 ± 0.02
0	100	-13.80 ± 0.03	-23.64 ± 0.07	-8.68 ± 0.06
1.0	0	-14.10 ± 0.01	-24.60 ± 0.01	-9.66 ± 0.01
1.5	0	-14.04 ± 0.02	-24.47 ± 0.06	-9.49 ± 0.08
2.0	0	-13.98 ± 0.01	-24.04 ± 0.01	-9.36 ± 0.02
2.5	0	-13.90 ± 0.02	-23.57 ± 0.08	-9.17 ± 0.01
3.0	0	-13.80 ± 0.01	-23.24 ± 0.02	-8.93 ± 0.01
3.5	0	-13.79 ± 0.01	-22.98 ± 0.06	-8.88 ± 0.02
4.0	0	-13.70 ± 0.00	-22.49 ± 0.01	-8.68 ± 0.01
5.0	0	-13.64 ± 0.01	-22.23 ± 0.03	-8.50 ± 0.02
15	0	-13.79 ± 0.01	-22.15 ± 0.00	-8.70 ± 0.03
1.5	15	-13.94 ± 0.01	-23.96 ± 0.02	-9.23 ± 0.02
1.5	30	-13.89 ± 0.01	-23.80 ± 0.05	-9.10 ± 0.00
1.5	45	-13.85 ± 0.02	-23.57 ± 0.07	-8.99 ± 0.05
1.5	60	-13.81 ± 0.01	-23.39 ± 0.07	-8.86 ± 0.01
1.5	75	-13.77 ± 0.01	-23.27 ± 0.02	-8.73 ± 0.01
1.5	100	-13.72 ± 0.02	-23.11 ± 0.02	-8.59 ± 0.01

[a]GTP concentration, ionic strength, pH, and temperature were maintained at 5 mM, 0.15 M, 7.4, and 37 °C, respectively; trimethyl phosphate served as the external reference.

Table 4. ^{31}P NMR Chemical Shifts of GDP with Various Li^+ and Mg^{2+} Concentrations (n=2)[a]

$[Mg^{2+}]$/mM	$[Li^+]$/mM	δ_α/ppm	δ_β/ppm
0	0	-13.77 ± 0.04	-9.78 ± 0.05
0	15	-13.53 ± 0.02	-9.57 ± 0.03
0	30	-13.47 ± 0.05	-9.54 ± 0.02
0	45	-13.26 ± 0.01	-9.37 ± 0.07
0	60	-13.22 ± 0.04	-9.31 ± 0.05
0	75	-13.10 ± 0.02	-9.25 ± 0.06
0	100	-12.93 ± 0.04	-9.00 ± 0.01
1.0	0	-13.62 ± 0.00	-9.69 ± 0.00
1.5	0	-13.57 ± 0.01	-9.63 ± 0.01
2.0	0	-13.53 ± 0.01	-9.59 ± 0.01
2.5	0	-13.47 ± 0.02	-9.50 ± 0.01
3.0	0	-13.42 ± 0.02	-9.41 ± 0.04
3.5	0	-13.37 ± 0.02	-9.40 ± 0.02
4.0	0	-13.33 ± 0.01	-9.34 ± 0.00
5.0	0	-13.24 ± 0.02	-9.26 ± 0.02
15	0	-13.00 ± 0.01	-9.04 ± 0.01
30	0	-12.96 ± 0.02	-9.12 ± 0.02
3.0	15	-13.34 ± 0.00	-9.32 ± 0.05
3.0	30	-13.27 ± 0.01	-9.27 ± 0.01
3.0	45	-13.19 ± 0.01	-9.16 ± 0.01
3.0	60	-13.11 ± 0.01	-9.06 ± 0.03
3.0	75	-13.04 ± 0.01	-9.01 ± 0.03
3.0	100	-12.92 ± 0.01	-8.91 ± 0.00

[a]GDP concentration was 5 mM; other conditions are the same as for Table 3.

Table 5. ^{31}P NMR Chemical Shift Data Analysis in the Presence of LiCl or $MgCl_2$ Alone

	GTP			GDP	
	α	β	γ	α	β
A) LiCl Alone[a]					
1:1 species only					
K (M^{-1})	4	6	2	6	3
δ_{theor}[b]	-12.76	-21.18	-0.50	-11.64	-6.44
Σ^2[c]	0.0006	0.0013	0.0054[g]	0.0078	0.0118[g]
2:1 species only					
K (M^{-2})	535	734	372	75	48
δ_{theor}[b]	-13.73	-23.48	-8.34	-12.87	-8.90
Σ^2[c]	0.0024	0.0326	0.0104	0.0255	0.0311
1:1 and 2:1 species					
1:1 K (M^{-1})	253	174	166	394	414
2:1 K (M^{-2})	1981	6217	1990	408	357
1:1 δ_{theor}[b]	-14.01	-25.14	-9.58	-13.58	-9.65
2:1 δ_{theor}[b]	-13.32	-22.50	-7.69	-6.11	-1.39
Σ^2[c]	0.0001	0.0001	0.0010	0.0053[g]	0.0084[g]
δ_{exp}[d]	-13.80	-23.64	-8.68	-12.93	-9.00
B) $MgCl_2$ Alone[e]					
1:1 species					
K (M^{-1})	20,000	20,000	20,000	10,000	10,000
δ_{thoer}[b]	-13.58	-22.02	-8.45	-13.06	-9.13
δ_{exp}[f]	-13.64	-22.23	-8.50	-13.24	-9.26
Σ^2[c]	0.0035	0.1100	0.0378	0.0007	0.0047

Footnote for Table 5:

[a]Binding constants for Li-GTP and Li-GDP calculated from ^{31}P NMR chemical shift data. The nucleotide concentration was 5 mM, and the LiCl concentrations ranged from 0 to 100 mM. [b]δ_{theor} values were calculated from equations similar to (12) through (15). [c]Σ^2 values are the sums of squared deviations. [d]δ_{exp} were measured from ^{31}P NMR spectra for $[Li^+]$ = 100 mM. [e]Binding constants for Mg-GTP and Mg-GDP were calculated from ^{31}P NMR chemical shift data. The nucleotide concentration was 5 mM, and the $MgCl_2$ concentrations ranged from 0 to 15 mM. [f]δ_{exp} values were measured from ^{31}P NMR spectra for $[Mg^{2+}]$ = 5.0 mM. [g]No convergence was found.

Table 6. ^{31}P NMR Chemical Shift Data Analysis in the Presence of Both LiCl and $MgCl_2$[a]

	GTP			GDP	
	α	β	γ	α	β
A) 1:1 species only					
K (M^{-1})	68	49	67	2	4
δ_{theor}[b]	-13.76	-23.62	-8.62	-6.58	-5.49
Σ^2[c]	0.0810	0.1496	0.1120	0.0002[e]	0.0012[e]
B) 2:1 species only					
K (M^{-2})	1250	799	1521	12940	645
δ_{theor}[b]	-13.76	-23.62	-8.62	-13.37	-8.48
Σ^2[c]	0.1020	0.8320	0.0820	0.4870	0.0045
C) 1:1 and 2:1 species					
1:1 K (M^{-1})	15	1.4×10^{-6}	1.8×10^{-7}	542	2683
2:1 K (M^{-2})	712	1666	805	3327	21640
1:1 δ_{theor}[b]	-14.02	-24.53	-9.40	-13.56	-9.50
2:1 δ_{theor}[b]	-13.71	-23.65	-8.65	-11.61	-8.06
Σ^2[c]	0.0013	0.0530	0.0177	0.0000	0.0008
δ_{exp}[d]	-13.80	-23.64	-8.68	-12.92	-8.91

[a]For the competition experiments, the nucleotide was 5.0 mM, and the Li^+ concentration ranged from 0 to 100 mM. The Mg^{2+} concentrations in the GTP and GDP experiments were 1.5 mM and 3.0 mM, respectively. [b]δ_{theor} values were calculated from equations similar to (12) through (15). K_{MgGTP} and K_{MgGDP} were fixed at 2×10^4 M^{-1} and 1×10^4 M^{-1}, respectively. [c]Σ^2 values are the corresponding sums of squared deviations. [d]δ_{exp} were measured from ^{31}P NMR spectra for $[Li^+]$ = 100 mM, and $[Mg^{2+}]$ = 1.5 mM for GTP, and $[Mg^{2+}]$ = 3.0 mM for GDP. [e]No convergence was found.

Figure 10. Structures of cAMP, AMP and IP_3. In AMP and cAMP, the primed symbols indicate the numbering of the sugar atoms, and the unprimed symbols the numbering of the base atoms.

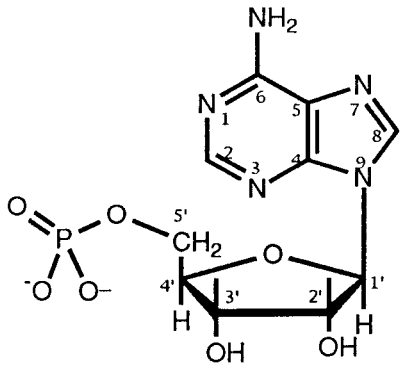

AMP

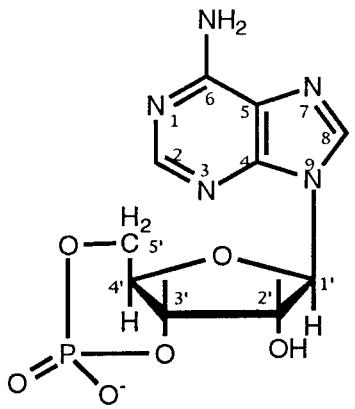

cAMP

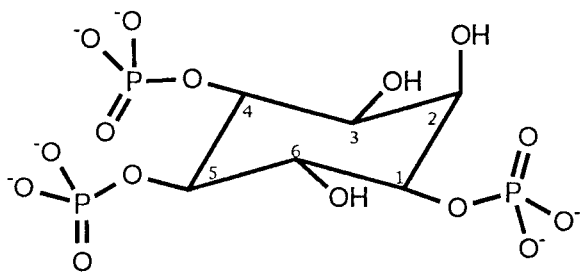

IP_3

Table 7. ^{7}Li T_1 Values of cAMP and AMP (n=2)[a]

[cAMP]/mM	[AMP]/mM	$[Li^+]$/mM	T_1/s
0	0	5	24.5 ± 1.0
5	0	5	24.3 ± 0.9
7	0	5	26.7 ± 1.8
10	0	5	25.8 ± 1.0
10	0	2	25.5 ± 0.2
0	5	5	24.3 ± 0.3
0	10	5	25.1 ± 0.9
0	10	2	25.1 ± 1.0

[a]Ionic strength, pH, and temperature were maintained at 0.15 M, 7.4, and 37 °C, respectively.

or Mg^{2+} (Table 8). No significant changes in the ^{31}P chemical shifts were observed, except in 5 mM AMP solution containing 50 mM Mg^{2+}, where the phosphate resonance experienced a 0.4 ppm upfield shift (Table 9). Two resonances separated by 21 Hz were observed in the ^{31}P spectrum of cAMP but not in that of AMP. This is due to a particular spin-spin coupling pattern mainly induced by the nonequivalence of the two protons at the 5' position of the sugar moiety whose couplings to phosphorus are very different (117).

Table 10 and Figure 11 depict the ^{7}Li T_1 values of a solution containing 2 mM IP_3 and 2 mM to 1.4 M Li^+, and a solution of 6 mM Li^+ and 2 mM IP_3 and various concentrations of Mg^{2+}, respectively. As the amount of Li^+ increased, T_1 values increased due to the increment in the fraction of free Li^+ in solution; however, for a fixed Li^+ concentration, as the amount of Mg^{2+} in solution increased, the T_1 values increased which indicated that Mg^{2+} replaced Li^+ bound to IP_3.

Figure 12 shows ^{31}P and ^{1}H NMR spectra of IP_3. The inorganic phosphate (P_i) resonance in the ^{31}P NMR spectrum is due to the hydrolysis of IP_3, which was 4% of the total amount. Table 11 shows ^{1}H chemical shifts of the inositol moiety in the absence and presence of Li^+ and Mg^{2+}. The resonances correspond to -CH- groups; -OH groups can not be resolved because they exchanged rapidly with water. Since phosphate groups were in an intermediate state of exchange at neutral pH, a pH value of 9.5 was used in both ^{31}P NMR and ^{1}H NMR spectra of IP_3 (118). Almost no changes in the ^{1}H chemical shifts of IP_3 were observed upon addition of either excess Li^+ or Mg^{2+}. In contrast, upfield shifts in the ^{31}P NMR spectra of IP_3 were observed for the P_4 and P_5 resonances upon addition of Li^+, whereas the P_1 resonance also experienced an upfield shift with excess Mg^{2+} (Table 12).

Table 8. ^{13}C NMR Chemical Shifts (in ppm) of cAMP and AMP [a,b]

	cAMP			AMP		
Resonance	No metals	w/ Li^+	w/ Mg^{2+}	No Metals	w/ Li^+	w/ Mg^{2+}
C_2	156.9	156.7	156.6	155.2	155.0	155.0
C_4	152.3	152.1	152.0	152.9	152.6	152.6
C_5	122.7	122.6	122.5	122.5	122.2	122.2
C_6	159.5	159.3	159.2	159.5	159.2	159.2
C_8	143.8	143.7	143.5	142.7	142.4	142.5
$C_{1'}$	95.6	95.4	95.3	91.5	91.7	91.9
$C_{2'}$	71.2	71.0	70.9	74.6	74.3	74.5
$C_{3'}$	75.9	75.8	75.7	78.4	78.1	78.7
$C_{4'}$	81.2	81.0	80.8	89.6	89.3	89.2
$C_{5'}$	63.9	65.0	65.0	65.4	65.3	65.5

[a]Primed resonances are due to sugar protons or carbons, whereas unprimed resonances are due to atoms in the guanine base. [b]The nucleotide concentration was 10 mM and the concentrations of LiCl and $MgCl_2$ were 150 mM and 50 mM, respectively. Each value is an average of two readings on separately prepared samples. The errors are less than 0.5 ppm.

Table 9. ^{31}P NMR Chemical Shifts of cAMP and AMP (n=2)[a]

$[Li^+]$/mM	$[Mg^{2+}]$/mM	δ/ppm cAMP (5 mM)[b]	AMP (5 mM)
0	0	2.61	7.93
100	0	2.63	7.90
500[c]	0	2.64	8.08
0	5	2.64	7.79
0	50	2.60	7.54

[a]Ionic strength, pH, and temperature were maintained at 0.15 M, 7.4, and 37 °C, respectively. No line broadening or proton decoupling was used, and 85 % H_3PO_4 served as the external reference. The errors are less than 0.1 ppm. [b]Midpoint between doublet resonances. [c]Sample ionic strength was larger than 0.15 M.

Table 10. ^{7}Li T_1 Values of Li^+-Containing IP_3 Solutions [a]

$[Li^+]$/mM	T_1/s
2.0	2.06 ± 0.09
4.0	2.46 ± 0.07
10	2.91 ± 0.01
20	3.49 ± 0.09
50	4.81 ± 0.15
80	5.82 ± 0.12
120	7.19 ± 0.44
160	7.37 ± 0.12
220	8.23 ± 0.09
300	8.82 ± 0.21
400	9.83 ± 0.27
600	10.54 ± 0.20
800	11.61 ± 0.19
1200	12.61 ± 0.27
1400	13.23 ± 0.26
free[b]	21.59 ± 0.88

[a] IP_3 in Na^+ form was used in this experiment; pH was adjusted to 9.5 by NaOH and ionic strength was not controlled. NMR measurements were conducted in a 5 mm probe and at room temperature (20 °C). [b] Value was obtained in 10 mM LiCl solution without IP_3.

Figure 11. ^{7}Li T_1 Values for Li^{+}-IP_3 Solution Containing Various Mg^{2+} Concentrations. The Li^{+} concentration was 6.0 mM, IP_3 was 2 mM and the solution pH was 7.4. NMR measurements were performed at room temperature and in 5 mm probe. Each value is an average of two readings made on the same sample.

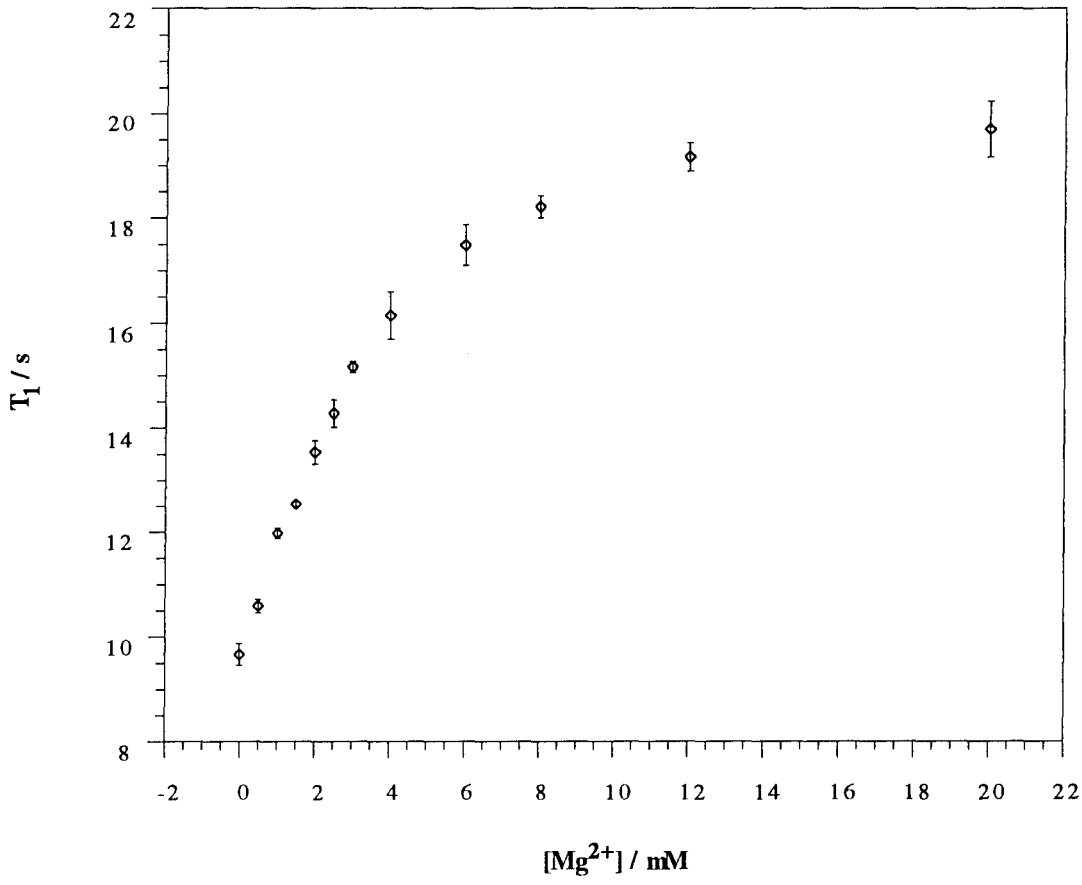
22
20
18
16
14
12
10
8
T_1 / s
-2
0
2
4
6
8
10
12
14
16
18
20
22
$[Mg^{2+}]$ / mM

Figure 12. ^{1}H (A) and ^{31}P (B) NMR Spectra of IP_3. The concentration of IP_3 (in the sodium salt form) was 4 mM. Samples were prepared in 99.5% D_2O, the pH adjusted to 9.5 with NaOH, and the spectra obtained at 20 °C. The presaturation technique was employed to suppress the water resonance in the ^{1}H NMR spectrum. ^{31}P chemical shifts were referenced to external 85% H_3PO_4; ^{1}H chemical shifts were quoted relative to TMS but referenced to ^{2}HHO at 4.8 ppm at pH 9.5; 0.5 Hz line broadening was used in both spectra. Chemical shift assignments were according to reference 118.

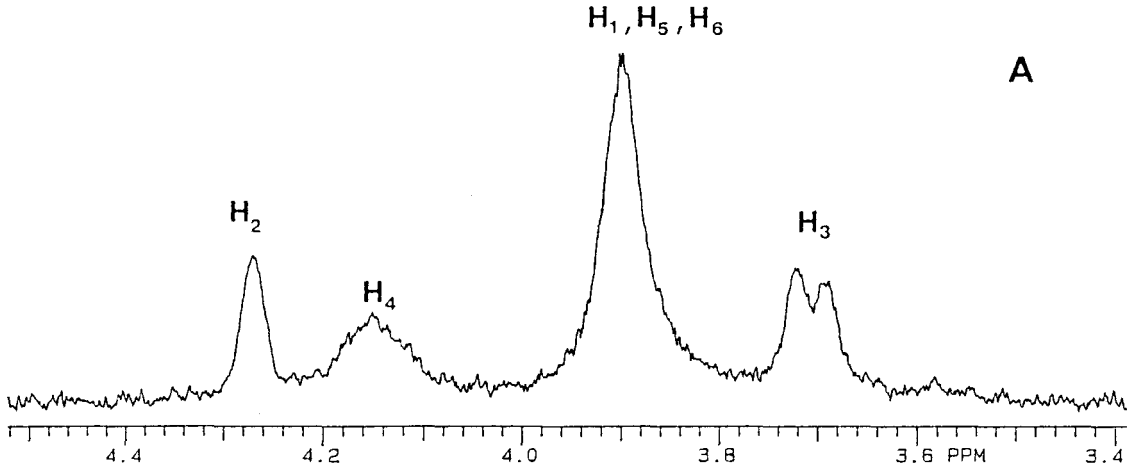
H1, H5, H6
A
H2
H4
H3
4.4
4.2
4.0
3.8
3.6 PPM
3.4

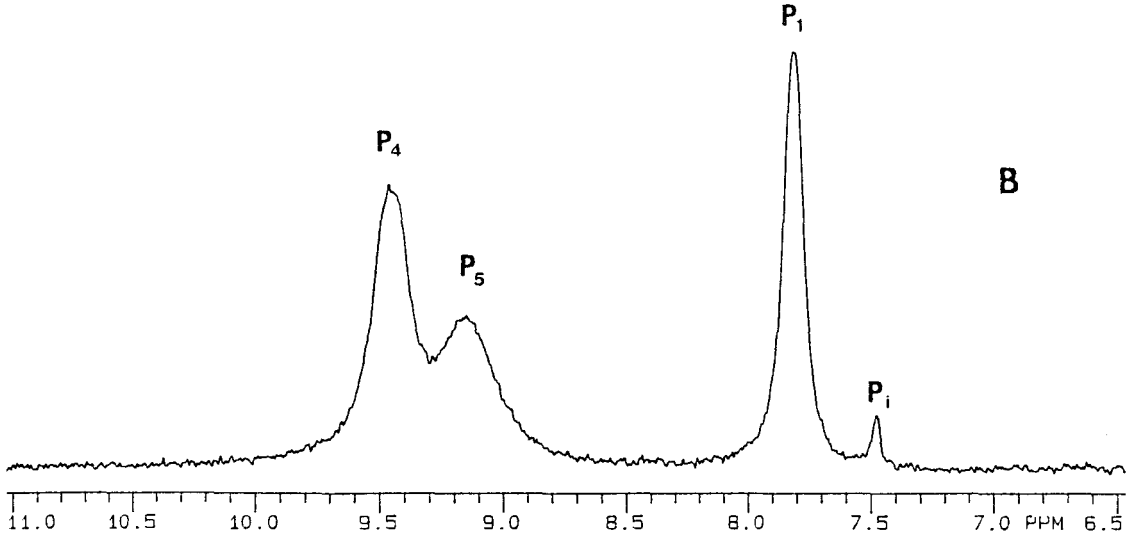
P1
P4
B
P5
Pi
11.0
10.5
10.0
9.5
9.0
8.5
8.0
7.5
7.0 PPM
6.5

Table 11. ^{1}H Chemical Shifts of IP_3 With or Without Saturating Amounts of Li^+ and Mg^{2+}.[a]

	H_1[b]	H_2	H_3	H_4	H_5[b]	H_6[b]
IP_3 alone	3.88	4.27	3.69	4.15	3.88	3.88
IP_3 with 50 mM Li^+	3.89	4.27	3.69	4.14	3.89	3.89
IP_3 with 100 mM Li^+	3.90	4.27	3.70	4.15	3.90	3.90
IP_3 with 20 mM Mg^{2+}	3.92	4.26	3.70	4.16	3.92	3.92

[a]Conditions were the same as for Figure 12. [b]H_1, H_5 and H_6 resonances overlapped; the data for these three resonances are approximate chemical shift values.

Table 12. ^{31}P Chemical Shifts (in ppm) of IP_3 [a]

$[Li^+]$/mM	$[Mg^{2+}]$/mM	P_1	P_4	P_5
0	0	7.80	9.40	9.12
10	0	7.89	9.38	9.10
20	0	7.90	9.31	9.07
0	2.5	7.77	8.91	8.51
0	5	7.63	8.69	8.20

[a]The concentration of IP_3 in the Na^+ form was 2 mM; other conditions were the same as for Figure 12. The errors are less than 0.1 ppm

IV.1C. Competition Between Li^+ and Mg^{2+} for RBC Membrane and ATP

Many enzymes are activated by Mg^{2+} including G proteins and adenylate cyclase present in RBC membrane (16,119). Therefore, Mg^{2+} competition must be considered when studying the interaction of Li^+ with membranes.

^7Li T_1 measurements were conducted at 37 °C in RBC membrane suspensions (at a concentration of 3.0 $\pm$ 0.5 mg/ml) in the presence of 0 to 1.0 mM Mg^{2+}. For each Mg^{2+} concentration in RBC membrane suspension, we then varied the Li^+ concentration between 1.0 mM and 150 mM. For a fixed Mg^{2+} concentration (Fig. 13), an increase in Li^+ concentration resulted in an increase in the ^7Li T_1 values because of an increase in the fraction of free Li^+. For a fixed Li^+ concentration, an increase in Mg^{2+} concentration caused an increase in the ^7Li T_1 values because of metal ion competition for binding sites in membrane. From the observed ^7Li T_1 values we calculated by using equation 19 the apparent Li^+ binding constants in the presence of Mg^{2+}. The Li^+ and Mg^{2+} binding constants to the RBC membrane was calculated by using equation 20 and found to be 174 M^{-1} and 3300 M^{-1}, respectively, with a regression coefficient of 0.91.

^7Li T_1 values were also measured for 7.0 mM ATP solutions containing varying Li^+ (1.0 - 1000 mM) and Mg^{2+} (0 - 2.5 mM) concentrations. We fitted the ^7Li T_1 relaxation data (Table 13) measured for 7.0 mM ATP solutions containing LiCl alone and $LiCl/MgCl_2$ mixtures to three different models (see III.3C) to generate binding constants and limiting R_1 values for Li^+ bound to ATP.

For ATP in the presence of LiCl alone and assuming an R_1 value of 0.05 s^{-1} for free Li^+, the Li^+ binding constants and the R_1 values for bound Li^+ were 12 M^{-1} and 1.5 s^{-1} (Σ^2 = 1.9 x 10^{-5}) for the model based on the LiATP species, 1.0 x 10^5 M^{-2} and 0.47 s^{-1} (Σ^2 = 4.9

Figure 13. ^{7}Li T_1 Values for Membrane Suspensions in Presence of Various Concentrations of Mg^{2+}. The Li^{+} concentrations were in the range of 2 mM to 20 mM, the concentrations of Mg^{+} were 0 (open squares), 0.2 mM (closed diamonds), 0.6 mM (closed squares) and 1.0 mM (closed circles). Membrane concentration was 3.0 $\pm$ 0.5 mg/mL.

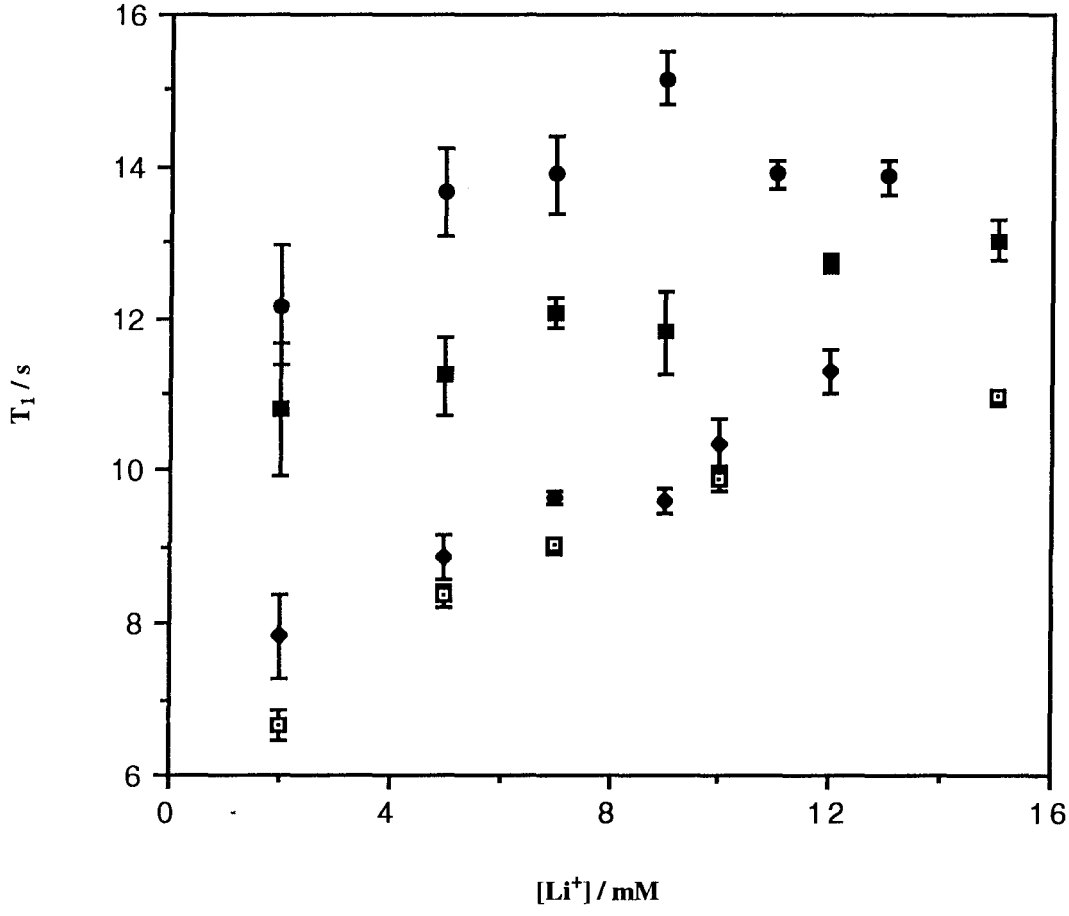
16
14
12
10
8
6
0
4
8
12
16
T_1 / s
[Li^+] / mM

Table 13. ^{7}Li T_1 Values in ATP Aqueous Solutions in the Presence of Various Concentrations of Mg^{2+}.[a]

	$[Mg^{2+}]$/mM					
$[Li^{+}]$/mM	0	0.5	1.0	1.5	2.0	2.5
1.0	6.4 ± 0.4	8.3 ± 0.4	8.1 ± 0.3	8.8 ± 0.7	9.2 ± 0.4	10.2 ± 0.8
10	6.7 ± 0.1	7.7 ± 0.2	8.8 ± 0.3	9.0 ± 0.3	9.8 ± 0.1	10.2 ± 0.3
20	7.1 ± 0.1	8.1 ± 0.3	8.9 ± 0.3	9.4 ± 0.2	10.7 ± 0.3	11.3 ± 0.5
40	7.8 ± 0.2	9.0 ± 0.5	9.4 ± 0.1	9.9 ± 0.2	11.2 ± 0.2	11.5 ± 0.4
60	8.7 ± 0.3	9.7 ± 0.5	10.4 ± 0.7	10.4 ± 0.1	11.4 ± 0.2	12.7 ± 0.8
80	9.3 ± 0.6	9.6 ± 0.1	11.1 ± 0.4	11.1 ± 0.2	12.4 ± 0.4	12.9 ± 0.4
100	9.4 ± 0.2	10.5 ± 0.4	11.3 ± 0.3	11.5 ± 0.3	13.1 ± 0.2	13.4 ± 0.5
120	10.2 ± 0.6	11.0 ± 0.2	11.7 ± 0.3	11.6 ± 0.4	13.1 ± 0.6	13.8 ± 0.9
1000	16.6 ± 0.7	16.7 ± 0.8	17.1 ± 0.5	16.9 ± 0.8	16.4 ± 0.4	16.3 ± 0.3

[a]The units of the T_1 values are in seconds. The concentration of ATP was 7 mM, buffered in 0.1 M Tris-Cl at pH 7.4. Measurements were conducted at 37 °C.

x 10^{-3}) for the model based on the Li_2ATP species, and 3.2 x 10 M^{-1} and 0.21 s^{-1} for LiATP and 3.2 x 10^3 M^{-2} and 1.6 s^{-1} for Li_2ATP (Σ^2 = 1.7 x 10^{-5}) for the model based on a mixture of LiATP and Li_2ATP. The Σ^2 values obtained for calculations with the ^7Li data in the presence of LiCl alone indicate that the best nonlinear least-squares fit to the ^7Li T_1 data was provided by the model based on a mixture of LiATP and Li_2ATP in which the species Li_2ATP predominates. Based on nonlinear least-squares fitting of ^{31}P chemical shift data, we had previously found that the 2:1 species also predominated in aqueous solutions of ATP or GTP in the presence of Li^+ alone (23,120; section IV.1A.c).

For ATP in the presence of mixtures containing 0.5 mM $MgCl_2$ and varying concentrations of LiCl and assuming an R_1 value of 0.05 s^{-1} for free Li^+ and a binding constant of 2 x 10^4 M^{-1} for MgATP (23), the Li^+ binding constants and the R_1 values for bound Li^+ were 7.3 M^{-1} and 1.8 s^{-1} (Σ^2 = 1.3 x 10^{-4}) for the model based on the LiATP species, 3.8 x 10^4 M^{-2} and 0.46 s^{-1} (Σ^2 = 3.0 x 10^{-3}) for the model based on the Li_2ATP species, and 8.7 x 10^2 M^{-1} and 0.14 s^{-1} for LiATP and 1.1 x 10^4 M^{-2} and 0.13 s^{-1} for Li_2ATP (Σ^2 = 6.2 x 10^{-5}) for the model based on a mixture of LiATP and Li_2ATP. The Σ^2 values obtained for calculations with ^7Li data in the presence of $LiCl/MgCl_2$ mixtures also indicate that the best nonlinear least-squares fit to the ^7Li T_1 data was provided by the model based on a mixture of LiATP and Li_2ATP in which the species Li_2ATP predominates. Based on nonlinear least-squares fitting of ^{31}P chemical shift data, we had previously found that the 2:1 species also predominated in aqueous solutions of ATP or GTP in the presence of Li^+/Mg^{2+} mixtures (23,120). The Li^+ binding constants appear to be greater in Li^+/Mg^{2+} mixtures than in the presence of Li^+ alone. The large error involved in the calculation of the binding constants suggests, however, that this difference may not be significant.

IV.2. Multinuclear NMR Study of Li^+-Loaded Erythrocytes

IV.2A. The Effects of Hematocrit on ^7Li NMR T_1 Values, and on the Rate of Li^+ Uptake in Human RBC Suspensions

Figure 14 shows our results for the hematocrit dependence of intra- and extracellular $^7Li^+$ T_1 values in human RBC suspensions at 37 °C. Whereas the intracellular $^7Li^+$ T_1 values were independent of the hematocrit used, the extracellular $^7Li^+$ T_1 values decreased at 84% hematocrit. Using a Newman-Keuls statistical test (114), we found that the extracellular $^7Li^+$ T_1 value at 84% hematocrit was significantly lower ($p < 0.05$) than the values at 11, 33, 45, and 67% hematocrit; however, the extracellular T_1 values in the 11 to 67% hematocrit range were not significantly different. For all hematocrits studied, we found that the extracellular $^7Li^+$ T_1 values were at least three times greater than the corresponding intracellular $^7Li^+$ T_1 values.

Slight, statistically insignificant variations in T_1 values were observed among different blood batches. In a separate experiment, the T_1 value of 14.8 $\pm$ 0.5 s (n=2) for extracellular Li^+ in Li^+-free RBCs suspended at 85% hematocrit in an isotonic-choline medium was observed. It was not statistically different (Student's t-test, $p > 0.05$) from that shown in Fig. 13 (16.7 $\pm$ 1.3 s, $n = 4$), which was measured for a different blood batch at approximately the same hematocrit (84%) and under the same suspensions conditions.

For the studies of Li^+ uptake in RBCs, packed washed RBCs loaded with 3 mM Li^+ were suspended at either 44% or 85% hematocrit in an isotonic medium containing 50 mM LiCl, 12 mM choline chloride, 50 mM KCl (shift reagent contribution included), 10 mM glucose, 85 mM sucrose, 5 mM $Dy(PPP)_2^{7-}$(in the K^+ form), and 10 mM HEPES, pH 7.4. The areas under the intracellular ^7Li NMR resonance curve were measured every hour during

Figure 14. Hematocrit Dependence of Intra- (crosses) and Extracellular (squares) $^7Li^+$ T_1 Values for Human RBC Suspensions at 37 °C. The media used for each measurement are described in detail in the Methods section. The extra- and intracellular Li^+ concentrations were 50 mM and 3.0 mM, respectively. The extracellular T_1 measurements were obtained with 1 transient for each τ value, except for the sample at 84% hematocrit for which 2 transients were used. The intracellular T_1 measurements were obtained with 2 transients for each τ value, except for samples with 25% hematocrit for which 4 transients were used. The total accumulation time for each T_1 measurement never exceeded 20 min. Each point represents the average of at least four experiments performed on separately prepared samples. The error bars indicate the range of T_1 values obtained.

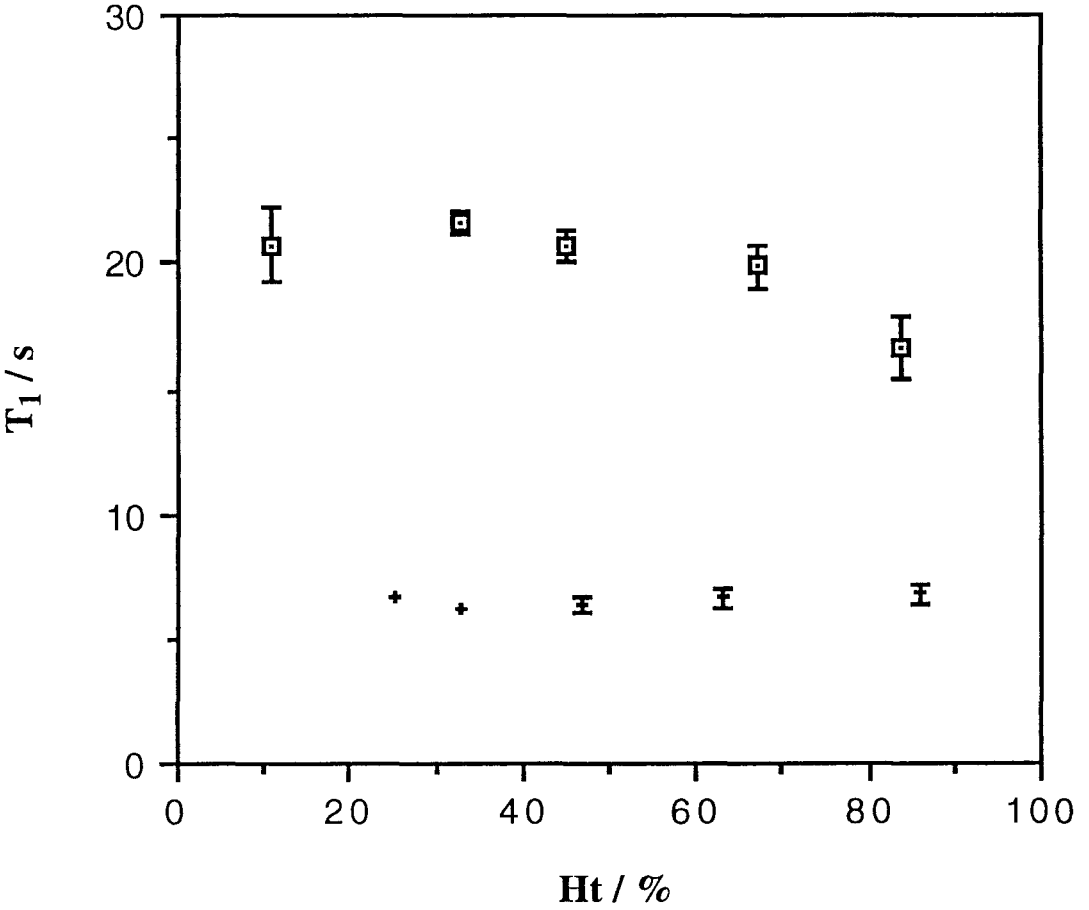
30
20
10
0
T_1 / s
0
20
40
60
80
100
Ht / %

an 8 h period and were converted into intracellular Li^+ concentrations, $[Li^+]_i$, with the equation (16).

Figure 15 shows the kinetics of Li^+ influx in human RBC suspensions at two different hematocrits. At the same temperature and for the same initial extracellular Li^+ concentration, the rise in the intracellular Li^+ concentration in fresh RBC suspensions was faster at the lower hematocrit. The initial rates of Li^+ uptake, which were calculated from the first derivative of the curves at time zero, were 1.40 and 1.27 mmol of Li^+/L RBC•h at 44% and 85% hematocrit, respectively (Table 14A). The time constant for Li^+ influx, which was calculated from the time dependence of intracellular Li^+ concentrations (see III.3B.), was 8.7 h at 44% hematocrit and 4.1 h at 85% hematocrit (Table 14A). The time constant that we obtained at 44% hematocrit is in good agreement with the time constant of 8.5 h reported by Andrasko (121) with fresh RBCs suspended at 40% hematocrit in 155 mM LiCl at 34 °C. The equilibrium concentration gradient increased with increasing hematocrit; the limiting intracellular Li^+ concentration, $[Li^+]^{\infty}_{in}$, decreased, however, with an increase in hematocrit whereas the percentage of intracellular Li^+ remained approximately constant (Table 14A). These results are in agreement with those reported previously by us and others using ^7Li NMR or AA (27,35,87,95). The literature data from reference 109 and corresponding calculated values are also listed in Table 14 (B & C).

IV.2B. Identification of Li^+ Binding Sites in Erythrocytes

IV.2B.a. ^7Li Intracellular Relaxation Study in Li^+-Loaded RBCs

Measurements of intracellular $^7Li^+$ T_1 and T_2 relaxation times for Li^+-loaded RBCs are summarized in Table 15. For all the intracellular Li^+ concentrations studied, T_1 values were

Figure 15. Time Dependence of RBC Intracellular Li^+ Uptake at 37 °C and at 44% (upper curve) or at 85% Hematocrit (lower curve). Fresh packed human RBCs are suspended in an isotonic medium containing 50 mM LiCl, 12 mM choline chloride, 50 mM KCl (shift reagent contribution included), 10 mM glucose, 85 mM sucrose, 5 mM $Dy(PPP)_2^{7-}$ (in the K^+ form), and 10 mM HEPES, pH 7.4. ^7Li NMR spectra were obtained after 171 scans, requiring a total of 1 h. Li^+ influx was measured every hour for an 8 h period. Each concentration is that at the midpoint for each hour of accumulation time. Each point represents the average of two experiments performed on separately prepared samples. The error bars indicate the range of intracellular Li^+ concentrations obtained.

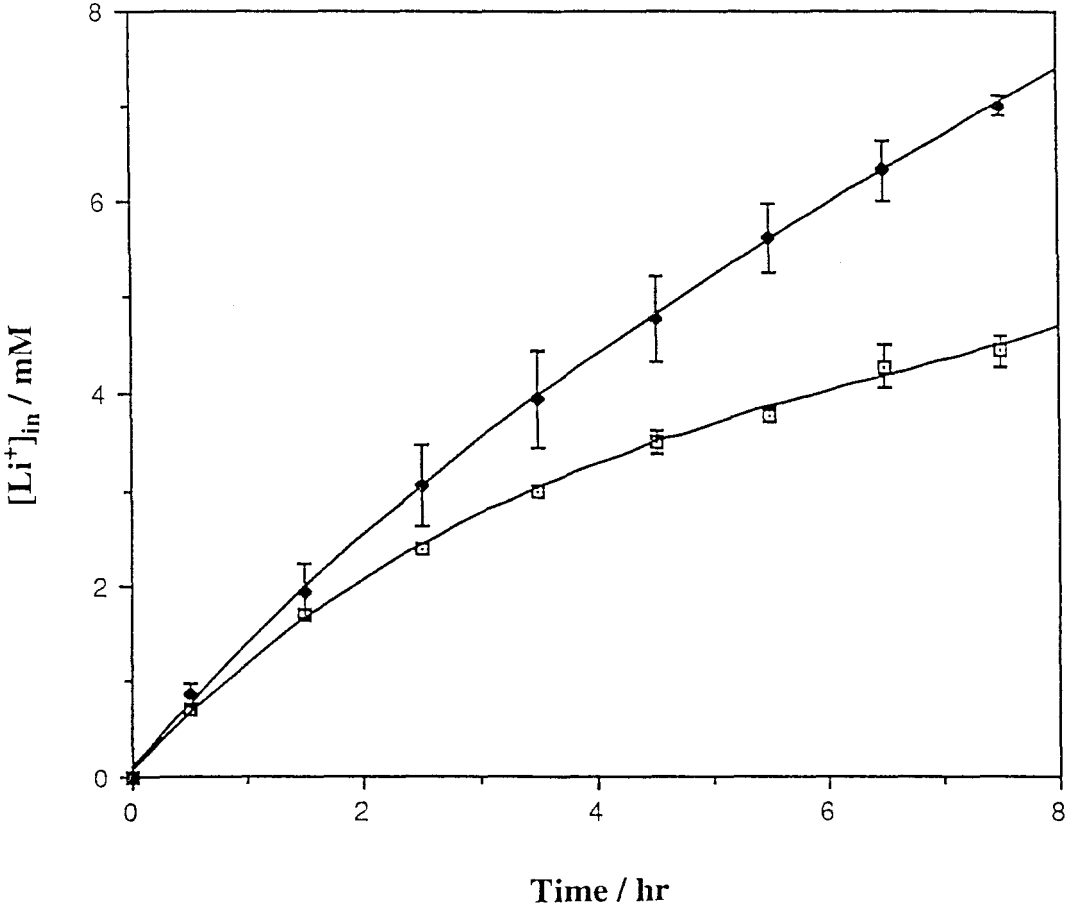
8
6
4
2
0
0
2
4
6
8
[Li+]in / mM
Time / hr

Table 14. Effect of Hematocrit on Li^+ Transport Parameters in Human RBC Suspensions

Hematocrit	Time Constant/h	Initial Rate of Li^+ Influx (mmol Li^+/L RBC.h)	Equilibrium Concentration Gradient ($[Li^+]^{\infty}_{out}/[Li^+]^{\infty}_{in}$)	$[Li^+]^{\infty}_{in}$/mM	$\%Li^{+\infty}_{in}$
A. Starting $[Li^+]_{out}$: 50 mM[a]					
44%	8.7[b]	1.40	6.7	12.0	10.6
85%	4.1[c]	1.27	57.2	5.3	9.0
B. Starting $[Li^+]_{out}$: 1.8 mM at 45% Ht and 50 mM at 85% Ht[d]					
45%	11.6	0.12	1.5	1.43	4.8
85%	16.5	0.82	19.8	13.1	22.2
C. $[Li^+]$ over entire sample (RBCs + medium): 3.5 mM[e]					
20%	[f]	[f]	1.9	2.1	12.0
44%	[f]	[f]	4.4	1.2	14.0
85%[g]	[f]	[f]	33.3	0.6	15.0

[a]Calculated from data shown in our Fig. 15. [b]Σ^2, the sum of squared deviations, was 5.5 x 10^{-2}. [c]Σ^2 was 4.0 x 10^{-2}. [d]Estimated from data published in Fig. 1 of ref. 109. [e]Estimated from data published in Fig. 2 of ref. 109. [f]Can not be calculated from data in ref. 109. [g]Estimated by extrapolation of data published in Fig. 2 of ref. 109.

Table 15. ^{7}Li T_1 and T_2 Relaxation Values of Packed Li^+-Loaded RBCs [a]

Samples	$[Li^+]$/mM	T_1/s	T_2/s	R (T_1/T_2)
Regular RBC	1.0	5.6 ± 0.1	0.21 ± 0.04	24
	1.4	6.0 ± 0.1	0.30 ± 0.03	20
	2.3	6.3 ± 0.1	0.35 ± 0.01	18
	3.5	6.5 ± 0.2	0.46 ± 0.06	14
CORBC	3.5	5.9 ± 0.1	0.53 ± 0.01	11
deoxy RBC	3.5	6.7 ± 0.1	0.44 ± 0.05	15
Glycerol 50:50% (v/v)	1.5	4.6 ± 0.1	4.0 ± 0.2	1.2

[a] All samples were run at 37 °C, and the concentrations of intracellular Li^+ were confirmed by atomic absorption. Viscosity of the glycerol sample was 5 cP.

much higher than the corresponding T_2 values. As the intracellular Li^+ concentration increased, so did T_1 and T_2 values because the fraction of free intracellular Li^+ also increased. These relaxation data are in agreement with those previously reported (122). The large difference between T_1 and T_2 values indicates that Li^+ interactions with a long correlation time (116) must be present in Li^+-loaded RBCs.

The viscosity of the intracellular volume in RBCs is about 5 cP (115). Viscosity alone could be responsible for the observed difference in intracellular $^7Li^+$ T_1 and T_2. We therefore measured ^7Li T_1 and T_2 values for glycerol/water solutions of 1.5 mM LiCl. The viscosity of these samples was in the 0.7 to 5 cP range and was obtained with 0:100% to 50:50% (v/v) glycerol/water mixtures. Unlike RBCs containing 1.5 mM intracellular Li^+ in which there was a drastic difference between T_1 and T_2 values (Table 15), for 1.5 mM LiCl in 50:50% glycerol/water (with a viscosity of 5 cP) there was only a slight difference between the T_1 (4.6 $\pm$ 0.1 s) and T_2 (4.0 $\pm$ 0.2 s) values. The T_1/T_2 ratio obtained for the viscosity-adjusted 1.5 mM LiCl solution was 1.2, which is considerably less than the T_1/T_2 ratio observed for RBCs loaded with 1.4 mM intracellular Li^+ (20; see Table 15). The values that we obtained for Li^+-containing glycerol/water mixtures are in agreement with previously reported data (121). The large difference in intracellular RBC $^7Li^+$ T_1 and T_2 values is therefore not due to viscosity effects.

^7Li T_1 and T_2 for packed deoxyRBC and packed CORBC were also measured. The oxygenation state of Hb was checked by ^{31}P NMR spectra (Fig. 16). N_2 treated RBCs were paramagnetic, showed broad line shape and downfield shifted ^{31}P NMR resonances (Fig. 16C), while the opposite trend was observed in CO treated RBCs (Fig. 16B). In packed RBCs loaded with 3.5 mM Li^+, the T_1 and T_2 values for Li^+-loaded deoxyRBC were 6.7 $\pm$ 0.1 s

Figure 16. ^{31}P NMR Spectra of Packed RBCs in Various Oxygenation States. TMP was used as external reference and spectra line broadening was 3.0 Hz.

(A) Regular RBCs; (B) CORBCs; (C) DeoxyRBCs.

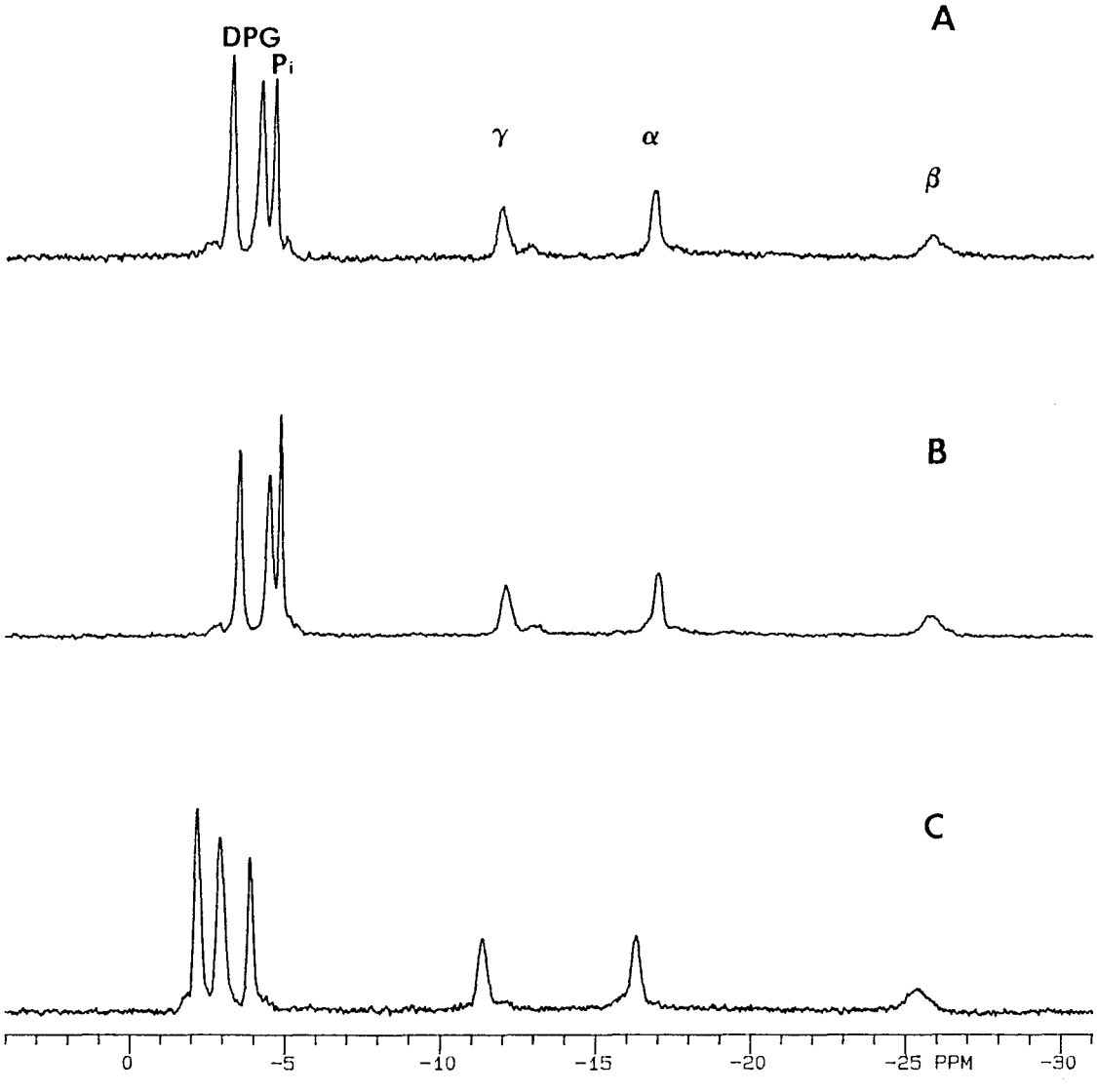
A
DPG
Pi
γ
α
β
B
C
0
-5
-10
-15
-20
-25 PPM
-30

and 0.44 ± 0.05 s (R = 15; *n* = 2), whereas the NMR relaxation parameters for Li^+-loaded CORBC were: T_1 = 5.9 ± 0.1 s, T_2 = 0.53 ± 0.01 s (R = 11; *n* = 2). However, the ^7Li T_2 and R values found in packed Li^+-loaded CORBCs are slightly larger and smaller, respectively, than the values obtained in packed Li^+-loaded deoxyRBCs and oxygenated RBCs (Table 15) suggesting that the paramagnetic relaxation induced by deoxyHb is small. Oxygenated Li^+-loaded RBCs may contain trace amounts of paramagnetic deoxyHb and metHb; not surprisingly, the T_2 and R values of oxygenated RBCs are intermediate between those observed for CORBCs and deoxyRBCs. Because the large difference in intracellular ^7Li T_1 and T_2 values was present in packed Li^+-loaded RBCs regardless of the state of oxygenation, we conclude that ^7Li NMR relaxation in RBCs is not controlled by paramagetic relaxation induced by high-spin Fe^{2+} or by Fe^{3+} present in deoxy Hb or metHb, respectively.

IV.2B.b. Interactions of Li^+ with RBC Components

RBC is most often thought of as a packet of hemoglobin. COHb is diamagnetic and is an irreversible analogue of oxy Hb, while deoxy Hb and metHb are paramagnetic. The oxygenation states of Hb were characterized by UV-Vis spectrophotometry. A red shift in the λ_{max} of the Soret band was observed when converting the oxy form (415 nm) to the CO form (419 nm), while that of the deoxy form had a blue shifted band (430 nm). Due to the difficulty in preparing concentrated Hb, the concentration used (2.7 mM per tetramer) was half the value of the physiological concentration (5.4 mM). The viscosity of the Hb solution was adjusted to 5 cP with glycerol.

The Hb results are shown on Table 16. By increasing the concentration of Li^+ from 1.5 to 8 mM, the T_1 and T_2 values stayed almost constant for all oxygenation states.

Compared with deoxyHb and COHb, both the T_1 and the T_2 values for metHb were lower which may be the result of higher paramagnetism induced by the high spin Fe^{3+} center. However, the difference between T_1 and T_2 relaxation values for different forms of Hb was essentially the same. The R values were small, and were independent of Li^+ concentration which indicated that Li^+ bound weakly to Hb. This agrees with published results (122,123).

^7Li T_1 and T_2 relaxation times were also measured for ATP, DPG (Table 17), spectrin (Table 18) and membrane (Table 19). Table 20 is a summary of ^7Li relaxation in RBC and its components at 1.5 mM Li^+ concentration. The T_1/T_2 ratio ranged from 1.3 to 1.6 in ATP and DPG at physiological concentrations, implying that at the Li^+ concentrations typically present in Li^+-loaded RBCs Li^+ binds weakly to ATP and DPG. The T_1/T_2 ratio of spectrin (1.9 mg/ml) was around 4, while it was in the range of 30 to 50 for membranes at the same protein concentration, suggesting weak Li^+ binding to spectrin. In solutions of ATP, DPG, and spectrin, an increase in Li^+ concentration resulted in increases of both T_1 and T_2 values; this effect was also observed for Li^+-loaded RBCs (Table 15) and is due to an increase in the mole fraction of free Li^+. The absolute values of the T_1 and T_2 values observed in Hb and spectrin solutions are significantly larger than those observed in ATP and DPG solutions; the higher T_1 and T_2 values are associated with the longer correlation times for Li^+ bound to the high molecular weight proteins Hb and spectrin.

The large difference in intracellular ^7Li T_1 and T_2 relaxation values characteristic of Li^+-loaded RBCs is also present in unsealed RBC membrane suspensions whose viscosity was adjusted to 5 cP with glycerol (Table 19), indicating that binding of Li^+ to the RBC membrane is responsible for the unique relaxation behavior of Li^+-loaded RBCs. The NMR parameters for a 1.5 mM Li^+-containing RBC membrane suspensions (2.0 mg/mL) whose viscosity was

Table 16. ^{7}Li T_1 and T_2 Relaxation Values of 2.7 mM Hemoglobin Solutions (n=2) [a]

Sample	$[Li^+]$/mM	T_1/s	T_2/s	R (T_1/T_2)
COHb	1.5	4.5 ± 0.5	2.0 ± 0.1	2.2
	3.0	5.3 ± 0.4	2.0 ± 0.3	2.7
	5.0	5.0 ± 0.6	2.0 ± 0.3	2.5
	8.0	4.9 ± 0.1	2.1 ± 0.1	2.3
Met Hb	1.5	4.2 ± 0.3	1.5 ± 0.1	2.8
	3.0	4.4 ± 0.1	1.7 ± 0.1	2.6
	5.0	4.3 ± 0.2	1.6 ± 0.1	2.7
	8.0	4.4 ± 0.4	1.7 ± 0.1	2.6
Deoxy Hb	1.5	4.7 ± 0.1	2.0 ± 0.2	2.4
	3.0	4.8 ± 0.1	2.1 ± 0.2	2.3
	5.0	4.6 ± 0.2	2.0 ± 0.1	2.3
	8.0	5.0 ± 0.2	2.1 ± 0.1	2.4

[a] All samples were buffered at pH 7.4; viscosities were adjusted by glycerol to approx. 5 cP, and NMR measurements were run at 37 °C.

Table 17. ^{7}Li T_1 and T_2 Relaxation Values in Aqueous Solutions of ATP and DPG (n=2)[a]

Sample	$[Li^+]$/mM	T_1/s	T_2/s	R (T_1/T_2)
2.0 mM ATP	1.5	0.85 ± 0.03	0.53 ± 0.03	1.6
	3.0	0.98 ± 0.03	0.66 ± 0.00	1.5
	5.0	1.08 ± 0.01	0.69 ± 0.09	1.6
	8.0	1.22 ± 0.02	0.92 ± 0.00	1.3
5.4 mM DPG	1.0	1.17 ± 0.01	0.76 ± 0.05	1.5
	3.0	1.18 ± 0.02	0.73 ± 0.05	1.6
	5.0	1.17 ± 0.09	0.77 ± 0.04	1.5
	8.0	1.25 ± 0.03	0.94 ± 0.10	1.3

[a]Experimental conditions were the same as for Table 16.

Table 18. ^{7}Li T_1 and T_2 Relaxation Values of Spectrin Solutions (n=2) [a]

	$[Li^+]$/mM	T_1/s	T_2/s	R (T_1/T_2)
w/o glycerol				
	1.5	16.7 ± 0.5	6.2 ± 0.7	2.7
	3.0	16.4 ± 0.3	6.1 ± 0.7	2.7
	5.0	15.8 ± 0.1	6.6 ± 0.3	2.4
w/ glycerol adjusted to 5 cP				
	1.5	3.0 ± 0.1	0.68 ± 0.10	4.4
	3.0	3.3 ± 0.2	0.77 ± 0.12	4.9
	5.0	3.7 ± 0.2	0.95 ± 0.20	3.9

[a]The protein concentration of spectrin was 1.9 mg/mL. The NMR samples were run at 37 °C, and buffered at pH 7.6 with the extraction buffer (0.3 mM sodium phosphate).

Table 19. ^{7}Li T_1 and T_2 Relaxation Values of RBC Membrane Suspensions (n=2) [a]

	$[Li^+]$/mM	T_1/s	T_2/s	R (T_1/T_2)
w/o glycerol				
	1.5	9.1 ± 0.1	0.13 ± 0.02	70
	3.0	11.3 ± 0.2	0.17 ± 0.03	66
	5.0	12.7 ± 0.2	0.26 ± 0.03	49
	8.0	14.5 ± 0.2	0.33 ± 0.02	44
w/ glycerol (adjusted to 5 cP)				
	1.5	3.4 ± 0.1	0.07 ± 0.01	49
	3.0	4.2 ± 0.1	0.08 ± 0.01	52
	5.0	4.7 ± 0.2	0.13 ± 0.01	39
	8.0	5.1 ± 0.1	0.17 ± 0.02	30

[a]The protein concentration of RBC membranes was 2.0 mg/mL. The NMR samples were run at 37 °C, and buffered at pH 8 with the extraction buffer 5 mM HEPES.

Table 20. ^{7}Li Relaxation Values for RBCs and Its Components at 1.5 mM Li^{+} Concentration (n=2) [a]

	T_1/s	T_2/s	R (T_1/T_2)	Concentration
RBC	6.0 ± 0.1	0.30 ± 0.03	20	-
ATP	0.85 ± 0.03	0.53 ± 0.03	1.6	2.0[b]
DPG	1.2 ± 0.1	0.82 ± 0.02	1.5	5.4[c]
COHb	4.5 ± 0.5	2.0 ± 0.1	2.2	2.7[b]
deoxy Hb	4.7 ± 0.1	2.0 ± 0.2	2.4	2.7[b]
metHb	4.2 ± 0.3	1.5 ± 0.1	2.8	2.7[b]
spectrin	3.0 ± 0.1	0.68 ± 0.10	4.4	1.9[c]
RBC membrane	3.4 ± 0.1	0.07 ± 0.01	49	2.0[c]
glycerol	4.6 ± 0.1	4.0 ± 0.2	1.2	50:50% (v/v)

[a]The viscosities of all samples were adjusted to 5 cP with glycerol. All NMR samples were run at 37 °C. ATP, DPG and glycerol were buffered with 10 mM Tris-Cl to pH 7.4; RBCs, Hb, spectrin and membranes were suspended in the same media as the extraction buffer. [b]The concentration unit is mM. [c]The unit is mg/mL protein.

not adjusted with glycerol were: T_1 = 9.1 ± 0.1 s, T_2 = 0.13 ± 0.02 s (R = 70; *n* = 2). The globular Hb protein is present in RBCs but absent in RBC membrane suspensions; the larger R values observed in RBC membrane suspensions relative to those found with intact RBCs, are presumably due to differences in viscosity between the two samples, and additional Li^+ binding sites in packed RBCs.

IV.2B.c. Li^+ Interaction with IOV and ROV

To determine which side of the RBC membrane contributes the most toward Li^+ binding, we measured ^7Li T_1 values for IOV and ROV suspensions containing Li^+ in the 2.0 to 9.0 mM range (Table 21, Figure 17). The preparations of the two types of RBC vesicles were characterized by glyceraldehyde-3-phosphate dehydrogenase and acetylcholine esterase sidedness assays. Whereas glyceraldehyde-3-phosphate dehydrogenase is located in the inner leaflet of the RBC membrane, acetylcholinesterase is located in the outer leaflet. The percentages of sidedness accessibility that we found (see III.2.G.) agree with literature values (104). We also added a shift reagent, 3.0 mM $Dy(PPP)_2^{7-}$, to the RBC vesicle suspensions and observed only one ^7Li NMR resonance; the ^7Li T_1 data obtained in RBC vesicle suspensions are therefore due to extravesicular Li^+, and not due to an average of intra- and extravesicular Li^+.

For the same extravesicular Li^+ and membrane concentrations, the T_1 values observed in ROV suspensions are two to three times larger than those found in IOV suspensions (Figure 17). Because ROVs were generated from a Mg^{2+}-containing buffer (0.5P8-0.1Mg), Mg^{2+} may compete with Li^+ for binding sites on the surface of ROVs; this metal ion competition could provide an alternative explanation for the larger T_1 values observed in ROV suspensions.

Table 21: ^{7}Li T_1 Relaxation Values for IOV and ROV (n=4)

$[Li^+]$/mM	T_1/s (IOV)	T_1/s (ROV)
2	3.2 ± 0.3	9.3 ± 0.7
3	3.8 ± 0.4	10.3 ± 1.0
5	4.5 ± 0.4	10.9 ± 0.8
7	5.3 ± 0.5	11.2 ± 0.7
9	5.9 ± 0.5	11.5 ± 0.6
Prot.(mg/mL)	3.5 ± 0.3	3.5 ± 0.7
% Sidedness Accessibility[a]	80 ± 8	21 ± 3
% Sidedness Accessibility[b]	19 ± 4	94 ± 2

[a] Glyceraldehyde-3-phosphate dehydrogenase
[b] Acetylcholinesterase

Figure 17. ^{7}Li T_1 Values for Li^{+}-Containing IOV (closed circles) and ROV (open circles). The data reported are an average of four separately prepared samples. The membrane protein concentrations in the IOV and ROV preparations were 3.5 $\pm$ 0.3 and 3.5 $\pm$ 0.7 mg/mL, respectively.

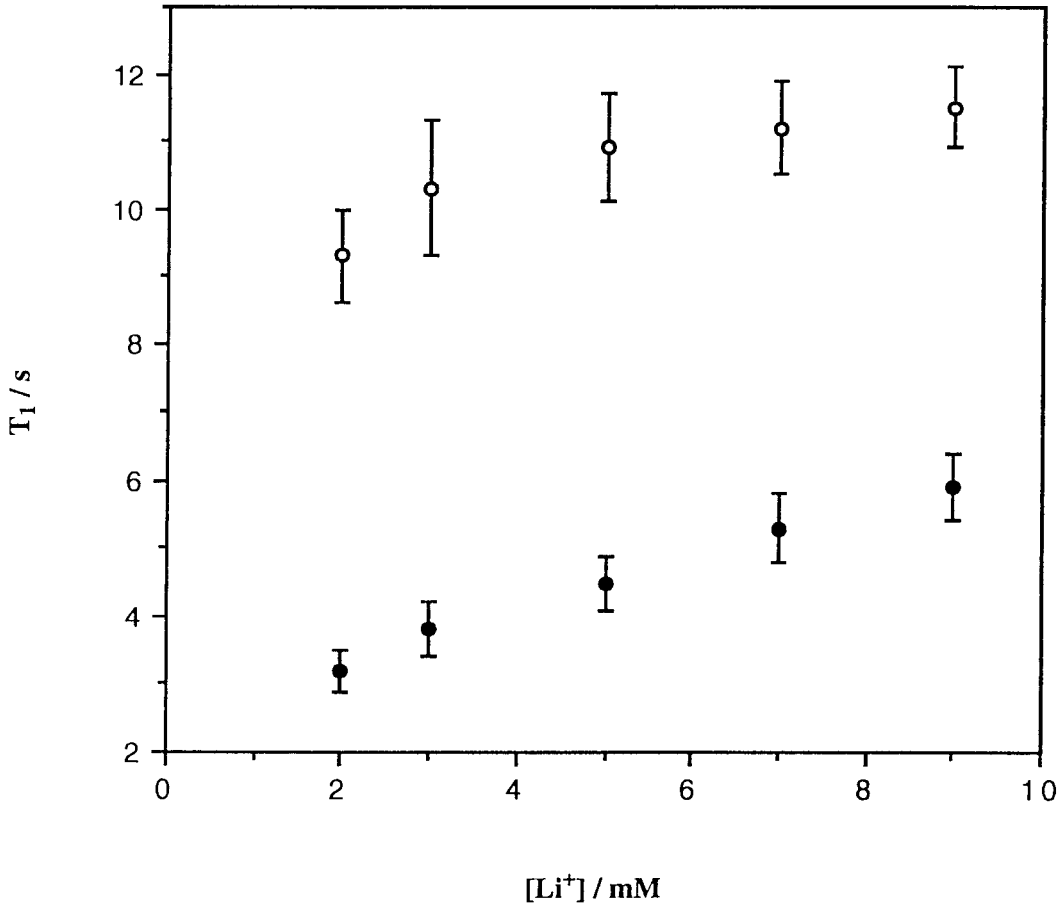
12
10
8
6
4
2
0
2
4
6
8
10
T1 / s
[Li+] / mM

To rule out this latter possibility, we conducted a control experiment where we added 0.1 mM $MgSO_4$ to an IOV suspension containing 7.0 mM Li^+. Although the T_1 value increased by 15% (from 5.3 s to 6.1 s), the T_1 value observed in Mg^{2+}-containing IOV suspensions (6.1 s; n = 2) was significantly shorter than that observed for ROV suspensions containing 7.0 mM Li^+ (11.2 s; n = 4). The large ^7Li T_1 values observed in ROV suspensions relative to IOV suspensions indicate weaker binding of Li^+ to the outer leaflet of the RBC membrane than to the inner leaflet; the difference in ^7Li T_1 values in ROV and IOV suspensions is not due to competition between Li^+ and Mg^{2+} for binding sites in the RBC membrane.

IV.2B.d. ^7Li Relaxation Behavior in RBC Membrane Suspensions

To understand the relaxation behavior of Li^+ in the presence of RBC membrane, partially relaxed ^7Li NMR spectra of 20 mM LiCl in the presence of 6.0 $\pm$ 0.2 mg/mL of unsealed RBC membrane were measured (Fig. 18). For a single Lorentzian line, the ratio of $\Delta\nu_{1/8}/\Delta\nu_{1/2}$ should be approximately 2.7 (80). At a pulse interval, τ, of 0.75 s, the $\Delta\nu_{1/8}/\Delta\nu_{1/2}$ value of 3.4 is larger than the theoretical value of 2.7; the inverted resonance observed for τ = 0.75 s is therefore composed of broad and narrow components. Similarly, the completely relaxed ^7Li NMR resonance observed for τ = 11.0 s yields a $\Delta\nu_{1/8}/\Delta\nu_{1/2}$ value of 3.5 also indicating biexponential relaxation for the ^7Li nucleus in the presence of RBC membrane. As the negative intensity decreases, we observed that the broad (or fast) component nulled and the $\Delta\nu_{1/8}/\Delta\nu_{1/2}$ value reached a minimum for a τ value of 6.3 s; on division by ln 2 it gives a T_{1f} value of 9.0 s. For τ = 6.3 s, only the narrow (or slow) component was observed; a value of 0.21 s for T_{2s} was calculated by fitting the $\Delta\nu_{1/2}$ value into the equation $T_{2s} = (\pi\nu_{1/2})^{-1}$. For a τ value of 8.0 s, the $\Delta\nu_{1/8}/\Delta\nu_{1/2}$ value is close to 2.7

Figure 18. Partially Relaxed ^{7}Li NMR Spectra in RBC Membrane Suspension. Suspension contained 20 mM LiCl, 80% (v:v%) unsealed RBC membrane (6.0 $\pm$ 0.2 mg/mL) and 20% of 5H8 (prepared by D_2O). The pulse sequence (D - 180° - τ - 90°)$_n$ was used for recording the ^{7}Li NMR spectra. The interpulse delay (τ) values are indicated by the side of the spectra, and the preacquisition delay (D) values were ten times the value of T_1. Each spectrum was obtained by averaging 30 transients (n).

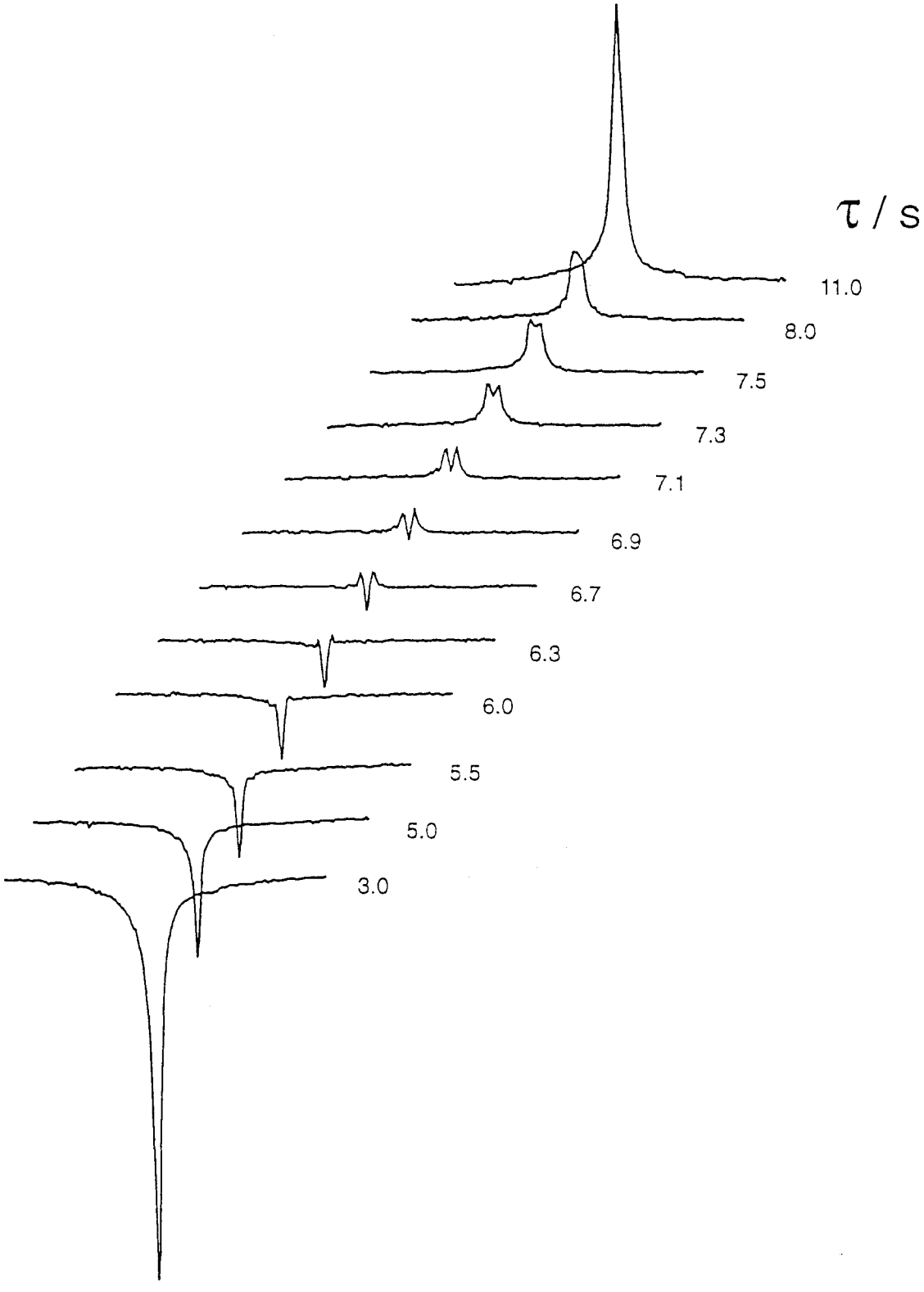
τ / s
11.0
8.0
7.5
7.3
7.1
6.9
6.7
6.3
6.0
5.5
5.0
3.0

indicating that the narrow component reached its null point making only the broad component visible; the T_{1s} and T_{2f} values calculated from the τ value of 8.0 s and the $\Delta\nu_{1/2}$ were 11.5 s and 0.06 s, respectively. Whereas biexponential relaxation was observed for membrane suspensions containing 20 mM LiCl, only one relaxation component with Lorentzian line shape was observed in membrane suspensions (with the same protein concentration) containing 150 mM LiCl or in a glycerol/water mixture containing 150 mM LiCl (no membrane). Therefore, a large fraction of bound Li^+ must be present in the membrane suspension to observe biexponential relaxation.

We measured the areas of the ^7Li NMR resonances and the T_1 values in RBC membrane suspensions (at a protein concentration of 3.0 $\pm$ 0.5 mg/mL) containing Li^+ in the range of 2.0 mM to 22.0 mM (Figure 19). The areas of the ^7Li NMR resonances were directly proportional to the Li^+ concentrations present in the RBC membrane suspension and, in the presence of RBC membrane, the areas were at least 95% of the areas observed in the absence of membrane indicating that there were no significant changes in the ^7Li NMR observable pool of Li^+ ions. From the observed ^7Li T_1 values, which are a weighted average of T_{1f} and T_{1s} values, we calculated the binding constant of Li^+ to the RBC membrane by using equation 19; the K_b value was 215 $\pm$ 36 M^{-1} ($r^2 \geq 0.95$; $n = 10$).

IV.3. Relationship Among Na^+/Li^+ Countertransport Rates, Phospholipid Composition, and Li^+ Binding to Human RBC Membranes from Bipolar Patients Receiving Lithium Carbonate

IV.3A. Demography of Patients and Controls

Whole blood from ten bipolar patients who were receiving lithium carbonate and from

Figure 19. James-Noggle Plot of RBC Membrane Suspension Containing Li^+. The membrane protein concentration was 3.0 $\pm$ 0.5 mg/mL.

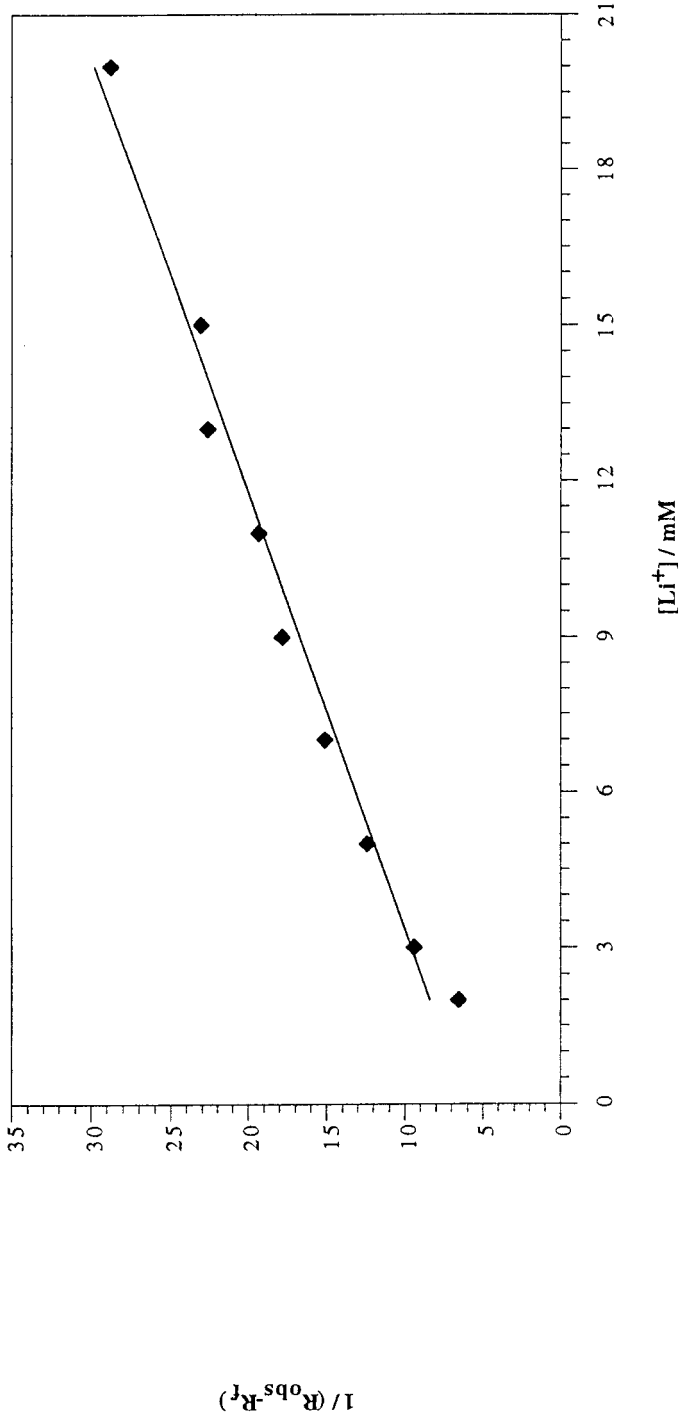
35
30
25
20
15
10
5
0
0
3
6
9
12
15
18
21
[Li+] / mM
1 / (Robs-RL)

ten normal individuals were obtained from the Department of Psychiatry, Loyola University Medical Center, Maywood, IL. Each bipolar patient was matched to a normal individual according to gender, race, age, and weight. Patients were diagnosed according to the Diagnostic and Statistical Manual of Mental Disorders (DSM-IIIR, 1990) (99). The patients in this study received between 300 and 2100 mg of lithium carbonate per day and had been taking lithium for a minimum of 3 weeks or for as long as 17 years. Some patients were taking other psychotropic drugs, including phenothiazines and benzodiazepines. Because Na^+-Li^+ exchange rates are related to the occurrence of hypertension (95,96), blood pressure was measured at the time of blood drawing, and individuals suffering from hypertension were excluded from the study. Tables 22 and 23 are the demography of patients and controls, respectively.

IV.3B. Na^+/Li^+ Countertransport Rates

Washed packed RBCs (2 ml) were incubated in 10 ml Li^+-loading medium containing 150 mM LiCl, 10 mM glucose, and 10 mM HEPES, pH 7.4 at 37°C for 3 hours. After incubation in the Li^+-containing medium, to remove extracellular Li^+ from the Li^+-loaded RBCs we washed the cells five times by centrifugation at 7,000 g for 5 min in the choline wash solution. The Li^+-loaded RBCs (0.6 ml) were suspended in 6 ml in either isotonic Na^+ medium (150 mM NaCl, 10 mM glucose 0.1 mM ouabain, 10 mM HEPES, pH 7.4) or choline medium (100 mM choline chloride, 85 mM sucrose, 10 mM glucose, 0.1 mM ouabain, 10 mM HEPES, pH 7.4) at 37 °C for a 75 min-period measurement of the rates of Na^+-Li^+ exchange (95) by means of AA. Aliquots were taken every 15 min from each of the

Table 22. Demography of Bipolar Patients[a]

Patient	Sex	Race	Age	Weight (LBs)	Blood Pressure	$[Li^+]_s$ (mM)	Smoker	Inpatient
P1	F	W	69	242	124/60	0.074	N	Y
P2	F	B	43	230	125/75	0.010	N	N
P3	M	W	40	159	138/73	0.162	Y	Y
P4	M	W	53	205	143/90	0.133	Y	Y
P5	M	W	57	163	171/98	0.210	Y	Y
P6	M	W	22	132	120/80	0.196	Y	N
P7	M	W	34	205	131/69	0.173	Y	Y
P8	M	W	36	200	140/98	0.167	Y	Y
P9	M	W	30	151	100/70	0.258	Y	Y
P10	M	W	62	193	120/70	0.318	Y	N

[a]M = Male, F =Female, W = White, B = Black, Y = Yes, N = No, $[Li^+]$ = starting intracellular Li^+ concentration

Table 23. Demography of Matched Controls[a]

Controls	Sex	Race	Age	Weight (LBs)	Blood Pressure	Smoker
C1	F	W	65	149	134/78	N
C2	F	B	42	127	112/72	Y
C3	M	W	43	189	130/80	Y
C4	M	W	52	180	120/75	N
C5	M	W	55	197	160/100	N
C6	M	W	22	185	135/80	N
C7	M	W	37	210	124/90	N
C8	M	W	39	151	110/70	Y
C9	M	W	28	184	140/102	N
C10	M	W	63	185	160/70	Y

[a]Abbreviations are the same as for Table 21.

Li^+-loaded RBC suspensions and collected into precooled polyethylene tubes and centrifuged at 10,000 g for 2 min at 4 °C, and the supernatants were collected and analyzed by AA. Li^+ standards (10 - 200 μM Li^+) prepared in both Na^+ and choline media were used for construction of calibration curves. Li^+ transport in the choline medium occurred via the leak pathway; that observed in the Na^+ medium was mediated by both the Na^+-Li^+ exchange and the leak pathway. The rates of Na^+-Li^+ exchange were obtained by subtraction of the measured rates of Li^+ transport in the choline medium from those measured in the Na^+ medium (27,95).

Tables 24 and 25 list the rates of Na^+-Li^+ exchange in Li^+-loaded RBCs, the phospholipid composition, and the Li^+ binding constants for the RBC membranes of the ten bipolar patients receiving lithium carbonate and the ten matched normal individuals, respectively.

The rates of RBC Na^+-Li^+ exchange measured by AA were found to be significantly lower for the ten bipolar patients receiving lithium carbonate than for the ten normal individuals (0.14 $\pm$ 0.02 mmol Li^+/L of RBCs x h vs. 0.21 $\pm$ 0.06, mean $\pm$ SD, paired Student's t-test, $p < 0.003$, $n = 10$). The top two Na^+-Li^+ exchange rates shown in each table are for female, whereas the remaining values are for males; the exchange rates for female were lower than for males in the patient and control groups. These results are in agreement with those previously reported (27,35,95,124-127).

IV.3C. Interaction of Li^+ with RBC Membranes

We measured ^7Li T_1 values in the presence of isolated RBC membranes (containing Li^+ in the 1.0 - 15 mM range) from lithium-treated patients and matched normal individuals at

Table 24. Na^+-Li^+ Exchange Rates (in mmol Li^+/L RBCs x h), Phospholipid Composition (%), and Li^+ Binding Constants (M^{-1}) to RBC Membranes of Bipolar Patients Receiving Lithium Carbonate.[a]

Patient No.	Na^+-Li^+	PC	PS	PI	PE	Sph	K_b
P1	0.12	31.5	17.3	0.8	25.1	25.4	314
P2	0.13	29.6	15.7	1.3	26.1	27.3	333
P3	0.12	32.1	17.1	0.8	26.6	23.6	291
P4	0.11	34.3	15.8	0.9	25.2	23.8	285
P5	0.14	28.0	17.4	0.6	30.9	23.0	326
P6	0.20	33.7	18.7	0.7	26.7	20.3	243
P7	0.14	28.5	16.0	1.0	27.0	27.5	362
P8	0.12	30.0	15.7	0.4	30.3	23.7	297
P9	0.14	26.5	18.1	0.8	28.4	26.2	285
P10	0.14	29.2	17.8	0.6	31.4	21.1	247
Average[b]	0.14 ± 0.02	30.3 ± 2.5	17.0 ± 1.1	0.8 ± 0.2	27.8 ± 2.3	24.2 ± 1.1	298 ± 37

[a]The r^2 values are greater than 0.98 and 0.95, respectively, for the rates of Na^+-Li^+ exchange and for K_b values. The areas under the ^{31}P NMR resonances were normalized to 100% for the five major classes of phospholipids. The accuracy of the percentage composition for PC, PS, PE, and Sph is within ± 10% of the values listed in the table, whereas the accuracy of the PI values is within ± 20% because of baseline noise (108). For abbreviations, see text. [b]Values expressed as mean ± standard deviation.

Table 25. Na^+-Li^+ Exchange Rates (in mmol Li^+/L RBCs x h), Phospholipid Composition (%), and Li^+ Binding Constants (M^{-1}) to RBC Membranes of Matched Normal Individuals.[a]

Control No.	Na^+-Li^+	PC	PS	PI	PE	Sph	K_b
C1	0.15	28.8	17.0	0.7	29.2	24.2	276
C2	0.15	31.1	13.7	0.6	24.8	29.9	185
C3	0.32	25.9	16.2	0.4	32.5	25.6	224
C4	0.23	29.5	15.7	1.1	28.3	25.4	166
C5	0.19	29.1	17.7	1.1	27.8	24.3	178
C6	0.26	31.3	14.9	1.2	29.1	23.4	228
C7	0.17	28.3	15.1	1.4	29.7	25.4	253
C8	0.19	31.7	16.9	0.6	24.7	26.1	213
C9	0.18	29.3	14.7	0.5	31.7	23.4	183
C10	0.26	31.9	16.9	0.9	28.8	22.0	243
Average[b]	0.21 ± 0.06	29.7 ± 1.9	15.8 ± 1.2	0.9 ± 0.3	28.7 ± 2.5	25.0 ± 2.1	215 ± 36

[a] and [b] Same as for Table 23.

the same membrane protein concentration (2.9 ± 0.8 mg/mL). Figure 20 shows the ^7Li T_1 values observed upon titration with Li^+ of the unsealed membrane prepared from the RBCs of a lithium-treated patient and that from the RBCs of a matched normal individual. A statistically significant difference ($p < 0.05$) in ^7Li T_1 values was observed between the samples from the patient and the normal individual for Li^+ concentrations ≥ 15 mM. Similar results were obtained for the remaining matched pairs of patients and normal individuals. Li^+ ions are in fast exchange on the ^7Li NMR time scale; the observed ^7Li T_1 values therefore represent the weighted average of free Li^+ in the suspension medium and Li^+ bound to the RBC membrane. Free nuclei have large T_1 values, whereas those that are bound to the RBC membrane have relatively small T_1 values. The T_1 values for ^7Li increased in the presence of increasing concentrations of Li^+ in membrane samples of both patients and normal individuals (Figure 20) because of increasing fractions of free Li^+. These observations confirm that ^7Li T_1 values are dependent on Li^+ binding to RBC membranes. For a given Li^+ concentration, the amount of Li^+ bound to the T_1 values of ^7Li were greater for membrane samples (with the same protein concentration) from normal individuals than for samples from matched lithium-treated patients. For a given Li^+ concentration, the amount of Li^+ bound to the same amount of RBC membrane was larger for patients than for normal individuals. The Li^+ binding constants, as calculated from James-Noggle plots (see III.3C. and Fig. 19), to the RBC membranes from bipolar patients receiving lithium carbonate were significantly higher than those for normal individuals (298 ± 37 M^{-1} vs. 215 ± 36 M^{-1}, $p < 0.001$, $n = 10$). The observed ^7Li T_1 data and the calculated K_b values (Tables 24 & 25) indicate that Li^+ has a stronger affinity for RBC membranes of lithium-treated patients than for those of normal individuals.

Figure 20. ^{7}Li T_1 Values of RBC Membrane Samples from Patient 4 (open squares) and Normal Individual 4 (closed diamonds) in the Presence of Increasing Concentrations of Li^{+}. The numbering for the samples is the same as for Tables 12 and 13. The membrane protein concentration for this paired samples was 3.5 $\pm$ 0.1 mg/mL.

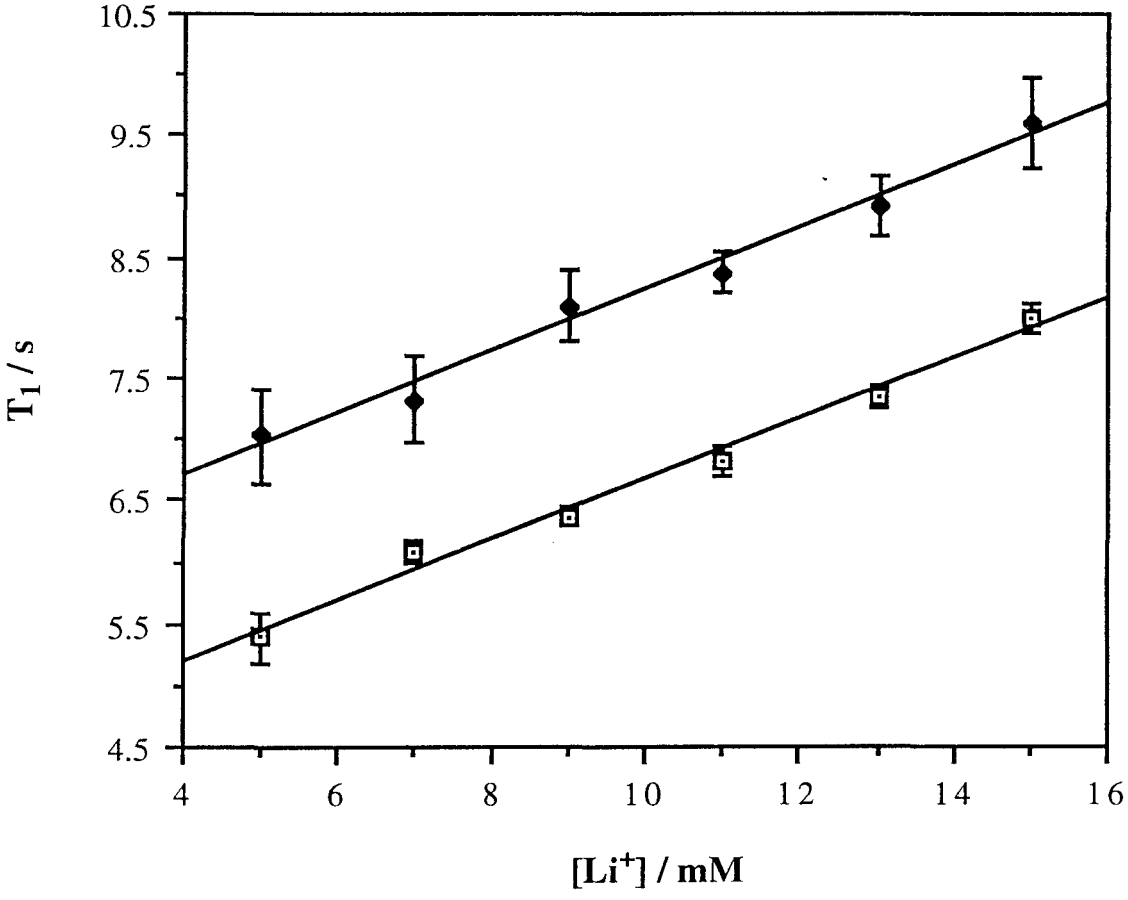
10.5
9.5
8.5
7.5
6.5
5.5
4.5
T_1 / s
4
6
8
10
12
14
16
[Li^+] / mM

IV.3D. Phospholipid Composition Analysis

Figure 21 shows a typical ^{31}P NMR spectrum of a phospholipid extract from a human RBC membrane. The assignments of the phospholipid resonances are indicated in the spectrum and were obtained as described in Section III.2I. The unassigned resonances downfield from the PE resonances are presumably due to derivatives of lysophosphatidic acid (107). Two types of PE and PC are clearly resolved in ^{31}P NMR spectra of phospholipid extracts of human RBC membranes. Regular PE or PC has alkyl ethers on the glyceride backbone, whereas PE plasmalogen (PEp) has an alkenyl ether and AAPC is an alkylacyl derivative of PC. The resolution of the two forms of PE and PC in ^{31}P NMR spectra was also observed in phospholipid extracts of other cell membranes (107,108,128). We added the areas under the two PE resonances to obtain the total PE composition. When one uses the areas under the ^{31}P NMR resonances to measure phospholipid composition, it is important to ensure that all the resonances are fully relaxed under the conditions used for recording the NMR spectrum. We compared the relative intensities of the signals obtained when using a delay between successive radiofrequency pulses of 4.0 s and 10 s. No statistically significant difference occurred between the percentage phospholipid compositions obtained with the two instrument settings, indicating that the experimental conditions specified in the caption to Figure 21 result in reliable quantitation of phospholipids in the RBC membrane. Edzes et al. (108) reported that, by increasing the percentage of chloroform in the solvent mixture, one can shift the PS resonance away from the PE/Sph envelope. We tested two different chloroform/methanol/water solvent mixtures (in ratios of 100:40:10, Fig. 21A, and 125:8:3, Fig. 21B) and found that, by increasing the percentage of chloroform in the solvent mixture, one can shift the PS resonance upfield and past the Sph resonance and completely resolve the

Figure 21. ^{31}P NMR Spectra of Phospholipid Extracts from Human RBC Membrane. The solvent mixture ratio of chloroform/methanol/0.2 mM EDTA was (A) 100:40:10 and (B) 125:8:3. The assignments of each resonance to the various phospholipids are shown on the spectrum. The symbols are: AAPC, alkylacyl PC; PC, phosphatidyl choline; PE, phosphatidyl ethanolamine; PEp, PE plasmalogen; PI, phosphatidyl inositol; PS, phosphatidyl serine; Sph, sphingomyelin. The positions of the resonances (chemical shifts) are reported relative to that of PC set at -0.84 ppm (parts per million). The spectrometer settings used for recording the one-dimensional spectrum were: pulse width, 7 μs (60° flip angle); acquisition time, 1.4 s; delay between successive radiofrequncy pulses, 4.0 s; number of scans, 10,000; spectral width, 1,050 Hz; spinning rate, 16 Hz; high power proton broadband decoupling, 55 dB.

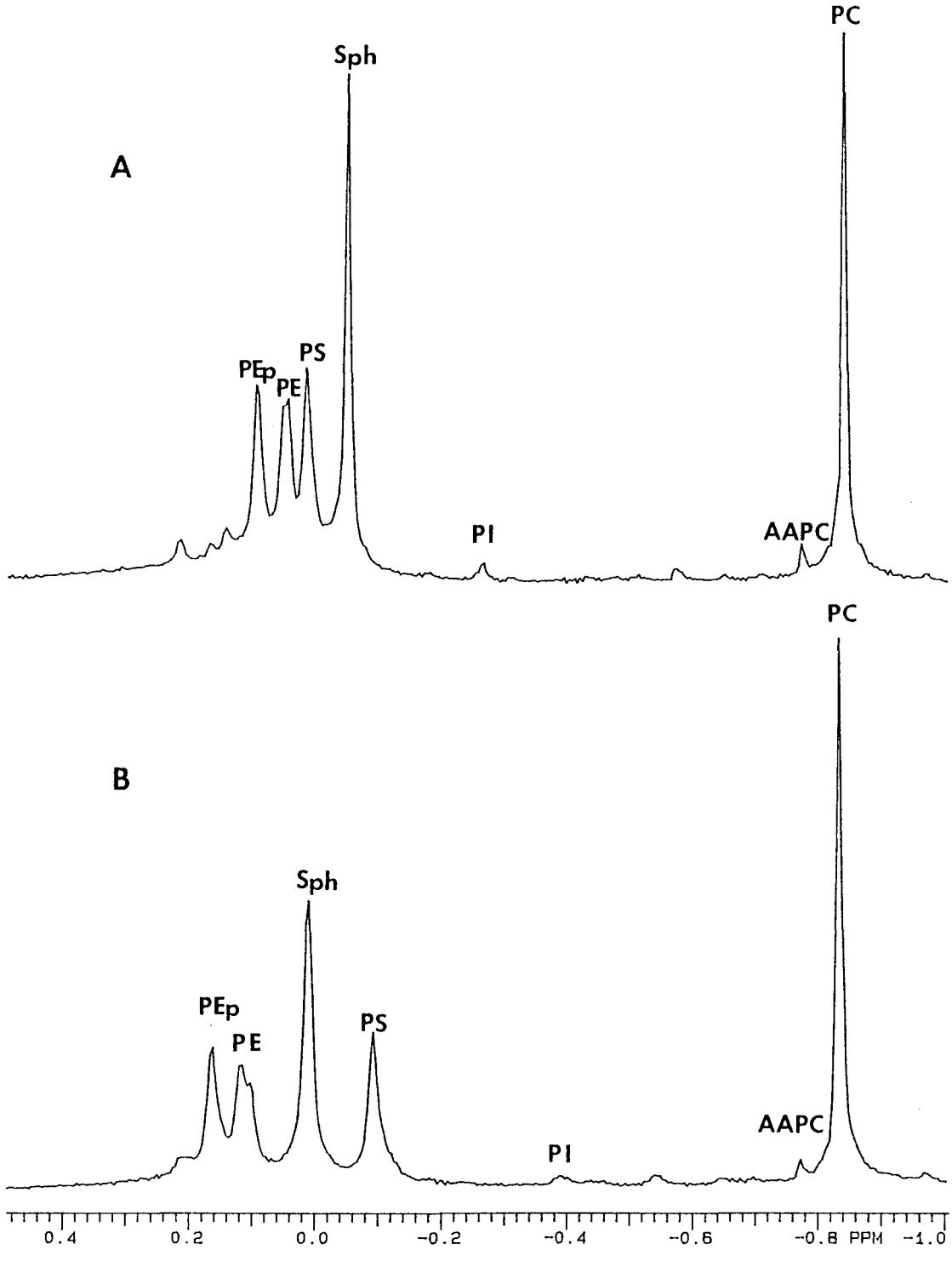
A
PC
Sph
PEp
PE
PS
PI
AAPC
B
PC
Sph
PEp
PE
PS
AAPC
PI
0.4
0.2
0.0
-0.2
-0.4
-0.6
-0.8 PPM
-1.0

PS resonance from other ^{31}P signals. We found no statistically significant difference in phospholipid composition between the two different solvent mixtures. The 125:8:3 ratio is recommended for future studies of phospholipid extracts of human RBC membranes because it simplifies the integration of the ^{31}P NMR spectra.

By using ^{31}P NMR spectroscopy, we found that the PS content in phospholipid extracts from RBC membranes was significantly lower for lithium-treated patients than for normal individuals ($17.0 \pm 1.1\%$ vs. $15.8 \pm 1.2\%$, paired Student's t-test, $p < 0.05$, $n = 10$). No significant differences were found between the patients and normal individuals for the anionic phospholipid PI and for the neutral phospholipids PE, PC, and Sph.

IV.3E. Correlation Analysis

Table 26 are data for a Pearson product-moment correlation. Significant positive correlations between the patient and control groups for the PS ($r = 0.46$, $p < 0.04$) and K_b ($r = 0.77$, $p < 0.001$) values, and significant negative correlations for the rates of Na^+-Li^+ exchange ($r = -0.67$, $p < 0.001$). These correlations are in agreement with the conclusions from the paired Student's t-test mentioned above. The rates of RBC Na^+-Li^+ exchange measured under standard assay conditions were significantly negatively correlated ($r = -0.56$, $p < 0.01$) with the Li^+ binding constants calculated from T_1 values measured in the presence of RBC membranes. No significant correlations were found between the Li^+ binding constants or the rates of Na^+-Li^+ exchange and the other phospholipids percentages.

Table 26. Pearson Product Moment Correlation For Li^+ Binding and Transport Parameters in RBCs from Bipolar Patients Receiving Lithium Carbonate and from Matched Normal Individuals.[a]

	Type[b]	PC	PS	PI	PE	Sph	Na^+-Li^+	K_b
Type[b]	1.00							
PC	0.15	1.00						
PS	0.46	-0.02	1.00					
PI	-0.11	0.07	-0.17	1.00				
PE	-0.19	-0.64	-0.01	-0.29	1.00			
Sph	-0.18	-0.30	-0.50	0.17	-0.42	1.00		
Na^+-Li^+	-0.67	-0.19	-0.13	0.01	0.38	-0.14	1.00	
K_b	0.77	-0.05	0.25	0.08	-0.13	0.05	-0.56	1.00

[a]Correlation coefficients ≥ 0.4 are considered significant ($p \leq 0.05$). [b]Type refers to a comparison of parameters between lithium-treated bipolar patients and normal matched individuals.

CHAPTER V

DISCUSSION

V.1. Competition Between Li^+ and Mg^{2+} for the Substrates of Second Messenger Systems, and RBC Membrane

Because of the similarity between Li^+ and Mg^{2+}, it is possible that Li^+ exerts its pharmacological effects by competing with Mg^{2+} for its enzyme binding sites in second messenger systems. G proteins and adenylate cyclase are magnesium activated, and the phosphoinositide turnover system which is G protein activated also has potential binding sites for cations (14,16). Therefore, I addressed the question of competition between Li^+ and Mg^{2+} for substrates of the second messenger systems, including GTP, GDP, AMP, cAMP and IP_3. pH, ionic strength, and temperature are factors on which metal ion binding to nucleotides are known to be dependent (129); we controlled all these factors in our experiments except for IP_3. The bulky organic cations Tris and tetramethylammonium were selected to adjust pH and ionic strength because they would not compete with metal cation binding to the enzymes. Because of the stacking property of nucleotides (130) and the low sensitivity of the NMR measurement, the concentrations of the nucleotides were in the range of 5 mM to 10 mM. The concentration of IP_3 was between 2 mM and 4 mM.

In aqueous solutions of AMP, cAMP, GTP and GDP, we investigated whether metal ion binding to nucleotides takes place via the base, sugar, or phosphate moiety. We probed

metal ion binding to the base and sugar domains by using ^{1}H and ^{13}C NMR, whereas we studied metal ion binding to the phosphate groups by ^{31}P NMR. We also studied competition between Li^{+} and Mg^{2+} ions for binding sites in guanine nucleotides by using ^{7}Li NMR relaxation measurements and ^{31}P NMR chemical shifts.

^{7}Li spin-lattice relaxation values decreased with increasing concentration of GTP or GDP (Figure 6), confirming that ^{7}Li T_1 values are dependent on Li^{+} binding to guanine nucleotides. This behavior was similar to that previously reported for ATP and ADP (23). In the presence of increasing concentrations of Mg^{2+}, the ^{7}Li T_1 values increased because of displacement of Li^{+} by Mg^{2+} from GTP- and GDP-binding sites, which indicated that simultaneous binding of Li^{+} and Mg^{2+} to GTP and GDP had occurred, in a manner analogous to what were observed for ATP and ADP (23). However, no differences were observed in LiCl solutions upon addition of AMP or cAMP; the interaction between Li^{+} and AMP or cAMP was too weak to be detected by relaxation measurements.

No significant chemical shift changes were observed in the ^{1}H and ^{13}C NMR spectra of GTP and GDP upon addition of saturating amounts of Li^{+} and Mg^{2+} (Table 2); no direct metal ion binding to the base or sugar moieties of GTP or GDP was present. The small ^{13}C chemical shift changes observed are probably due to proximity of metal ions to the sugar or base domains, or to a change in nucleotide conformation upon addition of metal ions. Similar ^{13}C NMR results were obtained with aqueous solutions of cAMP and AMP.

By using ^{31}P NMR spectroscopy, downfield shifts of the phosphate resonances were observed upon addition of metal ions to GTP or GDP solutions. This probably occurred from polarization of the electron density away from the phosphorus atoms when metal cations were bound to the phosphate groups of GTP or GDP. The shifts experienced by the α-

phosphate resonance were very small, while the γ-phosphate resonance, and to a greater extent that of the β-phosphate, moved downfield. Therefore, the α-phosphate resonance was used as an internal standard; the chemical shift separation between α- and β-phosphate resonances of GTP or GDP ($\delta_{\alpha\beta}$) reflects the extent of metal ion binding to GTP and GDP. As shown in Figure 9, the value $\delta_{\alpha\beta}$ of GTP decreased in the presence of saturating concentrations of either Li^+ or Mg^{2+}. An intermediate value of $\delta_{\alpha\beta}$ was observed in Li^+ saturated GTP solutions containing 1.5 mM Mg^{2+}, suggesting competition of these two cations for phosphate groups in GTP (Figure 9C). Similar observations were found in GDP solutions; however, the chemical shift changes of the two phosphate resonances were not as large as for GTP at the same concentrations because of the lower affinity of Li^+ and Mg^{2+} to GDP.

Using the ^{31}P NMR chemical shifts for the phosphate resonances of GTP and GDP, three different models (see III.3A.) were applied to generate binding constants. For GTP in the presence of LiCl alone, the Σ^2 values in Table 5 suggest that the best nonlinear least-squares fit to the ^{31}P NMR data was the model based on a mixture of 1:1 (LiGTP) and 2:1 (Li_2GTP) species (third model). The theoretical chemical values (δ_{theor}) for this model, as well as those for the first model based on 1:1 species, however, are unrealistic and showed no convergence in some cases. The binding constants for the 2:1 species were larger than those for the 1:1 species for both the Li-GTP and Li-GDP complexes, irrespective of the fitting model used. Based on both Σ^2 and δ_{theor} values, the overall best fits for the stoichiometry of Li^+ complexes of GTP or GDP are those in which Li_2GTP and Li_2GDP species predominate with binding constants, respectively, of $550 \pm 200\ M^{-2}$ and $60 \pm 15\ M^{-2}$. The 2:1 species also predominated in aqueous solutions of ATP or ADP in the presence of Li^+ alone (23). The calculated binding constants were higher for Li_2GTP than for Li_2GDP because of the

higher charge of GTP than of GDP.

The fit of the ^{31}P chemical shift data for the Mg-GTP and Mg-GDP complexes (Table 5) yielded δ_{theor} values which were consistent with the observed data. The binding constants obtained, $2x10^4$ M^{-1} and $1x10^4$ M^{-1}, agree with those reported previously for GTP and GDP (131,132). The fit of the ^{31}P chemical data for the Mg^{2+} titration of GTP or GDP was insensitive, however, to the absolute values of the binding constants as manifested by large Σ^2 values (Table 5).

The ^{31}P chemical shifts for Li^+/Mg^{2+} mixtures of GTP or GDP were interpreted based on the three models for the predominant species in solution; the binding constants and the theoretical limiting chemical shifts are summarized in Table 6. For GTP, the third model which assumed the presence of both LiGTP and Li_2GTP species in Li^+/Mg^{2+} mixtures yielded the best Σ^2 values and reasonable δ_{theor} values. The binding constants for the 1:1 species, however, were very small, indicating that the Li_2GTP species predominates in Li^+/Mg^{2+} mixtures, having an overall binding constant of 1060 ± 350 M^{-2}. The overall binding constant of Li^+ to GTP is not significantly different in the absence (550 ± 200 M^{-2}) or in the presence of Mg^{2+} (1060 ± 350 M^{-2}). For GDP in Li^+/Mg^{2+} mixtures, no convergence was found when only the presence of LiGDP species in solution was assumed (first model). While good convergence was found for the β-phosphate resonance of GDP when we used the second model (Li_2GDP species only), better convergence was found for both the α- and β-phosphate resonances with the third model (mixture of LiGDP and Li_2GDP). The third model, however, yielded unrealistically high Li^+ binding constants for GDP and poor agreement between observed and theoretical limiting ^{31}P chemical shifts. The most reliable Li^+ binding constant for GDP in the presence of Mg^{2+} is that of the β-phosphate resonance of the Li_2GDP species

with the second model, 645 M^{-2}, which is higher than that calculated from ^{31}P data measured in the absence of Mg^{2+} (60 $\pm$ 15 M^{-2}). The large error involved in the calculation of the binding constants indicates, however, that this difference may not be significant. The increase in the calculated Li_2GDP binding constant in the presence of Mg^{2+} suggests that simultaneous binding of Li^+ and Mg^{2+} to the two phosphate groups of GDP may be present. The ^7Li T_1 values in Li^+/Mg^{2+} mixtures in the presence of GDP (Figure 6) are consistent with competition between Li^+ and Mg^{2+} for the same binding sites in GDP. Thus, the common Li^+ and Mg^{2+} binding sites in GDP are not the sugar and base domains (Table 6), but presumably the α- and β-phosphate groups of GDP.

^{31}P NMR measurements of cAMP and AMP showed no changes in chemical shifts upon metal ion addition, except for the sample of AMP containing a high concentration of Mg^{2+} (50 mM) where a small upfield shift was found. The stability constant of AMP to Mg^{2+} is known to be very weak (93 M^{-1}) (133) compared to those of ATP (1.15 x 10^5 M^{-1}) and GTP (1.05 x 10^4 M^{-1}); therefore only small changes are observed in the ^{31}P NMR spectrum of AMP at high Mg^{2+} concentration. The upfield shift was due to the interaction between Mg^{2+} and AMP which changed the torsion angle of the phosphate group of AMP; an increase in bond angle results in an upfield chemical shift (134). The charge of cAMP is lower than that of AMP at the same pH; Li^+ and Mg^{2+} binding to cAMP should be weaker than to AMP and can ont be observed by ^{31}P NMR spectroscopy (Table 9). Though Li^+ and Mg^{2+} interact weakly with cAMP, it is still possible for competition between Mg^{2+} and Li^+ to exert an effect on the activity of adenylate cyclase via metal ion competition to the phosphate groups of ATP.

Similar ^7Li spin-lattice relaxation measurements were obtained for IP_3 as for GTP and

GDP, indicating competition between Li^+ and Mg^{2+} for binding sites in IP_3 (Figure 11). No changes were observed in the ^1H NMR spectra of IP_3 in the presence of excess amounts of Li^+ or Mg^{2+} (Figure 12A; Table 12), suggesting that the phosphate groups are the only potential binding sites for metal ions in IP_3.

Upfield shifts in the ^{31}P phosphate resonances, predominantly with the 4- and 5-phosphates of IP_3 were found upon addition of Li^+ or Mg^{2+}, suggesting interaction of Li^+ and Mg^{2+} to the 4- and 5-phosphate groups of IP_3. This observation is consistent with the previous study in 50 mM-Tris/100 mM-KCl, and at pH 7.1 (135). The metal ion interactions probably affected the conformation of IP_3, which caused the change in *p*-orbital symmetry and in the O-P-O torsion angle (134). No study on conformational changes was reported for Ins(1,4,5)P_3 upon addition of Li^+ or Mg^{2+}, but a similar conformational change was observed in sodium phytate by addition of Li^+ (136).

The binding constant of Mg^{2+} to Ins(1,4,5)P_3 was measured by ^1H NMR to be 281 M^{-1} at pH 6.9 and low ionic strength; and it decreased with the ionic strength (135). Though the Li^+ binding constants to Ins(1,4,5)P_3 have not been reported, they have already been studied by potentiometry in solutions of Ins(1,2,6)P_3 at 25 °C in 0.1 M But_4NBr; they were 240 M^{-1} and 4000 M^{-2} at 1:1 and 2:1 ratio, respectively (137). However, the binding constant for Mg^{2+} to Ins(1,2,6)P_3 was 4.0 x 10^5 M^{-1} under similar conditions (138). It seems that the affinity of Mg^{2+} changed drastic from Ins(1,2,6)P_3 to Ins(1,4,5)P_3; this may not be real but due to the different experimental conditions and methods used. Nonetheless, based on the information currently available, we conclude that the interaction of Li^+ and Mg^{2+} to phosphate groups in Ins(1,4,5)P_3 is not negligible.

By using NMR spectroscopy, we found that ATP, GTP, GDP and IP_3 are the potential

target sites for Li^+ in second messenger systems. As a result, we conclude that Li^+ may achieve its pharmacological effect on G proteins, adenylate cyclase and phosphoinositide turnover by competing with Mg^{2+} for phosphate-binding sites, in ATP, GTP, GDP and IP_3.

The mechanism of Li^+ action on second messenger systems is not clear. It could exert its effect via G proteins, by competition with Mg^{2+} binding sites, and regulate adenylate cyclase and phosphatidyl inositol turnover. However, it is also possible for Li^+ to exert its effect directly on adenylate cyclase by the same mechanism via competition with Mg^{2+} binding sites in ATP. The phosphatidyl inositol turn over system is complex with many potential sites for Li^+ interaction. The inhibition of Mg^{2+} on Ins(1,4,5) binding to its receptor was also found in human uterine membranes (139) and in dog cerebellum (140), suggesting Mg^{2+} may exert an important regulatory control on the release of Ca^{2+} by Ins(1,4,5)P_3. The proposed mechanism involves direct chelation of Mg^{2+} by Ins(1,4,5)P_3 or by its receptor. White et al. (135) suggested the latter postulation based on the low affinity of Mg^{2+} for Ins(1,4,5)P_3 which they observed at physiological ionic strength. It has been reported that Li^+ inhibited the Mg^{2+}-dependent inositol monophosphatase enzyme (22). The effect of Li^+ is not simply restricted to inositol monophosphatase; it can also inhibit other enzymes involved in phosphatidyl inositol turnover such as $InsP_2$, $InsP_3$ and $InsP_4$ phosphatase (141). It is therefore still questionable whether Li^+ exerts its effect directly on Ins(1,4,5)P_3 or indirectly by changing its accumulation rate. Nevertheless, Li^+ could compete with Mg^{2+} for binding to Ins(1,4,5)P_3. Metal ion competition could potentially lead to a change in the interaction between IP_3 and its receptor resulting in different amounts of released Ca^{2+}.

We used Li^+ concentrations that were approximately ten times higher than those present in the intracellular compartments of bipolar patients receiving lithium carbonate. The

sensitivity of the NMR methods used in this investigation would not enable us to observe appreciable changes at lower concentrations of Li^+. With more sensitive methods of Mg^{2+} analysis, such as fluorescence, it may be possible to determine whether a Li^+/Mg^{2+} competition mechanism for phosphate-binding sites in GTP bound to a purified G protein or other substrates of the second messenger systems operates at therapeutic Li^+ concentrations.

Most ligands that bind Li^+, including ATP, will also bind Mg^{2+} and Ca^{2+} with even higher affinity (142). When ligands with high Mg^{2+} affinity (e.g., the RBC membrane) are also present, the absolute values of the stoichiometric binding constants do not necessarily reflect the tendency of Li^+ to bind preferentially to ATP. Based on the calculations of conditional binding constants, it was found that the organic ligands uramildiacetate and o−carboxyphenyliminodiacetate, which have a set of three oxygens and one nitrogen coordination sites, can compete for one-fourth or one-half of the Mg^{2+} bound to 3.2 mM ATP (142). The intracellular Li^+ and Mg^{2+} concentrations are of the same order of magnitude in tissues of manic-depressive patients undergoing lithium therapy; the Ca^{2+} concentrations are however four to five orders of magnitude smaller than those of Li^+ implying that Ca^{2+} dose not appreciably compete with Li^+ for binding to biological ligands. The intracellular Na^+ and K^+ concentrations are approximately two orders of magnitude larger than those of Li^+; any ligand with conditional binding constants which are two log units smaller for Na^+ and K^+ than for Li^+ will preferentially bind Li^+. Most ligands meet this criterion, and therefore competition between Li^+ and Mg^{2+} can conceivably take place in the presence of physiologically relevant intracellular Na^+ and K^+ concentrations (142).

Based on ^7Li T_1 data, the calculated stoichiometric binding constants of Mg^{2+} and Li^+ to the RBC membrane were approximately 3.3×10^3 M^{-1} ($K_{Mg\text{-}M}$) and 1.7×10^2 M^{-1} ($K_{Li\text{-}M}$).

Based on ^{31}P chemical shift data (23), the binding constant for the species MgATP was calculated to be approximately 2.0 x 10^4 M^{-1} (K_{MgATP}), whereas from ^7Li T_1 data, the overall binding constants for the species LiATP and Li_2ATP were approximately 8.7 x 10^2 M^{-1} (K_{LiATP}), and 1.1 x 10^4 M^{-2} (β_{Li_2ATP}), respectively.

In the presence of ATP, the conditional binding constants for Mg^{2+} ($K'_{Mg\text{-}M}$) and Li^+ ($K'_{Li\text{-}M}$) binding to the RBC membrane were derived (Section III.3C.). The conditional binding constants are dependent on free concentrations of ATP ($[ATP]_f$) and Li^+ ($[Li^+]_f$). Figure 22 shows the calculated conditional binding constants, obtained from equation (21) and (22), as a function of free ATP concentration (in the range 10^{-4} M to 1 M). Equation 22 requires an estimate of the free Li^+ concentration; to obtain an approximate concentration of free Li^+, we assumed that most Li^+ was bound to ATP in the form of Li_2ATP. For a typical total intracellular Li^+ concentration of 1.0 mM, the free Li^+ concentrations are of the order of 10^{-4} M; therefore, the term $2[ATP]_f[Li^+]_f\beta_{Li_2ATP}$ in equation 22 does not significantly affect the estimation of $K'_{Li\text{-}M}$. For $[ATP]_f$ values larger than 1.0 mM (Fig. 22), Li^+ will bind as strongly as Mg^{2+} to the RBC membrane. Typical free intracellular ATP concentrations in RBCs are of the order of 0.2 mM. From Figure 22, we estimate, for typical free intracellular ATP concentrations ($-\log[ATP]_f = 3.69$), that the ratio of the conditional binding constants of Mg^{2+} over Li^+ to the RBC membrane is approximately 4. In contrast, in the absence of ATP the ratio of the stoichiometric binding constants of Mg^{2+} over Li^+ to the RBC membrane is approximately 20. These calculations indicate that, for typical intracellular $[ATP]_f$ values, Li^+ can compete with approximately 25% of Mg^{2+} binding sites in the RBC membrane. As the total intracellular Li^+ concentration increases in RBCs, the free concentration of ATP decreases and the ratio of conditional binding constants increases.

Figure 22. Logarithmic Plot of Mg^{2+} (dots) and Li^{+} (crosses) Conditional Binding Constants to the RBC Membrane against Free ATP Concentration.

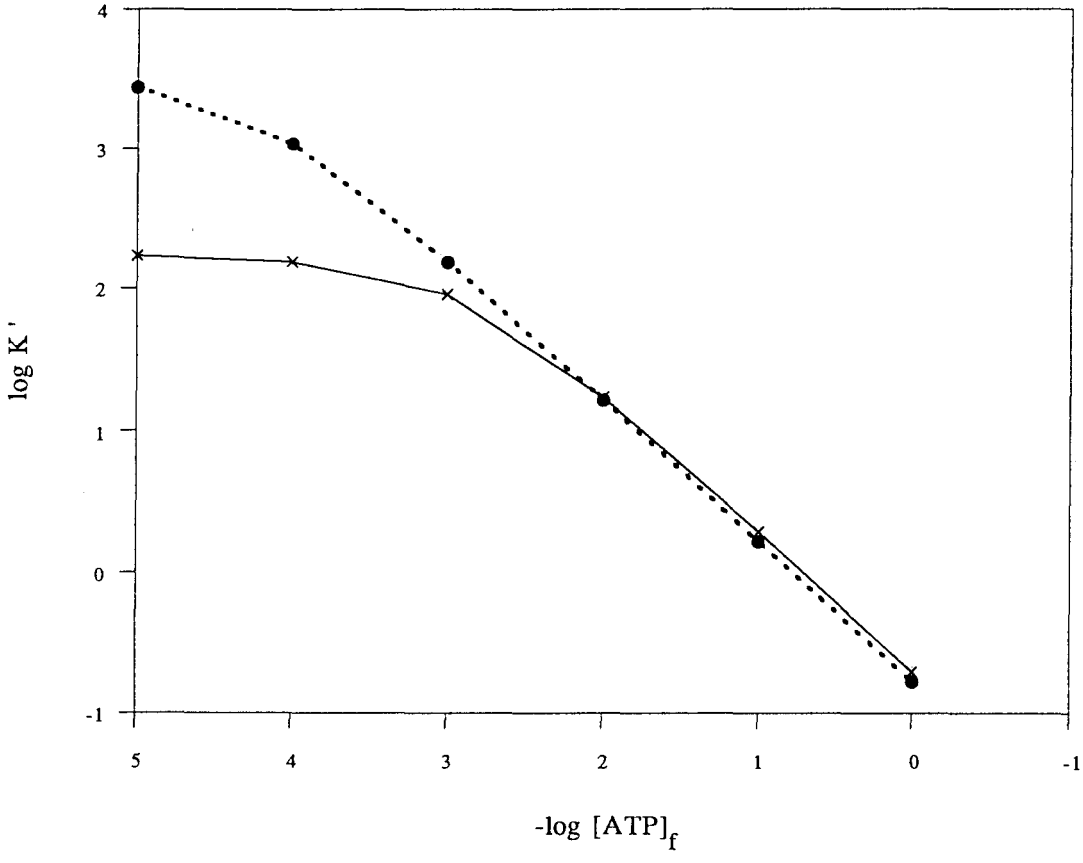
4
3
2
1
0
-1
log K '
5
4
3
2
1
0
-1
-log [ATP]f

Thus, in the presence of both ATP and RBC membrane, Li^+ can compete with some of the Mg^{2+} bound to ATP and to the RBC membrane. Competition between Mg^{2+} and Li^+ for ATP coupled with binding of the displaced Mg^{2+} to the RBC membrane of Li^+-loaded RBCs is therefore energetically favorable.

V.2. Transmembrane Difference on ^7Li NMR T_1 Values, and on the Rate of Li^+ Uptake in Human RBCs

RBCs contain hemoglobin (Hb) which is a mixture of oxy and deoxy forms. Whereas the form of Hb present in deoxyRBC is paramagnetic, that present in CORBC is diamagnetic (98,99). Two types of RBCs were prepared to examine the paramagnetic effect on intracellular ^7Li T_1 values. Despite the different magnetic environments of intracellular Li^+ in deoxyRBC and CORBC samples, the intracellular ^7Li T_1 values observed in the two cell suspensions are in good agreement (6.7 ± 0.1 s vs. 5.9 ± 0.1 s, n=2); thus, a transmembrane difference in ^7Li T_1 values can be observed in human RBC suspensions irrespective of the state of cell oxygenation.

Komoroski and coworkers (109) found that, for a Li^+ concentration of 50 mM at a high hematocrit (85%) and at 37 °C, the extracellular $^7Li^+$ T_1 value was 8.2 ± 0.8 s, whereas the intracellular $^7Li^+$ T_1 value was 6.5 ± 1.0 s. In contrast, our intracellular $^7Li^+$ T_1 value at 85% hematocrit and at 37 °C was consistent with theirs, but our extracellular T_1 value was at least twice as great, though the extracellular $^7Li^+$ T_1 value at 84% hematocrit was significantly lower ($p < 0.05$) than the values obtained at hematocrits of 11, 33, 45 and 67%. The lower extracellular $^7Li^+$ T_1 value at 84% hematocrit may be associated with the rise in sample viscosity at this hematocrit. The hematocrit-independent intracellular $^7Li^+$ T_1 values

are controlled mostly by Li^+ binding to the RBC membrane, and not by intracellular viscosity (92,122).

It is difficult to establish the source for this discrepancy because the procedures for the sample preparations used in the previous relaxation studies were not explicitly stated (109). The observed $^7Li^+$ T_1 values in RBC suspensions are a weighted average of the T_1 values for free and bound Li^+ ions; the observed values are dependent on the Li^+ concentration in each cell compartment. We do not know whether the Li^+ concentrations shown in their Table 1 (109) refer to the concentration of the Li^+-loading medium or represent the actual intra- and extracellular Li^+ concentrations. Alternatively they may represent the average Li^+ concentration over the entire RBC suspension. The possibility that their reported Li^+ concentrations represent the actual concentrations of Li^+ in the two cell compartments is unlikely because the highest intracellular Li^+ RBC concentrations that can be obtained after 12 h of incubation are typically in the range of 10 to 15 mM (95,143), as opposed to the 50 mM concentration stated in their Table 1 (109).

The total accumulation time for their T_1 measurements was not specified (109). Within 1 h of incubation, an appreciable amount of Li^+ influx and efflux will occur, particularly with RBCs suspended in a Na^+-containing medium (27,95,143). The "NMR buffer" which was used in the previous study (109) contained a high concentration of Na^+, whereas in our relaxation experiments we minimized the amount of Na^+-Li^+ exchange by using a choline-medium. In our study, the extracellular $^7Li^+$ T_1 values for fresh Li^+-free RBCs suspended at 85% hematocrit in an isotonic medium containing 50 mM LiCl, 62 mM choline chloride, 10 mM glucose, 85 mM sucrose, and 10 mM HEPES, pH 7.4, after 15 and 75 min, respectively, were 14.8 $\pm$ 0.5 s and 13.5 $\pm$ 0.9 s (n = 2); the intracellular Li^+ concentration after 75 min

as determined by AA was 1.7 mM. However, the extracellular $^7Li^+$ T_1 value for fresh Li^+-free RBCs suspended at 85% hematocrit in an isotonic medium containing 5 mM LiCl, 105 mM choline chloride, 10 mM glucose, 85 mM sucrose, and 10 mM HEPES, pH 7.4, after 75 min was 10.5 $\pm$ 1.5 s (n = 2); the intracellular Li^+ concentration determined by AA was 0.3 mM. Thus, we were also able to observe shorter T_1 values in RBC suspensions incubated for at least 1 h with Li^+ at low extracellular concentrations; however, the T_1 values measured under these conditions are not due to extracellular Li^+ alone, but to a mixture of intra- and extracellular Li^+ ions.

Whether the ideal osmolarity of the incubation medium was maintained at 300 mosM in the previous study (109) is not clear. If the Li^+ concentrations reported in their Table 1 (109) refer to the average Li^+ concentration over the entire RBC suspension, their cell suspensions would be far from being isotonic. A solution of 50 mM LiCl has an ideal osmolarity of 100 mosM; if no other salts are added, it will constitute a hypotonic medium for RBCs which can induce cell lysis. We also observed T_1 values in the range of 8.0 to 13.0 s for Li^+-free RBCs incubated in a hypotonic medium containing 50 mM LiCl alone; an appreciable amount of cell lysis was present, however, in these RBC suspensions, as indicated by the high concentrations of hemoglobin (approximately 2.0 mM) present in the supernatant. The partial lysis of RBC suspensions, which occurs upon incubation in a hypotonic medium, affords decreased extracellular ^7Li T_1 values because the observed values represent a mixture of intra- and extracellular Li^+ ions, and because hemoglobin, which is known to bind Li^+ weakly, is present in the suspension (119,144).

Possible reasons for the inability of Komoroski et al. (109) to observe a transmembrane difference in T_1 values in human RBC suspensions (109) may be related to uncontrolled

osmolarity of the incubation medium and consequently to cell lysis, Na^+/Li^+ exchange induced by the presence of Na^+ in the suspension medium, and/or Li^+ redistribution across the RBC membrane during the course of a long relaxation measurement. The precautions have described in detail (82,86) to be taken during ^7Li MIR measurements of Li^+ transport in human RBC suspensions. Although the relaxation behavior of the spin 3/2 ^7Li nucleus is complex (77,109,122), it should be possible to explore both ^7Li T_1 and ^7Li T_2 values to obtain novel information concerning the biological action of Li^+ in manic-depressive patients (27,92,145).

Using nuclear magnetic resonance methods, we found, for a given starting Li^+ concentration in the extracellular medium, that the initial rate of Li^+ influx into fresh human red blood cells (RBCs) from an isotonic medium decreased with increasing hematocrit (Table 14A and Figure 15).

In previous ^7Li NMR transport experiments, Komoroski et al. (109) varied the hematocrit, initial extracellular Li^+ concentration, and temperature simultaneously (Fig. 1 of ref. 109). The initial rate of Li^+ uptake in RBC suspensions is expected to increase with increasing initial extracellular Li^+ concentration. With increases in both the hematocrit to 85% and in the starting extracellular Li^+ concentration to 50 mM, the percentage of intracellular Li^+ that they observed at 85% hematocrit was lower than that at 45% hematocrit and at a lower initial extracellular Li^+ concentration, 1.8 mM (Table 14B) (109). If they had monitored the initial Li^+ influx in terms of intracellular Li^+ concentrations, and not in percentages of intracellular Li^+ relative to the total amount of Li^+ present over the entire RBC suspension, they would also have found that the initial rate of Li^+ uptake increases with simultaneous increases in hematocrit and starting extracellular Li^+ concentration (Table 14B),

as predicted above. Although two different temperatures (25 °C and 37 °C) were used in their experiments (109), it is unlikely that this temperature difference significantly affected the pharmacokinetics of Li^+.

In separate procedures (Fig. 2 of ref. 109), Komoroski et al. observed that the percentage of intracellular Li^+ measured after 12 h of incubation in an RBC suspension having an average Li^+ concentration of 3.5 mM over the entire sample increased with increasing hematocrit; based on this observation, they concluded that the rate of Li^+ uptake into RBCs increased with increasing hematocrit. Because the amount of Li^+ added to the suspension medium was constant, the starting extracellular Li^+ concentration increased (from 3.7 mM to 11.7 mM) with increasing hematocrit (from 5% to 70%). Moreover, the percentage of intracellular Li^+ at a higher hematocrit may appear to be larger than that at a lower hematocrit because of the larger number of cells in the NMR window, and not because of an increase in intracellular Li^+ concentration with increasing hematocrit. If they had also monitored Li^+ influx in their second set of experiments in terms of intracellular Li^+ concentrations, they would again have found that the limiting intracellular Li^+ concentration decreases with increasing hematocrit after 12 h of incubation (Table 14C). The equilibrium concentration gradient also increases with increasing hematocrit (Table 14C), as under our experimental conditions. The "NMR buffer" used by Komoroski et al. (109) contained a high concentration of Na^+ (140 mM). Under these conditions, a significant amount of Li^+ efflux via the Na^+-Li^+ exchange pathway (intracellular Li^+ exchanging with extracellular Na^+) occurs after 12 h of incubation. The extent of Li^+ efflux via the Na^+-Li^+ exchange pathway also depends on hematocrit (27,95,143). In our experiments (Fig. 15), we minimized the contribution of Na^+-Li^+ exchange by using an incubation medium that contained the K^+, and not the Na^+, form

of the shift reagent, and by monitoring Li^+ influx every hour over a shorter incubation time (8 h vs. 12 h); the residual amount of Na^+ in the shift reagent (8.0 mM Na^+ concentration in the suspension) is unlikely to cause significant Li^+ efflux via the Na^+-Li^+ exchange pathway. Although the K^+ medium used in our studies is less relevant physiologically than is the Na^+ medium used in the previous study (109), no direct conclusions can be drawn concerning Li^+ influx into RBCs suspended in a Na^+ medium because of the existence of the Na^+-Li^+ exchange pathway (27,95,143). Thus, in their second set of experiments (Fig. 2 of ref. 109), Komoroski et al. (109) also varied two parameters simultaneously, both the starting extracellular Li^+ concentration and the hematocrit, and did not allow for Li^+ efflux via the Na^+-Li^+ exchange pathway. This led to a misleading conclusion concerning the effect of hematocrit on Li^+ uptake in RBC suspensions.

A comparison of the Li^+ transport results obtained from our experiments, in which only one experimental parameter was changed (Table 14A), with Komoroski's results in which three parameters (Table 14B) or two parameters (Table 14C) were changed simultaneously, could lead to misleading conclusions regarding the effect of hematocrit on Li^+ uptake in RBC suspensions. We clarified in the present study the effect of hematocrit on the pharmacokinetics of Li^+ through the definition of various Li^+ uptake transport parameters, namely, initial rate of Li^+ influx, limiting values of both intracellular Li^+ concentration ($[Li^+]^{\infty}_{in}$) and Li^+ percentage ($\%Li^{+\infty}_{in}$), and equilibrium concentration gradient. Table 14 shows that, in all experiments, the equilibrium concentration gradient increased with increasing hematocrit. The decrease in $[Li^+]^{\infty}_{in}$ values with increasing hematocrit obtained in our experiments (Table 14A) was in agreement with Komoroski's second set of experiments (Table 14C), but there were discrepancies with their first set of data (Table 14B) regarding the effect

of hematocrit on the initial rate of Li^+ uptake, and on $[Li^+]^{\infty}_{in}$ and $\%Li^{+\infty}_{in}$ values. These discrepancies result from the large increase in the starting extracellular Li^+ concentration, which limits the loading capacity of RBCs with Li^+ as manifested by the decreased $\%Li^{+\infty}_{in}$ values at high hematocrit (Table 14B). Regarding the initial rates of Li^+ influx, one would anticipate that, for a fixed starting extracellular Li^+ concentration and at a lower hematocrit, extracellular Li^+ can more rapidly populate the membrane transport sites, leading to a higher initial rate of Li^+ influx, which we indeed observed (Table 14A). At high starting extracellular Li^+ concentrations, the membrane transport sites may be saturated with Li^+ at all hematocrits, leading to an increase in initial rates of Li^+ influx with increasing hematocrit (Table 14B).

In conclusion, depending upon the way in which the Li^+ concentration is defined in the blood sample, it may appear that changes in hematocrit have opposite effects on the rate of Li^+ uptake in cell suspensions. Because bipolar patients receiving a given dose of lithium carbonate have the same starting extracellular Li^+ concentration, and not necessarily the same starting Li^+ concentration over the whole cell suspension (cells plus plasma), the uptake of Li^+ in cells from patients with reduced cytocrit values is expected to be faster initially than that in cells from patients with normal cytocrit values. Patients with reduced cytocrit values would also have an increased limiting intracellular Li^+ concentration. In patients with reduced cytocrit values, such as anemic patients or human immune deficiency virus-infected individuals on zidovudine therapy (146), toxicity could develop when lithium therapy is initiated. However, because Li^+ itself also induces the production of granulocytes (147), patients receiving long-term lithium therapy will most likely have normal rates of Li^+ uptake.

V.3. Identification of Li^+ Binding Sites in Erythrocytes

Slow motions contribute only to T_2 whereas fast motions such as those components of motions at the resonance frequency contribute to both T_1 and T_2 (116). The observation of a large difference between $^7Li^+$ T_1 and T_2 values in Li^+-loaded RBCs (Table 15) is indicative of a long correlation time for intracellular Li^+. When Li^+ ions are subject to substantial electric field gradients or are immobilized in the membrane, the ^7Li T_1/T_2 ratio increases; the larger the ratio, the stronger the interaction. We therefore used ^7Li T_1/T_2 ratio measurements to determine the internal and external Li^+ binding sites in RBC suspensions.

Based on the known RBC composition, one can predict what the Li^+ binding sites might be. Glycophorins account for 90% of the total sialic acid residues and thus the outer cell surface has a negative charge (148). In principle, these residues can interact or bind the positively charged Li^+ ion. No difference was found between the ^7Li T_1 and T_2 values of the extracellular Li^+ resonance for RBC suspensions treated and untreated with sialidase (93); the presumably weak interaction between Li^+ ions and sialic acid residues does not account for the large T_1/T_2 ratio observed in Li^+-loaded RBCs. It is possible that not all the sialic acid residues were released by treatment with sialidase. However, if specific sialic acid - Li^+ interactions were present, one would expect an increase in ^7Li relaxation times after treatment with sialidase, which was not observed. The relaxation data do not support the presence of specific sialic acid - Li^+ interactions.

RBCs are often thought of as packets of Hb. Intracellular Li^+ may also be interacting with hemoglobin. In the present study, Li^+ was also found to bind weakly to Hb (Table 16). Our Hb data are in agreement with published results (122,123) which indicate weak Li^+-Hb interactions. We also found that the paramagnetic properties of deoxyHb or metHb which

might be present in partially oxygenated Li^+-loaded RBCs is not responsible for the large value of the T_1/T_2 ratio. The small value of the T_1/T_2 ratio obtained for Li^+-containing glycerol/water mixtures indicates that the high intracellular viscosity, which is associated with large concentrations of Hb in RBCs, is not responsible for the large difference between ^7Li T_1 and T_2 values.

Pettegrew and coworkers (122) measured the ^7Li T_1 and T_2 relaxation values for RBCs incubated with 50 mM Li^+ (concentration expressed over total volume of cells and suspension medium) and found them to be approximately 5.1 and 0.15 s, respectively. They speculated that the large difference in relaxation times was due to diffusion of Li^+ ions across the heterogeneous electrostatic field gradients generated by the SA network of the RBC membrane. However, no direct investigation of Li^+ diffusion through the SA network or of Li^+-SA binding was conducted by Pettegrew et al. (122); their speculation was based on measurements obtained with agar gels. In this study, we investigated directly the contributions of Li^+ diffusion through the SA network and of Li^+-spectrin interactions by measuring ^7Li T_1 and T_2 values in spectrin solutions containing LiCl (1.5 - 5.0 mM) - see Table 16. From the small R values observed in Li^+-containing spectrin solutions, we conclude that diffusion of the Li^+ ion through the SA network is not responsible for the large T_1/T_2 ratio present in Li^+-loaded RBCs. From the small dependence of the observed ^7Li relaxation values on the spectrin concentration and the small R values, we conclude that only weak Li^+ interactions with SA are present for Li^+ levels typically present in RBCs. Ca^{2+}, and to a smaller extent Mg^{2+}, bind strongly to erythrocyte spectrin (149); it is therefore unlikely that therapeutic concentrations of Li^+ would compete with physiological intracellular concentrations of Ca^{2+} and Mg^{2+}. The small values of the T_1/T_2 ratios observed with Li^+ solutions containing

physiologic concentrations of DPG and ATP (Table 17) also indicate weak Li^+-DPG and Li^+-ATP interactions, which is agreement with the literature (23,133).

The large T_1/T_2 ratios observed with unsealed RBC membrane suspensions (Table 19) indicate that the large difference between T_1 and T_2 values observed in Li^+-loaded RBCs is due to specific interactions between Li^+ and membrane binding sites. Because stronger Li^+ binding was observed for extravesicular Li^+ in the presence of IOV than in ROV (Figure 17), we conclude that the inner leaflet of the RBC membrane provides the major Li^+ binding sites in Li^+-loaded RBCs. The lipids of the erythrocyte membrane are asymmetrically distributed (40). The outer leaflet of mature human RBC contains approximately 40-50% PC, 40-50% sphingomyelin (SM) and 10-15% phosphatidylethanolamine (PE) of the total outer leaflet phospholipids, whereas the inner leaflet contains approximately 10-20% PC, 10% SM, 40-50% PE, 20-30% PS and 1.4% PI of the total inner leaflet phospholipids (40,150,151). Both anionic phospholipids, PS and PI, are found only in the inner leaflet. The intrinsic binding constants for interactions between some alkali and alkaline earth metal ions and PS have been reported (152); they are 0.8 M^{-1} for PS - Na^+, 4.0 M^{-1} for PS -Mg^{2+}, and 35 M^{-1} for PS - Ca^{2+}. Evidence for Li^+ interactions with PS-containing liposomes was previously obtained from ^7Li relaxation data (153,154). Therefore, it is likely that the anionic phospholipids PS and PI present in the inner leaflet of the RBC membrane contribute toward Li^+ binding (Figure 17). The SA network is also present in the inner leaflet of the RBC membrane. For similar protein concentrations, however, the R value for spectrin solutions containing 1.5 mM Li^+ was 4.4 whereas that of RBC membrane suspensions was 49 (Table 19). We therefore conclude that the SA network is not responsible for the enhanced Li^+ binding present in IOV suspensions (Figure 17).

Apparent affinity binding constants for Na^+ and Li^+ ions to the internal and external binding sites of the RBC Na^+-Li^+ exchange (countertransport) membrane protein were previously determined from Lineweaver-Burk plots (155,156); on both membrane surfaces, a 15 to 18 fold preference of Li^+ over Na^+ was found. Interestingly, the absolute values for the binding affinities for Li^+ and Na^+ were 3 fold greater for the internal than for the external binding sites. The difference in ion affinities on the two RBC membrane surfaces may be due to excess internal negative charge associated with the presence of anionic phospholipids, PS and PI, in the inner RBC membrane surface. Previous studies (26,157) on the lipid composition of RBC membranes from bipolar and hypertensive patients have shown that the amounts of PS and PI are different from those present in RBCs from normotensive individuals.

Li^+ binding to RBC anionic phospholipids may be affecting the extent of lipid-protein interactions in the RBC membrane. Since the Na^+-Na^+ exchange protein, which mediates RBC Na^+-Li^+ countertransport, is a membrane protein, it is feasible that different extents of Li^+ binding to phospholipids, and in turn different extents of interactions between anionic phospholipids and the membrane-bound Na^+-Na^+ exchange protein, could be responsible for the variations in RBC Li^+ countertransport reported for bipolar (10,11,27) and hypertensive (95,96) patients relative to normotensive individuals. Although the Na^+-Na^+ exchange protein is known to bind Li^+ with high affinity (155,156), its low abundance in the RBC membrane makes it unlikely that Li^+ binding to the Na^+-Na^+ exchange protein is solely responsible for the drastically short intracellular ^7Li T_2 values observed in Li^+-loaded RBC suspensions. The contribution of the Na^+-Na^+ exchange toward the observed ^7Li T_1/T_2 ratio in Li^+-loaded RBCs cannot be determined directly at the present time because the RBC Na^+-Na^+ exchange

membrane protein has not been isolated yet, and highly specific transport inhibitors are not available.

V.4. ^{7}Li Relaxation Behavior in RBC Membrane Suspensions

The ^{7}Li nucleus has a nuclear spin, I, of 3/2, and is therefore a quadrupolar nucleus. The quadrupole moment of ^{7}Li is however small (75). Nuclear Overhauser enhancement measurements and H_2O-D_2O exchange experiments showed that dipolar coupling to ^{1}H contribute approximately 20% toward the relaxation of intracellular Li^+ in RBC suspensions (109,122). Contributions from spin rotation, chemical shift anisotropy, and scalar relaxation mechanisms have also been ruled out (109). Our observations of similar T_1/T_2 ratios for RBCs bubbled with either N_2 or CO, and of small T_1/T_2 ratios for both paramagnetic (deoxyHb and metHb) and diamagnetic (COHb) forms of Hb (Table 16) indicate that paramagnetic relaxation is not an important relaxation mechanism for intracellular Li^+ in RBCs. Despite its small quadrupole moment, the major mechanism for relaxation of the ^{7}Li nucleus in Li^+-loaded RBCs is therefore quadrupolar relaxation.

Under the extreme narrowing condition ($\omega^2\tau_2 << 1$, where ω is the NMR observation frequency, and τ is the correlation time), the T_1 value should be similar to the T_2 value (75). Because the intracellular ^{7}Li T_1 values are significantly larger than the T_2 values in Li^+-loaded RBCs (Table 15), the extreme narrowing condition does not apply to the relaxation of intracellular Li^+. Outside the domain of motional extreme narrowing, and assuming that the relaxation and exchange times in the bound state are much shorter than those in the free state, the quadrupolar relaxation decay for a nucleus with I = 3/2 is biexponential (158). In similarity to the two-state model for spin 3/2 nuclides undergoing chemical exchange, a model

that assumes asymmetric continuous distribution of correlation times for the fluctuating electric field gradients experienced by the spin 3/2 nuclides in biological samples also predicts biexponential relaxation (77). A Lorentzian line shape, which is observed in the extreme narrowing condition, is characterized by a $\Delta\nu_{1/8}/\Delta\nu_{1/2}$ ratio of 2.7 (80). Outside the domain of motional extreme narrowing, however, a non-Lorentzian line shape is observed which can be deconvoluted into a narrow Lorentzian curve, originating from the slow T_{2s} relaxation component and accounting for 40% of the total signal intensity, and a broad Lorentzian curve, owing to the fast T_{2f} relaxation component and accounting for the remaining 60% of the total signal intensity; similarly, the observed T_1 values under this condition can be decomposed into slow T_{1s} components that contribute 80%, and fast T_{1f} components that account for the remaining 20% of the observed T_1 relaxation. The narrow or slow component of T_1 or T_2 relaxation is associated with the -1/2 to +1/2 transition, whereas the broad or fast component is due to the -3/2 to -1/2 and the +1/2 to +3/2 transitions (80).

Our partially relaxed ^{7}Li NMR spectra of RBC membrane suspensions containing 20 mM LiCl (Figure 18) provided evidence for biexponential relaxation for the ^{7}Li nucleus. When the mole fraction of free Li^+ was very large relative to that of bound Li^+, as it was the case in RBC membrane suspensions containing 150 mM LiCl or in a glycerol/water mixture with the same Li^+ concentration, we were, however, unable to detect biexponential decay for the T_1 relaxation. The T_1 values observed in Li^+-containing RBC membrane suspensions represent weighted averages of free Li^+ in exchange with Li^+ bound to RBC membrane sites. Because the relaxation of Li^+ in the absence RBC membrane is monoexponential, the environment the Li^+ experienced is homogeneous. The relaxation behavior of 150 mM LiCl in the presence of RBC membrane appears to be monoexponential because of the large

fraction of free Li^+. The T_{1f} and T_{1s} values for 20 mM Li^+ in the presence of RBC membrane were 9.0 s and 11.5 s yielding a ratio of less than two for spin-lattice relaxation rates. Low sensitivity may preclude the separation of fast and slow relaxation components when they differ by a factor of less than two (158). Komoroski et al. (109) did not observe biexponential T_1 or T_2 relaxation, or a double-quantum ^7Li NMR resonance for Li^+-loaded RBCs; the inability to detect biexponential relaxation for the ^7Li nucleus in Li^+-loaded RBCs may be associated with a low signal to noise ratio for the intracellular ^7Li NMR resonance (158). We observed full visibility for the ^7Li nucleus in Li^+-containing RBC membrane suspensions (this study) and in Li^+-loaded RBCs (27). The observation of partial visibility of the intracellular ^7Li NMR resonance and the inability to detect biexponential relaxation (109) may be associated with low NMR sensitivity under the experimental conditions previously used. Precedents for biexponential relaxation and partial visibility of the ^{23}Na nucleus in human RBC and rat liver have been reported (109,159,160). Apparent monoexponential ^{23}Na relaxation and a large difference between T_1 and T_2 was also reported for intracellular Na^+ in human packed RBCs (161).

Changes in Li^+ binding sites, in particular anionic phospholipids, may be responsible for the abnormal Li^+ transport properties in RBCs from bipolar and hypertensive patients. Changes in the phospholipid composition (162) or activities of enzymes involved in phospholipid metabolism and interconversion (163) require investigation; such studies may contribute to an understanding of the etiology of bipolar illness, other neurological diseases as well as essential hypertension. Our ^7Li NMR relaxation results indicate the promise of relaxation measurements to probe Li^+ interactions in disease states.

V.5. Relationship Among Li^+/Na^+ Countertransport Rate, Phospholipid Composition, and Li^+ Binding to Human RBC Membrane from Bipolar Patients Receiving Lithium Carbonate

In this study, as in most reports (35,95,124-127) the rates of RBC Na^+-Li^+ exchange were measured as the efflux of Li^+ from Li^+-loaded RBCs in exchange with Na^+ present in the suspension medium. Under the standard assay conditions, Li^+ is present at saturating concentrations, but Na^+ is not (37,38,164), the dissociation constants (K_M) for extracellular Na^+ are of the same order of magnitude as extracellular Na^+ concentration, 140 mM, used in the standard assay indicating that the RBC Na^+-Li^+ exchange protein is far from saturated with Na^+ on the extracellular side of the RBC membrane. The rates that we obtained in this study, as well as the rates that have been reported by others (35,95,124-127) under the standard assay conditions are therefore not maximal velocities of RBC Na^+-Li^+ exchange; variations in Na^+ affinity (K_M) and maximal velocity (V_{max}) could change the observed rates in RBCs of lithium-treated patients. By monitoring bipolar patients for the first week after initiating lithium treatment, Ehrlich et al.(35) observed by using AA an increase in the K_M values and yet no change in the V_{max} values. In contrast, inter-individual differences observed in the rates of Na^+-Li^+ exchange in RBCs of lithium-treated patients were attributed to changes in the V_{max} values but not in the K_M values (29,35,165). These previous findings on the effect of lithium treatment on the kinetic properties of RBC Na^+-Li^+ exchange need, however, to be reevaluated in light of the now known transport Na^+ unsaturation under standard assay conditions (37,38,164).

When ^7Li relaxation measurements are used for probing variations in Li^+ binding to the RBC membrane, unsealed RBC membrane samples are preferable to intact Li^+-loaded RBCs

because the Li^+ concentration can be adjusted more precisely and the extent of Li^+ binding to the RBC membrane is enhanced. With intact Li^+-loaded RBCs, the intracellular Li^+ concentration may change during the course of a long ^7Li NMR relaxation measurement as a result of Na^+-Li^+ countertransport. The extent of Li^+ binding in intact Li^+-loaded RBCs is less than that in unsealed RBC membrane samples because of weak binding of intracellular Li^+ to anionic intracellular components such as hemoglobin, 2,3-diphosphoglycerate, and adenosine triphosphate.

The Li^+ binding constants that we calculated from the ^7Li T_1 values measured in Li^+-containing suspensions of unsealed RBC membranes are measures of Li^+ binding to the phosphate head groups of phospholipids and protein binding sites present in the internal and external surfaces of the RBC membrane. In contrast, the K_M values obtained by varying the intra- or extracellular Li^+ concentrations in the standard assay (29,35,165) are measures of Li^+ binding to intra- or extracellular sides of the membrane exchange protein. Not surprisingly, the Li^+ binding constants (which are the reciprocals of K_M values) reported for the transport measurements (which are in the range of 500 M^{-1} to 3800 M^{-1}) (35,155,156) are significantly different from the K_b values of Li^+ that we measured by using ^7Li NMR spectroscopy (Tables 24 and 25). Interestingly, the $1/K_M$ values of Li^+ for inner surface of the RBC membrane obtained under Li^+ efflux conditions was three-fold greater than K_M values for the outer surface (155,156); the larger negative surface charge, associated with a large percentage of the anionic phospholipids PS and PI, of the inner leaflet of the RBC membrane may also contribute toward the K_M values measured by the standard transport assay. Na^+-Li^+ exchange activity occurs only when Li^+ and Na^+ gradients are present across the RBC membrane (166). The values of K_b are smaller than those of $1/K_M$ presumably because the

^{7}Li NMR binding measurements were conducted on unsealed RBC membrane suspensions which contain an inactivated exchange protein, whereas the K_M values were obtained from transport experiments conducted on intact RBC suspensions.

The phospholipid composition of the human RBC membrane that we observed by ^{31}P NMR is in general agreement with that observed by Sengupta et al. (26), who used thin-layer chromatography. However, ^{31}P NMR yielded higher percentages of PC, Sph, and PS, and lower percentages of PI and PE, than those measured by thin-layer chromatography. The different percentage compositions measured by the two methods is attributed to the fact that ^{31}P NMR measures the total phosphate in each phospholipid; the visualization reagent used in thin-layer chromatography (iodine vapor or cupric acetate) results in detection of only unsaturated fatty acids by chromatographic methods (127,167).

Previous observations have suggested that alterations in plasma lipids and RBC membrane lipid composition may be associated with the decreased rates of RBC Na^+-Li^+ exchange reported for lithium-treated psychiatric patients and the elevated rates of Na^+-Li^+ exchange in RBCs of hypertensive patients (168-171). An alteration in plasma lipid composition, triggered by genetic or other unknown exogenous or endogeneous factors, could result in alterations in phospholipid membrane composition via exchange between plasma and membrane lipids. Alterations in lipid-protein interactions in cell membranes could result in variations in the rates of Na^+-Li^+ exchange (170). Changing the amount of cholesterol in the RBC membrane or replacing the native PC by derivatives of PC containing fatty acids with various degrees of saturation resulted in significant changes in the rates of RBC Na^+-Li^+ exchange (172). However, dietary supplementation with olive oil caused significant changes in plasma lipids and RBC membrane fatty acids, and yet the rates of RBC Na^+-Li^+ exchange

were maintained (173). Therefore, in previous measurements on the total amount of fatty acids in the RBC membrane it was not possible to identify the subclasses of phospholipids that regulate the activity of the RBC Na^+-Li^+ exchange protein. By using ^{31}P NMR spectroscopy, however, we were able to measure alterations in the percentage membrane composition of the anionic phospholipids PI and PS in lithium-treated bipolar patients.

Because PS is a phospholipid with a head group bearing a negative charge, the interaction of PS with Li^+ is expected to be strong. Evidence for binding of Li^+ to the negatively charged head group of PS comes from studies on synthetic membranes by ^7Li, ^{31}P, and ^2H NMR and by neutron diffraction (153,154,174). We found that the percentage of PS in RBC membrane of lithium-treated patients was significantly stronger binding of Li^+ to the head groups of PS located in the inner leaflet of RBC membrane, and in slower rates of RBC Na^+-Li^+ exchange. Because Li^+ causes inhibition of myo-inositol-1-phosphatase (91), lithium treatment is associated with decreased levels of myo-inositol and decreased biosynthesis of PI in the brain (175,176). Moscovich et al. (177) have also shown decreased activity of inositol-1-phosphatase in RBCs of lithium-treated bipolar patients. The non-significant decrease in PI content that we observed by ^{31}P NMR spectroscopy in RBC membranes of lithium-treated patients agrees with previous observations. Because of baseline noise and small amounts of PI present in RBC membranes, it is only possible to determine the PI content with an accuracy of $\pm$ 20%; the low accuracy of the PI content measured by ^{31}P NMR spectroscopy may explain our failure in observing a significant difference in PI levels between the patients and control groups.

Our NMR measurements of phospholipid composition and Li^+ binding to the RBC membrane provided a clear discrimination between lithium-treated bipolar patients and normal

individuals. To rule out a drug-induced effect, we are currently investigating whether a similar discrimination exists between lithium-free bipolar patients and normal individuals in RBC phospholipid composition and Li^+ binding constants. Measuring the affinity of Na^+ for the RBC membrane proved to be a promising tool to identify patients who are at risk of developing essential hypertension (38). By using ^{31}P NMR spectroscopy, Pettegrew et al. (178) obtained evidence for abnormal membrane phospholipid metabolism in the brains of schizophrenic patients. An investigation at the molecular level of the factors responsible for the abnormal rates of Na^+-Li^+ exchange in RBCs of bipolar patients may lead to the identification of the abnormalities in the RBC Na^+-Li^+ exchange protein. More precisely defined molecular parameters, such as phospholipid composition and Li^+ binding constants, may be useful for the diagnosis and prognosis of bipolar patients as well as for predicting the usefulness of lithium treatment.

In summary, we found that an alteration in the anionic phospholipid composition of the RBC membrane of manic-depressive patients receiving lithium carbonate resulted in stronger Li^+ binding to the RBC membrane and lower rates of Na^+-Li^+ exchange. Opposite trends were observed for normal individuals. We are now investigating Li^+ binding to RBC membranes from bipolar patients who are Li^+-free to establish whether abnormal Li^+ binding to RBC membranes is related to the etiology of manic depression (12,179) or is a result of Li^+ therapy (34,35).

REFERENCES

1. Jefferson, J.W., Greist, J.H., Baudhuin, M. Lithium in psychiatry. In "Lithium: Current Applications in Science, Medicine and Technology" (Bach, R.O., ed.). New York: Wiley Interscience, 1985; 345-352.

2. Schou, M. Biology and pharmacology of lithium ion. Pharmacol. Rev., 1957; 9: 17-58.

3. Cade, J.F.J. Lithium salts in the treatment of psychotic excitement. Med. J. Aust., 1949; 2: 349-352.

4. Fawcett, J. Lithium carbonate in medicine and psychiatry. In "Lithium Effects on Granulopoiesis and Immune Function" (Rossof, A.H., Robinson, W.A., ed.). New York: Plenum Press, 1980; 1-13.

5. Abraha, A., Mota de Freitas, D. Nuclear magnetic resonance study of differences between ^{6}Li and ^{7}Li ions in transport across human red blood cell membranes. Lithium, 1991; 2: 118-121.

6. Abraha, A., Mota de Freitas, D. Ionophore-induced Li^{+} transport across human erythrocyte membranes in the presence of a background of Na^{+} ions. Lithium, 1992; 3: 203-211.

7. Horronbin, D.F. Lithium and dermatological disorders. In "Lithium and Cell Physiology" (Bach, R.O., Gallichio, U.S. ed.), New York: Springer-Verlag, 158-168.

8. Frausto da Silva, J.J.R., Williams, R.J.P. Possible mechanism for the biological action of lithium. Nature, 1976; 263: 237-239.

9. Ramasamy, R., Mota de Freitas, D. Competition between Li^{+} and Mg^{2+} for ATP in human erythrocytes. FEBS Lett., 1989; 244, 1: 223-226.

10. Ramsey, T.A., Frazer, A., Mendels, J., Dyson, L. The erythrocyte lithium-plasma ratio in patients with primary affective disorder. Arch. Gen. Psychiatry, 1979; 36:457-461.

11. Frazer, A., Mendels, J., Brunswick, D., London, J., Pring, M., Ramsey, A., Rybakowski, J. Erythrocyte concentrations of lithium ion: Clinical correlates and mechanisms of action. Am. J. Psychiatry, 1978; 135: 1065-1069.

12. Meltzer, H.L. Is there a specific membrane defect in bipolar disorders? Biol. Psychiatry, 1991; 30: 1071-1074.

13. Lazarus, J.H. Lithium and the cell. In "Endocrine and Metabolic Effects of Lithium" (Lazarus J.H., ed.). New York: Plenum Medical Book Company, 1986; 31-54.

14. Avissar, S., Schreiber, G., Dennon, A., Belmaker, R.H. Lithium inhibits adrenergic and cholinergic increases in GTP binding in rat cortex. Nature, 1988; 331: 440-442.

15. Baraban, J.M., Worley, P.F., Snyder, S.H. Second messenger systems and psychoactive drug action: focus on the phosphoinositide system and lithium. Am. J. Psychiatry, 1989; 146: 10, 1251-1260.

16. Stryer, L. Hormone action. In "Biochemistry", 1988; 3rd edition: 975-1004.

17. Ha, J.M., Ito, Y., Kawai, G., Miyazawa, T., Miura, K., Ohtsuka, E. Conformation of guanosine 5'-diphosphate as bound to a human c-Ha-*ras* mutant protein: a nuclear overhauser effect study. Biochemistry, 1989; 28: 8411-8416.

18. Yamasaki, K., Kawai, G., Ito, Y., Muto, Y., Fujita, J., Miyazawa, T., Nishimura, S., Yokoyama, S. Conformation change of effector-region residues in antiparallel β-sheet of human c-Ha-*ras* protein on GDP→GTPγS exchange: a two-dimensional NMR study. Biochem. Biophys. Res. Commun., 1989; 162: 1054-1062.

19. Pai, E.F., Kabach, W., Krengel, U., Holmes, K.C., John, J., Wittinghofer, A. Structure of the guanine-nucleotide-binding domain of the Ha-*ras* oncogene product p21 in the triphosphate conformation. Nature, 1989; 341: 209-214.

20. Schlichting, I., Almo, S.C., Rapp, G., Wilson, K., Petratos, K., Lentfer, A., Wittinghofer, A., Kabsch, W., Pai, E.F., Petsko, G.A., Goody, R. Time-resolved x-ray crystallographic study of the conformational change in Ha-*ras* p21 protein on GTP hydrolysis. Nature, 1990; 345: 309-315.

21. Pai, E.F., Krengel, U., Petsko, G.A., Goody, R.S., Kabsch, W., Wittinghofer, A. Refined crystal structure of the triphosphate conformation of H-*ras* p21 at 1.35 Å resolution: implications for the mechanism of GTP hydrolysis. EMBO J., 1990; 9: 2351-2359.

22. Bone, R., Springer, J.P., Atack, J.R. Structure of inositol monophosphatase, the putative target of lithium therapy. Proc. Natl. Acad. Sci. USA, 1992; 89: 10031-10035.

23. Abraha, A., Mota de Freitas, D., Castro, M.M.C.A., Geraldes, C.F.G.C. Competition between Li^+ and Mg^{2+} for ATP and ADP in aqueous solution: A multinuclear NMR study. J. Inorg. Biochem., 1991; 42: 191-198.

24. Geisler, A., Mϕrk, A. The interaction of lithium with magnesium-dependent enzymes. In "Lithium and Cell Physiology" (Bach, R.O., Gallicchio, V.S., ed.). New York:

Springer-Verlag, 1990; 125-136.

25. Adragna, N.C., Canessa, M.L., Solomon, H., Slater, E., Tosteson, D.C. Red-cell lithium-sodium countertransport and sodium-potassium cotransport in patients with essential-hypertension. Hypertension (Dallas), 1982; 4: 795-804.

26. Sengupta, N., Datta, S.C., Sengupta, D. Platelet and erythrocyte-membrane lipid and phospholipid patterns in different types of mental-patients. Biochem. Med., 1981; 25: 267-275.

27. Mota de Freitas, D., Silberberg, J., Espanol, M.T., Dorus, E., Abraha, A., Dorus, W., Elenz, E., Whang, W. Measurement of lithium transport in RBC from psychiatric patients receiving lithium carbonate and normal indivials by ^{7}Li NMR spectroscopy. Biol. Psychiatry, 1990; 28: 415-424.

28. Egeland, J.A., Kidd, J.R., Frazer, A., Kidd, K.K., Neuhauser, V.I. Amish Study V: Lithium-sodium countertransport and catechol o-methyltransferase in pedigree of bipolar probands. Am. J. Psychiatry, 1984; 141: 1049-1054.

29. Greil, W., Esienried, F., Becker, B.F., Duhm, J. Interindividual differences in the Na^{+} dependent Li^{+} countertransport system and in the Li^{+} distribution ratio across the red cell membrane among Li^{+} treated patients. Psychopharmacologia, 1977; 53: 19-26.

30. Mallinger, A.G., Mallinger, J., Himmelhoch, J.M., Rossi, A., Hanin, I. Essential hypertension and membrane lithium transport in depressed patients. Psychiatry Res., 1983; 10:11-16.

31. Richelson, E., Snyder, K., Carlson, J. Lithium ion transport in erythrocytes of randomly selected blood donors and manic depressive patients: Lack of association with affective illness. Am. J. Psychiatry, 1986; 23: 465-475.

32. Rybakowski, J.K., Amsterdam, J.D., Dyson, W.L., Frazer, A., Winokur, A., Kurt, J. Factors contributing to lithium-sodium countertransport activity in lithium-treated bipolar patients. Pharmacopsychiatry, 1989; 22: 16-20.

33. Amsterdam, J.D., Rybakowski, J.K., Gottleb, J., Frazer, A. Kinetics of erythrocytes of sodium-lithium countertransport in patients with affective illness before and after lithium therapy. J. Affect. Disord., 1988; 14: 75-81.

34. Ehrlich, B.E., Diamond, J.M., Fry, V., Meier, K. Lithium erythrocyte cation transport involves a slow process in the erythrocyte membrane. J. Memb. Biol., 1983; 75: 233-240.

35. Ehrlich, B.E., Diamond, J.M., Gosenfield, L. Lithium-induced changes in sodium-lithium countertransport. Biochem. Pharmacol., 1981; 30: 2539-2543.

36. Nurnberger, J.I., Pandey, G.N., Gerson, E.S., Davis, J.M. Lithium ratio in psychiatric patients: A caveat. Psychiatry Res., 1983; 9: 201-206.

37. Aronson, J.K. Methods for expressing the characteristics of transmembrane ion transport systems. Clin. Sci., 1990; 78: 247-254.

38. Rutherford, P.A., Thomas, T.H., Wilkinson, R. Increased erythrocyte sodium-lithium countertransport activity in enssential hypertension is due to an increased affinity for extracellular sodium. Clin. Sci., 1990; 79: 365-369.

39. Dorus, E., Cox, N.J., Gibbson, R.D., Shaughnessy, R., Pandey, G.N., Cloninger, R. Lithium ion transport and affective disorders within families of bipolar patients: Identification of a major gene locus. Arch. Gen. Psychiatry, 1983; 40: 545-552.

40. Schwarz, R.S., Chiu, D.T.-Y., Lubin, B. Studies on the organization of plasma membrane phospholipids in human erythrocytes. In "Erythrocyte Membranes 3: Recent Clinical and Experimental Advances" (Back, N., Brewer, G.J., Eijsvogel, V.P., ed.). New York: Alan R. Liss, Inc., 1984; 89-122.

41. Birnbaumer, L. G proteins in signal transduction. Annu. Rev. Pharmacol. Toxicol., 1990; 30: 675-705.

42. Gilman, A.G. G proteins: Transducers of receptor-generated signals. Annu. Rev. Biochem., 1987; 56: 615-649.

43. Sternweis, P.C. The purified alpha-subunits of G_o and G_i from bovine brain require beta-gamma for association with phospholipid-vesicles. J. Biol. Chem., 1986; 261:631-637.

44. Neer, E.J., Clapham, D.E. Roles of G protein subunits in transmembrane signalling. Nature, 1988; 333: 129-134.

45. Codina, J., Carry, D.J., Birnbraumer, L., Iyenger, R. Purification of G proteins. In "Methods in Enzymology". Academic Press, 1991; 195: 177-188.

46. Masters, S.B., Stroud, R.M., Bourne, H.R. Family of G protein α chains: Amphipathic and predicted structure of functional domains. Protein Eng., 1986; 1: 47-54.

47. Halliday, K.R. Regional homology in GTP-binding proto-oncogene products and elongation-factors. J. Cyclic Nucleotide Protein Phosphor. Res., 1984; 9: 435-448.

48. Jurnak, F. Structure of the GDP domain of EF-tu and location of the amino-acids homologous to *ras* oncogene proteins. Science, 1985; 230:32-36.

49. La Cour, T.F.M., Nyborg, J., Thirup, S., Clack, B.F.C. Structural details of the binding of guanosine diphosphate to elongation-factor Tu from *Escherichia coli* as

studied by X-ray crystallography. EMBO J., 1985; 4: 2385-2388.

50. Hurley, J.B., Simon, M.I., Teplow, D.B. Homologies between signal transducing G-proteins and *ras* gene-products. Science, 1984; 226: 860-862.

51. Manji, H.K. G proteins: Implications for psychiatry. Am. J. Psychiatry, 1992; 149: 6, 746-760.

52. Smithers, G.W., Poe, M., Latwesen, D.G., Reed, G.H. Electron paramagnetic resonance measurements of the hydration of Mn(II) in ternary complexes with GDP and *ras* p21 proteins. Arch. Biochem. Biophy., 1990; 280: 416-420.

53. Bourne, H.R., Sanders, D.A., McCormick, F. The GTPase superfamily: Conserved structure and molecular mechanism. Nature, 1991; 349: 117-127.

54. Barbacid, M. *Ras* genes. Annu. Rev. Biochem., 1987; 56: 799-827.

55. Bourne, H.R., Sanders, D.A., McCormick, F. The GTPase superfamily: A conserved switch for diverse cell functions. Nature, 1990; 348: 125-132.

56. Nishimura, S., Sekiya, T. Human cancer and cellular oncogenes. Biochem. J., 1987; 243: 313-327.

57. Santos, E., Nebreda, A.R. Structural and functional properties of *Ras* proteins. FASEB J., 1989; 3: 2151-2161.

58. Gibbs, J.B., Schaber, M.D., Allard, W.J., Sigal, I.S., Scolnick, E.M. Purification of *ras* GTPase activating protein from bovine brain. Proc. Natl. Acad. Sci. USA, 1988; 85: 5026-5030.

59. Langen, R., Schweins, T., Warshel, A. On the mechanism of guanosine triphosphate hydrolysis in *ras* p21 proteins. Biochemistry, 1992; 31: 8691-8696.

60. Pfaffinger, P.J., Hunter, D.D., Hill, B., Martin, J.M., Nathanson, N.M. GTP-binding proteins couple cardiac muscarinic receptors to a K channel. Nature, 1985; 317: 536-538.

61. Breitwieser, G.E., Szabo, G. Uncoupling of cardiac muscarinic and β-adrenergic receptors from ion channels by a guanine nucleotide analogue. Nature, 1985; 317: 538-540.

62. Itoh, H., Kozasa, T., Nagata, S. Molecular cloning and sequence determination of cDNAs for alpha subnits of the guanine nucleotide-binding proteins G_s, G_i, and G_o from rat brain. Proc. Natl. Acad. Sci. USA, 1981; 83: 3776-3780.

63. Taylor, S.J., Smith, J.A., Exton, J.H. Purification from bovine liver membranes of a guanine nucleotide-dependent activator of phosphoinositide-specific phospholipase C:

immunologic identification as a novel G-protein alpha subunit. J. Biol. Chem., 1990; 265: 17150-17156.

64. Freissmuth, M., Casey, P.J., Gilman, A.G. G proteins control diverse pathways of transmembrane signalling. FASEB J., 1989; 3: 2125-2131.

65. Gilman, A.G. The Albert Lasker medical awards: G proteins and regulation of adenylyl cyclase. JAMA, 1989; 262: 1819-1825.

66. Hildebrandt, J.D., Kohnken, R.E. Hormone inhibition of adenylyl cyclase: differences in the mechanisms for inhibition by hormones and G protein beta gamma. J. Biol. Chem., 1990; 265:9825-9830.

67. Ross, E.M. Signal sorting and amplification through G protein-coupled receptors. Neuron, 1989; 3: 141-152.

68. Mota de Freitas, D.E., Espanol, M.T., Dorus, E. Lithium transport in red blood cells of bipolar patients. In "Lithium Therapy Monographs" (Lancaster, F.N.J., ed.). 1991; 4: 96-120.

69. Wheeling, K., Christian, G.D. Spectrofluorimetric determination of serum lithium using 1,8-dihydroxyanthraquinone. Anal. Lett., 1987; 160: 243-250.

70. Gadzepko, V.P.Y., Hungerford, J.M., Kadry, A.M. Comparative study of neutral carries in polymetric lithium ion-selective electrodes. Anal. Chem., 1986; 58: 1948-1953.

71. Metzger, E., Dohener, R., Simon, W. Lithium/sodium ion concentration ratio measurements in blood serum with lithium and sodium ion-selective liquid membrane electrodes. Anal. Chem., 1987; 59: 1600-1603.

72. Xie, R.Y., Christian, G.D. Serum lithium analysisby coated wire lithium ion selective electrodes in flow injection analysis dialysis system. Anal. Chem., 1986; 58: 1806-1810.

73. Veniero, J.C., Gupta, R.K. NMR measurements of intracellular ions in living systems. In "Annual Reports on NMR Spectroscopy" (Webb, G.A., ed.). London: Academic Press, 1992; 24: 219-265.

74. Ramasamy, R., Mota de Freitas, D., Geraldes, C.F.G.C., Peters, J.A. Multinuclear NMR study of the interaction of shift reagent lanthanide(III) bis(triphosphate) with alkali-metal ions in aqueous solution and in solid state. Inorg. Chem., 1991; 30: 3188-3191.

75. Mota de Freitas, D. Alkali metal NMR. In "Methods in Enzymology". Academic Press, 1993; 227: 78-106.

76. Detellier, C. Alkali metals. In "NMR of Newly Accessible Nuclei: Chemically and Biochemically Important Elements" (Laszlo, P., ed), Academic Press, New York, USA, 1987; 2: 105-151.

77. Rooney, W.D., Springer, C.S. A comprehensive approach to the analysis and interpretation of the resonances of spins 3/2 from living systems. NMR Biomed., 1991; 4: 209-226.

78. Monoi, H. Nuclear magnetic resonance of ions with quadrupole nuclei in aqueous heterogeneous systems: basic theory and application. Rev. Magn. Reson., 1986; 1: 73-122.

79. Laszlo, P. Sodium-23 nuclear magnetic resonance spectroscopy. Angew. Chem. Int. Ed. Engl., 1978; 17: 254-266.

80. Urry, W., Trapane, L., Venkatachalam, C.M., McMichens, R.B. Ion interactions at membranous polypeptide sites using nuclear magnetic resonance: determining rate and binding constants and site locations. Methods Enzymol., 1989; 171: 286-287.

81. Harris, R.K. In "Nuclear Magnetic Resonance Spectroscopy: a Physicochemical View". London: Pitman, 1983; 232-233.

82. In "Multinuclear NMR" (Mason, J., ed). New York: Plenum Press, USA, 1987; 625-629.

83. Espanol, M.T., Mota de Freitas, D. ^{7}Li NMR studies of lithium transport in human erythrocytes. Inorg. Chem., 1987; 26: 4356-4359.

84. Ramasamy, R., Espanol, M.T., Long, K.M., Mota de Freitas, D., Geraldes, C.F.G.C. Aqueous shift reagents for ^{7}Li NMR transport studies in cells. Inorg. Chim. Acta, 1989; 163: 41-52.

85. Espanol, M.T., Ramasamy, R., Mota de Freitas, D. Measurement of lithium transport across human erythrocyte membranes by ^{7}Li NMR spectroscopy. In"Biological and Synthetic Membranes". Alan R. Liss, Inc. 1989; 33-43.

86. Mota de Freitas, D., Espanol, M.T., Ramasamy, R., Labotka, R.J. Comparison of Li^{+} transport and distribution in human red blood cells in the presence and absence of dysprosium(III) complexes of triphosphate and triethylenetetraminehexaacetate. Inorg. Chem., 1990; 29: 3972-3978.

87. Ramasamy, R., Mota de Freitas, D., Jones, W., Wezeman, F., Labotka, R.J., Geraldes, C.F.G.C. Effects of negatively charged shift reagents on red blood cell morphology, Li^{+} transport, and membrane potential. Inorg. Chem., 1990; 29: 3979-3985.

88. Mota de Freitas, D., Rong, Q., Mo, S. Reinvestigation of transmembrane difference

in ^{7}Li NMR T_1 values in Li^{+}-loaded human erythrocyte suspensions. Magn. Reson. Med., 1993; 29: 256-259.

89. Seo, Y., Murakami, M., Suzuki, E., Watari, H. A new method to discriminate intracellular and extracellular K by ^{39}K NMR without chemical-shift reagents. J. Magn. Reson., 1987; 75: 529-533.

90. Birch, N.J., Goulding, I. Lithium-nucleotide interactions investigated by gel filtration. Anal. Biochem., 1975; 66: 293-297.

91. Hallcher, L.R., Sherman, W.R. The effects of lithium ion and other agents on activity of *myo*-inositol-1-phosphatase from bovine brain. J. Biol. Chem., 1980; 255: 10896-10901.

92. Mota de Freitas, D., Abraha, A., Rong, Q., Mo, S., Wittenkeller, L. Elucidation of transport mechanisms for alkali cations in human RBCs by metal NMR. J. Inorg. Biochem., 1991; 43: 386.

93. Espanol, M. Multinuclear magnetic resonance studies of lithium binding and transport in human erythrocytes. Ph.D. Dissertation, Loyola University of Chicago, 1989.

94. American Psychiatric Association: Diagnostic and Statistical Manual of Mental Disorders, 3rd ed rev. 1987; Washington, DC: American Psychiatric Press.

95. Canessa, M.L., Adragna, N.C., Solomon, H.S., Connolly, T.M., Tosteson, D.C. Increased sodium-lithium countertransport in red cells of patients with essential hypertension. N. Engl. J. Med., 1980; 302: 772-776.

96. Ramasamy, R., Mota de Freitas, D., Bansal, V.K., Dorus, E., Labotka, R.J. Nuclear magnetic resonance studies of lithium transport in erythrocyte suspensions of hypertensives. Clin. Chim. Acta, 1990; 188: 169-176.

97. Brophy, P.J., Hayer, M.K., Riddell, F.G. Measurement of intracellular potassium concentrations by NMR. Biochem. J., 1983; 210: 961-963.

98. Fabry, M.E., San George, R.C. Effect of magnetic susceptibility on nuclar magnetic resonance signals arising from red cells: a warning. Biochemistry, 1983; 22: 4119-4125.

99. Labotka, R.J. Measurement of intracellular pH and deoxyhemoglobin concentration in deoxygenated erythrocytes by phosphorus-31 nuclear magnetic resonance. Biochemistry, 1984; 23: 5549-5555.

100. Dozy, A.M., Kleihauer, E.F., Huisman, T.H.J. Studies on the heterogeneity of hemoglobin. J. Chromatog., 1968; 32: 723-727.

101. Huisman, T.H., Dozy, A.M. Studies On The Heterogeneity Of Hemoglobin. J.

Chromatog., 1965, 19, 160-169.

102. Winterbourn, C.C. Reaction of Superoxide With Hemoglobin. In "CRC Handbook of Methods for Oxygen Radical Research" (Greenwald, R.A., ed). Florida: CRC Press, Inc., 1985; 137-141.

103. Weissbluth, M. Molecular orbitals and optical spectra. In "Hemoglobin: Cooperativity and Electronic Properties". Springer-Verlag, Berlin, 1974; 125-141.

104. Steck, T.L., Kant, J.A. Preparation of impermeable ghosts and inside-out vesicles from human erythrocyte membranes. In "Methods in Enzymology" (Fleischer, S., Packer, L. eds), New York: Academic Press, 1974; 31: 172-180.

105. Macintyre, J.D. Properties and Uses of human erythrocyte membrane vesicles. In "Red Cell Membranes: A Methodological Approach" (Ellory, J.C., Young J.D., eds.). London, New York: Academic Press, 1982; 199-217.

106. Ungewickell, E, Gratzer, W. Self-association of human spectrin. Eur. J. Biochem., 1978; 88: 379-385.

107. Meneses, P., Glonek, T. High resolution ^{31}P NMR of extracted phospholipids. J. Lipid Res., 1988; 29: 679-689.

108. Edzes, H.T., Teerlink, T., Van der Knaap, M.S., Valk, J. Analysis of phospholipids in brain tissue by ^{31}P NMR at different compositions of the solvent system chloroform-methanol-water. Magn. Reson. Med., 1992; 26: 46-59.

109. Gullapalli, R.P., Hawk, R.M., Komoroski, R.A. A ^{7}Li NMR study of visibility, spin relaxation, and transport in normal human erythrocytes. Magn. Reson. Med., 1991; 20: 240-252.

110. James, T.L., Noggle, J.H. ^{23}Na nuclear magnetic resonance relaxation studies of sodium ion interaction with soluble RNA. Proc. Natl. Acad. Sci. USA, 1969; 62: 644-649.

111. Ong, R.L., Cheung, H.C. ^{23}Na NMR studies of Na^+ interaction with human red cell membranes from normotensives and hypertensives. Biophys. Chem., 1986; 23: 237-244.

112. Urry, D.W., Trapane, T.L., Andrews, S.K., Long, M.M., Overbeck, H.W., Oparil, S. NMR observation of altered sodium interaction with human erythrocyte membranes of essential hypertensives. Biochem. Biophys. Res. Commun., 1980; 96: 514-521.

113. Bollag, D.M., Edelstein, S.J. In "Protein Methods". New York: Wiley-Liss, 1991; 50-55.

114. Zar, J.H. In "Biostatistical Analysis", 2nd Edition, Prentice-Hall, New Jersey, 1984.

115. Morse, P.D., Lusczakoski, D.M., Simpson, D.A. Internal microviscosity of red blood cells and hemoglobin-free resealed ghosts: a spin-lable study. Biochemistry, 1979; 18: 5021-5029.

116. Gadian, D.G. In "Nuclear magnetic resonance and its applications to living systems". Oxford: Clarendon Press, 1982.

117. Cozzone, P.J., Jardetzky, O. Phosphorus-31 fourier transform nuclear magnectic resonance study of mononucleotides and dinucleotides. 2. Coupling constants. Biochemistry, 1976; 15: 4860-4865.

118. Lindon, J.C., Barker, D.J., Farrant, R.D., Williams, J.M. ^{13}C and ^{31}P NMR spectra and molecular conformation of *myo*-inositol 1,4,5-trisposphate. Biochem. J., 1986; 233: 275-277.

119. Andrasko, J. Measurement of membrane permeability to slowly penetrating molecules by a pulse gradient NMR method. J. Magn. Reson., 1976; 21: 479-484.

120. Pettegrew, J.W., Post, J.F.M., Panchalingam, K., Withers, G., Woessner, D.E. ^{7}Li NMR study of normal human erythrocytes. J. Magn. Reson. 1987; 71: 504-519.

121. Bull, T.E., Andrasko, J., Chiancone, E., Forsen, S. Pulsed nuclear magnetic resonance studies on ^{23}Na, ^{7}Li and ^{35}Cl binding to human oxy- and carbon monoxyhaemoglobin. J. Mol. Biol., 1973; 73: 251-259.

122. Antonny, B., Sukumar, M., Bigay, J., Chabre, M., Higashijima, T. The mechanism of aluminum-independent G-protein activation by fluoride and magnesium. J. Biol. Chem., 1993; 268, 2393-2402.

123. Rong, Q., Mota de Freitas, D., Geraldes, C.F.G.C. Competition between lithium and magnesium ions for guanosine di- and triphosphates in aqueous solution: a nuclear magnetic resonance study. Lithium, 1992: 3, 213-220.

124. Pandey, G.N., Ostrow, D.G., Haas, M., Dorus., E, Casper, R.C., Davis, J.M., Tosteson, D.C. Abnormal lithium and sodium transport in erythrocytes of a manic patient and some members of his family. Proc. Natl. Acad. Sci. USA, 1977; 74: 3607-3611.

125. Szentistvanyi, I, Janka, Z. Correlation between lithium ratio and Na-dependent Li transport in red blood cells during lithium prophylaxis. Biol. Psychiatry, 1979; 14: 973-977.

126. Ostrow, D.G., Pandy, G.N., Davis, J.M., Hurt, S.W., Tosteson, D.C. A heritable disorder of lithium transport in erythrocytes of a subpopulation of manic-depressive patients. Am. J. Psychiatry, 1978; 135: 1070-1078.

127. Diamond, J.M., Meier, K., Gosenfield, L.F., Jope, R.S., Jemden, D.J., Wrifht, S.M.

Recovery of erythrocyte Li^+/Na^+ countertransport and choline transport from lithium therapy. J. Psychiat. Res., 1983; 17:385-393.

128. Pearce, J.M., Shifman, M.A., Pappas, A.A., Komoroski, R.A. Analysis of phospholipids in human amniotic fluid by ^{31}P NMR. Magn. Reson. Med., 1991; 21: 107-116.

129. Sontheimer, G.M., Kuhn, W., Kalbitzer, H.R. Observation of Mg^{2+}.ATP and uncomplexed ATP in slow exchange by ^{31}P NMR at high magnetic fields. Biochem. Biophys. Res. Commun., 1986; 134: 1379-1386.

130. Corfù, N.A., Tribolet, R., Sigel, H. Comparison of the self-association properties of the 5'-triphosphates of inosine (ITP), guanosine (GTP), and adenosine (ATP). Eur. J. Biochem. 1990; 191: 721-735.

131. Walaas, E. Stability constants of metal complexes with mononucleotides. Acta. Chim. Scand., 1958; 12: 528-536.

132. Sari, J.C., Belaich, J.P. Microcalorimetric studies on the formation of magnesium complexes with 5' ribonucleotides of guanine, uracil, and hypoxanthine. J. Am. Chem. Soc., 1973; 95: 7491-7496.

133. Smith, R.M., & Martell, A.E. In "Critical Stability Constants". Plenum Press, 1974; 2: 280-284.

134. Gorenstein, D.G. Phosphorus-31 chemical shifts: principles and empirical observations. In"Phosphorus-31 NMR: principles and applications" (Gorenstein, D.G., ed.). Academic Press, Inc., 1984; 7-36.

135. White, A.M., Varney, M.A., Watson, S.P., Rigby, S., Changsheng, L. Influence of Mg^{2+} and pH on NMR spectra and radioligand binding of inositol 1,4,5-trisphosphate. Biochem. J., 1991; 278: 759-764.

136. Champagne, E.T., Robinson, J.W., Gale, R.J., Nauman, M.A., Rao, R.M., Liuzzo, J.A. Lithium ion association with sodium phytate and effects on the conformational equilibria. Implications in the physiological effects of lithium. Anal. Lett., 1985; 18: 2421-2443.

137. Bieth, H., Schlewer, G., Spiess, B. Complexation studies on inositol-phosphates. II. Alkali-metal complexes of D-*myo*-inositol 1,2,6 triphosphate. J. Inorg. Biochem., 1991; 41: 37-44.

138. Bieth, H., Jost, P., Spiess, B. Complexation studies on inositol-phosphates. I. Ca(II) and Mg(II) complexes of D-*myo*-inositol 1,2,6 triphosphate. J. Inorg. Biochem., 1990; 39: 59-73.

139. Rivera, J., Bernal, A.L., Varney, M., Watson, S.P. Inositol 1,4,5-triphosphate and

oxytocin binding in human myometrium. Endocrinology (Baltimore), 1990; 127: 155-162.

140. Volpe, P., Alderson-Lang, B.H., Nickols, G.A. Regulation of inositol 1,4,5-trisphosphate-induces Ca^{2+} release. 1. Effect of Mg^{2+}. Am. J. Physiol., 1990; 258: 1077-1085.

141. Gani, D., Downes, C.P., Batty, I., Bramham, J. Lithium and *myo*-inositol homeostasis. Biochim. Biophys. Acta, 1993; 1177: 253-269.

142. Frausto da Silva, J.J.R., Williams, R.J.P. Possible mechanism for the biological action of lithium. Nature, 1976; 263: 237-239.

143. Pandey, G.N., Sarkadi, B., Hass, M., Gunn, R.B., Davis, J.M., Tosteson, D.C. Lithium transport pathways in human red blood cells. J. Gen. Physiol., 1978; 72: 233-247.

144. Post, J.F.M. Cation nuclear magnetic resonance (NMR). ^{7}Li- and ^{23}Na-NMR results obtained with human erythrocytes. Scan. Micros., 1989; 3: 877.

145. Pettegrew, J.W., Panchalingam, K., Spiker, D. Na^{+} and Li^{+} NMR studies in affective illness. Biol. Psychiatry, 1989; 25: 136A.

146. Gallicchio, V.S., Hughes, N.K., Hulette, B.C., Noblitt, L. Effect of interleukin-1, GM-CSF, erythropoietin, and lithium on the toxicity associated with 3'-azido-3'-deoxythymidine (AZT) in vitro on hematopoietic progenitors (CFU-GM, CFU-MEG, and BFU-E) using murine retrovirus-infected hematopoietic cells. J. Leukoc. Biol., 1991; 50: 580-586.

147. Gallicchio, V.S. Lithium and granulopoiesis: mechanism of action. In "Lithium and cell physiology" (Bach, R.O., Gallicchio, V.S., eds.). New York: Springer-Verlag, 1990; 82-93.

148. Steck, T.L. The organization of proteins in the human red blood cell membrane. J. Cell. Biol., 1974; 62, 1-19.

149. Wallis, C.J., Babitch, J.A., Wenegieme, E.F. Divalent cation binding to erythrocyte spectrin. Biochemistry, 1993; 32, 5045-5050.

150. Cullis, P.R., Hope, M.J. Physical properties and functional roles of lipids in membranes. In "Biochemistry of Lipids and Membranes" (Vance, D.E., & Vance, J.E., eds.). Benjamin/Cummings Publ. Co., Menlo Park. 1985; 25-72.

151. Van Deenen, L.L.M., De Gier, J. Lipids of the red blood cell membrane. In "The Red Blood Cell" (Surgenor, M., ed.). New York: Academic Press, 1974; 2nd edition, I: 148-212.

152. Newton, C., Pangborn, W., Nir, S., Papahadjoupoulos, D. Specificity of Ca^{2+} and Mg^{2+} binding to phosphatidylserine vesicles and resultant phase changes of bilayer membrane structure. Biochim. Biophys. Acta, 1978; 506, 281-287.

153. Riddell, F.G., Arumugam, S. Surface charge effects upon membrane transport processes: the effects of surface charge on the monesin-mediated transport of lithium ions through phospholipid bilayers studied by ^{7}Li NMR spectrosopy. Biochim. Biophys. Acta, 1988; 945: 65-72.

154. Roux, M., Bloom, M. Ca^{2+}, Mg^{2+}, Li^{+}, Na^{+}, and K^{+} distributions in the headgroup region of binary membranes of phosphatidylcholine and phosphatidylserine as seen by deuterium NMR. Biochemistry, 1990; 29: 7077-7089.

155. Hannaert, P.A., Garay, R.P. A kinetics analysis of Na-Li countertransport in human red blood cells. J. Gen. Physiol., 1986; 87, 353-368.

156. Sarkadi, B., Alifimoff, J.K., Gunn, R.B., Tosteson, D.C. Kinetics and stoichiometry of Na-dependent Li transport in human red blood cells. J. Gen. Physiol., 1978; 78: 249-265.

157. Marche, P., Koutouzov, S., Girard, A., Elghozi, J.L., Meyer, B., Ben-Ishay, D. Phosphoinositide turnover in erythrocyte membranes in human and experimental hypertension. J. Hypertension, 1985; 3: 25-30.

158. Bull, T.E. Nuclear magnetic relaxation of spin-3/2 nuclei involved in chemical exchange. J. Magn. Reson., 1972; 8: 344-353.

159. Bansal, N., Germani, M.J., Seshan, V., Shires, G.T., Malloy, C.R., Sherry, A.D. Thulium 1,4,7,10-tetraazacyclododecane-1,4,7,10-tetrakis(methylene phosphonate) as a ^{23}Na shift reagent for the *in vivo* rat liver. Biochemistry, 1993; 32: 5638-5643.

160. Shinar, H., Knubovets, T., Eliav, U., Navon, G. Sodium interaction with ordered structures in mammalian red blood cells detected by Na-23 double quantum NMR. Biophys. J., 1993; 64: 1273-1279.

161. Pettegrew, J.W., Glonek, T., Minshew, N.J., Woessner, D.E. Na-23 NMR analysis of human whole blood, erythrocytes, and plasma-chemical shift, spinrelaxation, and intracellular sodium concentration studies. J. Magn. Reson., 1984; 57: 185-196.

162. Hitzemann, R.J., Garver, D.L. Abonrmalities in membrane lipids associated with deficiencies in lithium counterflow. In "Biological Markers in Psychiatry and Neurology" (Usdin, E., Hanin, I., eds.). Pergamon Press, Oxford. 1982; 177-182.

163. Callahan, J. Phospholipids in disorders of the nervous system. In "Phospholipids in Nervous Tissues" (Eichberg, J., ed.). New York: John Wiley, 1985; 297-320.

164. Rutherford, P.A., Thomas, T.H., Wilkinson, R. Erythrocyte sodium-lithium

countertransport: clinically useful, pathophysiologically instructive or just phenomenology? Clin. Sci., 1992; 82: 341-352.

165. Ehrlich, B.E., Diamond, J.M. Lithium, membrane, and manic-depressive illness. J. Membr. Biol., 1980; 52: 187-200.

166. Duhm, J., Eisenried, F., Becker, B.F., Greil, W. Studies on the lithium transport across the red cell membrane. I. Li^+ uphill transport by Na^+-dependent Li^+ countertransport system of human erythrocytes. Pflugers Arch., 1976; 364: 147-155.

167. Spillman, T., Bretaudiere, J.P., Cotton, D.B., Lynn, S.C. Influence of phospholipid saturation on classical thin-layer chromatographic detection methods and its effect on amniotic fluid lecithin sphingomyelin ratio. Clin. Chem., 1983; 29: 250-255.

168. Deuticke, B., Haest, C.W.M. Lipid modulation of transport proteins in vertebrate cell membranes. Annu. Rev. Physiol., 1987; 41: 1171-1178.

169. Corrocher, R., Steinmayr, M., Ruzzenente, O., Brugnara, C., Bertinato, L., Mazzi, M., Furri, C., Bonfanti, F., De Sandre, G. Elevation of red cell sodium-lithium countertransport in hyperlipidemias. Life Sci., 1985; 36: 649-655.

170. Duhm, J. Pathways of lithium transport across the human erythrocyte membrane. In "Lithium Kinetics" (Thellier, M., Wissocq, J-C., eds). Carnforth: Marius Press, 1992: 27-53.

171. Stubbs, C.D., Smith, A.D. The modification of mammalian membrane polyunsaturated fatty acid composition in relation to membrane fluidity and function. Biochim. Biophys. Acta, 1984; 779: 89-137.

172. Engelmann, B., Op den Kamp, J.A.F., Roelofsen, B. Replacement of molecular species of phosphatidylcholine: influence on erythrocyte Na transport. Am. J. Physiol., 1990; 258: C682-C691.

173. Pagnan, A., Corrocher, R., Ambrosio, G.B., Ferrari, S., Guarini, P., Picollo, D., Opportuno, A., Bassi, A., Oliveri, O., Baggio, G. Effects of an olive oil rich diet on erythrocyte membrane lipid composition and cation transport systems. Clin. Sci., 1989; 76: 87-93.

174. Hauser, H., Shipley, G.G. Crystallization of phosphatidyl serine bilayer induced by lithium. J. Biol. Chem., 1981; 256: 11377-11380.

175. Allison, J.H., Blisner, M.E., Holland, W.H., Hipps, P.P., Sherman, W.R. Increased brain myo-inositol-1-phosphate in lithium-treated rats. Biochem. Biophys. Res. Commun., 1976; 71: 664-670.

176. Berridge, M.J., Downes, C.P., Hanley, M.R. Lithium amplifies agonist-dependent phosphatidyl inositol responses in brain and salivary glands. Biochem. J., 1982; 206:

587-595.

177. Moscovich, D.G., Belmaker, R.H., Agam, G., Livne, A. Inositol-1-phosphatase in red blood cells of manic-depressive patients before and during treatment with lithium. Biol. Psychiatry, 1990; 27: 552-555.

178. Pettegrew, J.W., Keshavan, M.S., Panchaligam, K., Strychor, S., Kaplan, D.B., Tretta, M.G., Allen, M. Alterations in brain high-energy phosphate and membrane phospholipid metabolism in first-episode, drug-naive schizophrenics. A pilot study of the dorsal prefrontal cortex by in vivo phosphorus-31 nuclear magnetic resonance spectroscopy. Arch. Gen. Psychiatry, 1991; 48: 563-568.

179. Mendels, J., Frazer, A. Alterations in cell membrane activity in depression. Am. J. Psychiatry, 1974; 131: 1240-1246.

VITA

The author, Qinfen Rong, was born on December 3, 1965, in Shanghai, China.

In September of 1984, she started her undergraduate studies at Fudan University and obtained her Bachelor of Science degree in Chemistry in July of 1988.

In August 1989, she entered the Ph.D. program in Chemistry at Loyola University of Chicago. She received a graduate assistantship from August of 1989 until December of 1990. She was supported by a research assistantship from January of 1991 until August 1992, and from June of 1993 till October of 1993 by a NIMH grant awarded to Dr. Duarte Mota de Freitas. She was awarded the Schmitt Dissertation Fellowship for the period of September 1992 through May of 1993. In August 1993, she was awarded the Dumbach medal for "Excellence in Chemistry" by the Chemistry Department of Loyola University of Chicago.

APPROVAL SHEET

The dissertation submmitted by Qinfen Rong has been read and approved by the following committee:

Dr. Duarte Mota de Freitas, Director
Associate Professor of Chemistry, Loyola University

Dr. Kenneth Olsen
Professor of Chemistry, Loyola University

Dr. Charles Thompson
Associate Professor of Chemistry, Loyola University

Dr. David Crumrine
Associate Professor of Chemistry, Loyola University

Dr. David Lynn
Professor of Chemistry, The University of Chicago

The final copies have been examined by the director of the dissertation and the signature which appears below verifies the fact that any necessary changes have been incorporated and that the dissertation is now given final approval by the committee with reference to content and form.

The dissertation is therefore accepted in partial fulfillment of the requirements for the degree of Doctor of Philosophy.

11/19/93
Date


Director's Signature